POLITECNICO DI MILANO
Department of Bioengineering
PhD Program in Bioengineering

Development of innovative devices for reliable studies of in vitro models of Central Nervous System pathologies

PhD Thesis of
Emilia Biffi
Matr # 723986

Tutor: Prof. Giancarlo Ferrigno
Supervisors: Alessandra Pedrocchi, Gianfranco Beniamino Fiore
PhD Coordinator: MariaGabriella Signorini

XXIV Edition
2008-2011

Acknowledgment

I would like to thank my tutor, Professor Giancarlo Ferrigno for the great opportunity he gave me and for his important support throughout this work. I am grateful to my supervisor Dr. Alessandra Pedrocchi, whose encouraging advice guided me during these years and allowed me to successfully carry out my project. I am also thankful to my supervisor Dr. Gianfranco Beniamino Fiore, whose valuable comments and suggestions about my work helped me during some difficult moments. I would like to thank Dr. Andrea Menegon that taught me the basic knowledge of neurobiology and neuropharmacology through constructive debates. Sincere thanks to Diego, whose criticism and advice helped me to reach my scientific independence. I am also grateful to Dr. Luca Muzio with whom important idea exchanges put the basis for a meaningful collaboration. During this work I collaborated with many colleagues with whom I shared both disappointments and satisfactions. First, my warm thanks to "the girls", Emy, Cla, Simo, Marta, four good colleagues and really important friends who transformed even the worst moment in the best time. Then, many thanks to Marco that always supported me and who taught me the real meaning of working as a team. I also would like to thank my student Giulia, who never gave up in front of difficulties and failures and who always trusted me. Finally, thanks to all the people from NearLab, who shared my anxiety and my happiness. I wish to extend my thanks to all those who have helped me with my work. Many thanks to Roby, "my biological mind", who transformed boring Sundays at work into pleasant weekends. Thanks also to all the people from the Alembic facility, who taught me with patience all the biological protocols I did not know before. Thanks to all my friends, particularly thanks to Alice, Stefano, Roberto and Michele that were always present even when I was abroad. Thanks also to all the people I met in Leuven, above all to my German friend Andreas for his careful reading of part of this thesis. I owe my thanks to my great family: my mum and dad who believed in me since the beginning and particularly to my sister Giulia, whose determination always reminds me that we can do whatever we wish. Giulia, thanks also for your detailed and constructive comments on my thesis. Finally, thanks to Nico, my best friend and my life partner who always rejoiced and suffered with me during these years and hopefully for the rest of my life.

Summary

S.1. Introduction

Diseases of the Central Nervous System (CNS) are a crucial topic in neuroscience. Among these, neurodegenerative diseases constitute a considerable portion. Neurodegenerative diseases are chronic pathologies of the CNS that cause brain functional derangement. These brain diseases are growing in incidence due to increase in life expectancy, but still most of their causes and mechanisms are not well known. This raises the interest in studying brain alterations as well as developing and testing new molecules that could re-establish brain functionalities. Since the level of investigation is not ethical in human patients, researchers take advantage of using animal models of diseases with the purpose of better understanding these neuropathologies. The vast majority of the experimental models have a genetic origin. Due to the ease of its genetic manipulation, the mouse has become the preferred system to pattern neurodegenerative diseases. Examples of neurodegenerative diseases that are investigated by means of genetic mice models are Alzheimer's disease [Chen and Zhang, 2011], Parkinson's disease [Dawson et al., 2010], Down syndrome [Bartesaghi et al., 2011], Amyotrophic Later Sclerosis [Gurney et al., 1994] and Epilepsy [Barclay and Rees, 1999]. In addition to genetic animal models, several human diseases, including Multiple Sclerosis [Brown and Sawchenko, 2007] and stroke [Durukan and Tatlisumak, 2009], are patterned on inducible experimental mouse models. In particular Multiple Sclerosis (MS), a widespread autoimmune disease of young adults, has been deeply investigated by using the experimental autoimmune encephalomyelitis (EAE) model.

Given the complexity of the adult tissue, these studies take advantage of *in vitro* neuronal networks, which are widely used as a model for acquiring a basic understanding of the network functionality. Thanks to *in vitro* studies it is possible to address directly the effects of diseases and drugs at cellular and small network level. Moreover, they shorten the experimental timescales, offer a controlled environment and assist in the ease of experimental replication [Polikov et al., 2008]. For these reasons *in vitro* models are a powerful tool to characterize a pathological condition and to compare it to the physiological one.

One of the main mechanisms exploited by neurons to communicate is depicted by electrical signaling. Hence, the electrophysiology of the single neuron and of small networks is a widely accepted methodologies to study the *in vitro* physiopathology of the brain. Single cell analysis is usually carried out by means of patch clamp technique, whose target is mainly the study of single ion-channel currents or the investigation of the related changes in cell membrane potentials. The advantage and interest of the patch clamp technique is that it allows to carry out accurate measurements of voltage changes in up to twelve neurons at the same time; on the other hand, it is highly invasive and time consuming [Eckmann et al., 2007]. Thus, when the focus lies on networks rather than single cells, conventional electrodes suffer from two well-known limitations [Thakur et al., 2007]: the number of neurons recorded simultaneously and the time needed for electrode placement. These experimental difficulties can be overcome thanks to Micro Electrode Arrays (MEAs). These matrices of planar metallic electrodes allow to record extracellular activity of neuronal preparations from multiple sites simultaneously in a non-destructive manner [Gross, 1979, Pine, 1980]. MEAs offer a simple approach to examine the activities of neuronal cells on a large scale and provide new insights into the dynamics of *in vitro* networks. Therefore, they are considered a standard tool in the field of drug discovery and basic research [Jimbo et al., 1999, Demarse et al., 2001, Segev et al., 2004, Baruchi and Ben-Jacob, 2007, van Pelt et al., 2004b, Chiappalone et al., 2006, 2007, Chiappalone et al., 2003, Morin et al., 2005, Boehler et al., 2007, Chen et al., 2008]. Recently, they have also been used to study *in vitro* models of brain malfunctions, such as epilepsy [Faingold, 2004] and neurodegeneration [Hakkoum et al., 2007].

Within this framework, it is of great interest to use MEA technologies to characterize the spontaneous electrophysiological activity of *in vitro* models of pathologies and to pharmacologically modulate it in order to regain a physiological network activity. This goal gives rise to many technological challenges concerning the ability of studying the electrical activity during network maturation and of stimulating neurons locally with neuroactive molecules.

Nowadays, microfabricated arrays, recording hardware and software for data acquisition and analysis are commercially available and enable recordings from 60 or more electrodes. The standard experimental setup usually consists of an incubator, where cell cultures are grown on MEA chips, and freestanding electronics for neuronal activity recording. During experimental sessions, MEA chips have to be moved to the electrophysiological setup. Due to the high degree of sensitivity of neuronal networks to slight changes in the physical and chemical environment of the cell culture [Gross and Schwalm, 1994], the ability of controlling and maintaining the environmental parameters during electrophysiological tests is an important requirement in the experimental design. During neuronal activity recordings, changes in

temperature and contamination of the cellular environment may be induced; moreover, the content of CO_2 in the environmental air, lower than the peculiar percentage of an incubator, rapidly results in elevation of the cell culture medium pH. These issues get more crucial when the duration of electrophysiological experiments is increased from hours to days, which is the time extent required in order to study network functional plasticity [Shahaf and Marom, 2001, Chiappalone et al., 2008], long-term neuronal network phenomena [van Pelt et al., 2004b,a, Hofmann and Bading, 2006] and chronic treatment effects [Morefield et al., 2000, Xiang et al., 2008, Howell et al., 2011]. The shortcomings of the aforementioned setup cause a gradual decline in the health of these cell cultures and a decrease of data reproducibility, for which the environmental stability is critical [Gross and Schwalm, 1994]. Prototypes of temperature controlled bath chambers [Forsythe and Coates, 1988, Toyotomi and Momose, 1989, Heidemann et al., 2003, Ho et al., 2005], devices to improve the pH maintenance [Fantini et al., 1987, Bavister, 1988, Vukasinovic et al., 2009], flow chambers and sealing membranes coupled to MEAs [Gross and Schwalm, 1994, Blau and Ziegler, 2001, Potter and DeMarse, 2001, Pancrazio et al., 2003, Mukai et al., 2003, Blau et al., 2009] have been developed over the last years. However, so far there are no integrated devices available which allow growing neuronal cultures since the beginning of their maturation for a long period of time and simultaneously providing long term continuous multichannel recordings.

When a study aims at figuring out the effect of molecules on the activity of *in vitro* neuronal models, the pharmacological stimulation protocol is another crucial element. Currently, standard techniques make use of pipettes and require partial or complete change of the culture medium. Disadvantages of these protocols are the unknown kinetic of the interaction between molecules and cells and the rapid changes in the cellular environment, respectively. Moreover, these stimulation protocols often lack of defined spatio-temporal control [Kothapalli et al., 2011] and are demanding in terms of reagents consumption and costs [Sung et al., 2010]. These drawbacks indicate that the current *in vitro* systems for studying drug effects need to be refined. Recently, the potential importance of microfluidic techniques in improving pharmacological studies has been widely recognized. Microfluidics can precisely define pharmacological microenvironment [Taylor and Jeon, 2010], it allows a localized pharmacological intervention [Shi et al., 2010] and the delivery of micro-scale volumes of drugs to the desired neurons [Wang et al., 2009]. Hence, microfluidic systems with perfusion cell culture offer a great potential for drug screening [Sung et al., 2010].

S.2. Aim of the work

Within this framework, this thesis aims at improving the reproducibility and reliability of *in vitro* electrophysiological data. In this work, the scientific importance of MEA technology in the neurodegenerative field has been stressed by means of an electrophysiological and pharmacological study on EAE, the mice model of multiple sclerosis, which gave important results with possible outcomes for patients drug treatments (Chapter 3). During this project, I evidenced many restrictions related to the experimental equipments and techniques. First, it emerged the impossibility of recording neuronal activity continuously for many hours, because of the size of data and the huge memory space required. Furthermore, repeated acquisitions of the same neuronal culture were limited since they caused electrophysiological changes and cellular viability decline. Finally, the standard biochemical stimulation technique with pipettes showed its drawbacks by causing uncontrolled neuronal response and electrode saturation.

Consequently, several technological challenges have been tackled during my PhD. First, a custom chamber for neuronal growth and long term recording of network activity was developed and tested (Chapter 4). Then, dedicated electronic boards for signal conditioning and post-processing (i.e. spike detection and sorting) were designed to handle the huge amount of data due to continuous acquisition (Chapter 5). Besides, a cross-correlation algorithm was designed to provide a comprehensive functional evaluation of neuronal network communication properties (Chapter 6). Finally, a PDMS microfluidic device, coupled to an array of microelectrodes, was developed and validated first for neuronal extracellular electrophysiology and, subsequently, for local controlled biochemical stimulation (Chapter 7). To conclude, these technologies solve the problems concerning continuous and long term acquisitions and overcome the drawbacks of standard biochemical stimulation techniques. The benefits that these technologies bring to the neuroscience field and the perspective of their eventual integration into one device are discussed eventually in this thesis (Chapter 8).

S.3. Study of GABA transmission in Th1-treated neuronal cultures[1]

Multiple sclerosis (MS) is a chronic debilitating disease, generally thought to be immune mediated [Brown and Sawchenko, 2007]. It is usually investigated by using an animal model of neurodegeneration, called experimental autoimmune encephalomyelitis (EAE) model. EAE is generally induced in mice by the subcutaneous injection of myelin oligodendrocytes (MOG) peptides. MOG induces both an encephalitogenic T-cell response and a demyelinating autoantibody response. Thus, MOG-EAE mice develop a chronic disease, which evolves in a manner consistent with an ascending myelopathy. Moreover, both MS and EAE active lesions are characterized by the presence of pro-inflammatory cytokines, which are secreted by Th1 cells infiltrating the CNS. These pro-inflammatory molecules represent key molecules of adaptive immunity and have been found to alter neuronal functioning and glutamate transmission [Stellwagen et al., 2005]. Furthermore, it is known that glutamate-dependent excitotoxic damage plays a fundamental role in neuronal degeneration that accompanies EAE and MS [Centonze et al., 2009], while there is no evidence concerning the alteration of inhibitory transmission in the brain of EAE mice. To evaluate the effects of inflammatory events on gamma-Aminobutyric acid (GABA) signaling, Th1-treated neuronal cultures and striatal slices of EAE mice were investigated.

In the study, 28 primary neuronal cultures on MEAs were included, which were obtained from the dissociation of E17.5 mouse cerebral cortices. Each cell culture was firstly recorded after 12 days *in vitro*, then randomized MEAs were treated either with a cocktail of pro-inflammatory cytokines (Th1 treatment) or with saline as sham treatment. Cell cultures on MEAs were subsequently recorded 12 and 24 hours after cytokines or saline administration. Then, some neuronal cultures were treated with increasing amount of GABA (from $0.01\,\mu$M to the maximal concentration of $100\,\mu$M) and cell signals were recorded. Spikes were detected using MCRack Software (Multi Channel Systems, MCS GmbH) and further analyzed with standard algorithms [van Pelt et al., 2005, Chiappalone et al., 2005]. Pro-inflammatory cytokines did not affect the single channel activity, as well as burst activity. In contrast, pro-inflammatory cytokines significantly increased the network burst length, which was approximately doubled in cell cultures treated for 24 hours with Th1 cytokines (Figure 1A, $n = 14$, $p < 0.01$ Wilcoxon test inside groups, $p < 0.05$ Mannn-Whitney test between treated and untreated cell cultures at 24 hours). Moreover, Th1 in-

[1]The work has been published as Rossi S, Muzio L, De Chiara V, Grasselli G, Musella A, Musumeci G, Mandolesi G, De Ceglia R, Maida S, **Biffi E**, Pedrocchi A, Menegon A, Bernardi G, Furlan R, Martino G, Centonze D. Impaired striatal GABA transmission in experimental autoimmune encephalomyelitis. *Brain Behav Immun*, 2011, 25(5):947-56.

flamed neuronal networks treated with increasing amount of GABA showed a reduction of network burst length which became comparable to those of control neuronal cultures after 10 μM GABA treatment (Figure 1B). Finally, the expression levels of parvalbumin (PV), a calcium-binding protein, which is present in GABAergic interneurons, were examined with retro-transcription polymerase chain reaction (RT-PCR) both in Th1- and sham-treated cell cultures (24 hour treatments). According to the electrophysiological data, pro-inflammatory cytokines treatment significantly reduced the mRNA levels of paravalbumin. These results suggest that Th1 stimuli do not perturb single cell firing activity but alter network connectivity. Moreover, they prove that a cocktail of pro-inflammatory cytokines can perturb the GABAergic system *in vitro* when chronically administered. These results are in agreement with the observations made on cortico-striatal slices of EAE-induced mice. Indeed, a decrease in spontaneous GABAergic currents during acute neuro-inflammation and chronic phases of the disease was measured. Moreover, a significant reduction of striatal PV-positive GABAergic interneurons was determined. Altogether, these data suggest that chronic inflammatory stimulation of neuronal networks leads to profound alteration of GABA transmission. Furthermore, the evidence that this alteration can be induced by cytokines signaling *per se*, as demonstrated by MEAs experiments, supports the possibility that this mechanism is at the base of MS pathogenesis. To conclude, the general GABAergic down-regulation induced by cytokines chronic treatment that emerges from this study should drive the search of drugs able to control this alteration.

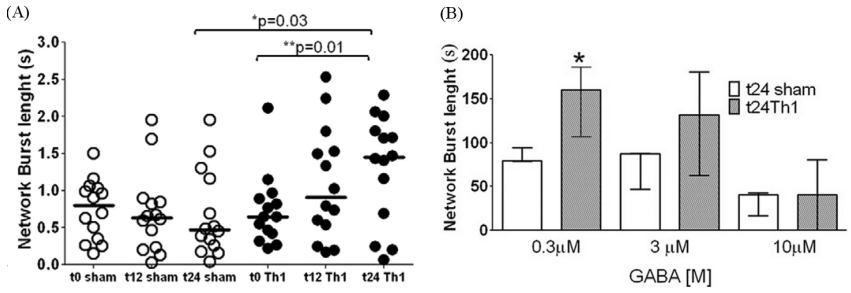

Figure 1: (A) Single experiments (solid circles: Th1-treated cell cultures; dashed circles: saline treated cell cultures) and median values (lines) before the treatment (1st time point) and after 12 and 24 h (2nd and 3rd time points). (B) GABA treatment of control (white) and Th1-treated (gray) neuronal cultures. In collaboration with the Neuroimmunology Unit, INSpe, Department of Neuroscience (San Raffaele Scientific Institute, Milan) and with the Advanced Light and Electron Microscopy Bio-Imaging Center (San Raffaele Scientific Institute, Milan).

S.4. Development of a chamber for long term MEA recordings[2]

MEA electrophysiological recordings are usually performed with systems which are separated by the incubating chambers. In my work, an integrated device for both neuronal growth and activity recording was developed and tested in order to overcome the drawbacks of the standard MEA recording setup and to increase the neurophysiopathological data reproducibility.

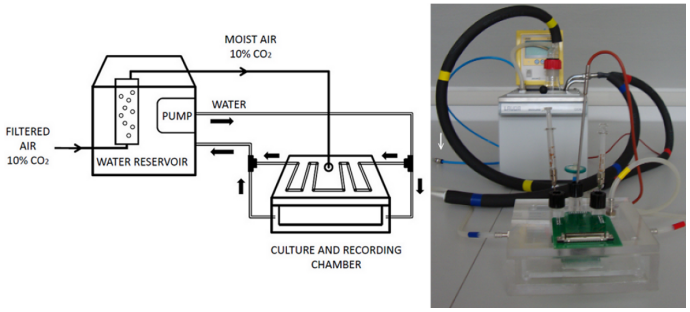

Figure 2: Schematic representation (left) and a picture (right) of the whole system configuration.

Figure 2 shows a scheme (left) and a picture (right) of the system developed. The chamber is made of polymethylmethacrylate (PMMA) plates and it is formed by an outer (180 mm x 180 mm) and an inner (150 mm x 150 mm) box, both covered by a top plate. A silicon membrane and eight small Rolez clamps guarantee the sealing of the closure and sterility. Proper airtight openings for needles insertion allow adding medium and drugs from the outside; moreover, joins for air exchange are provided. The chamber heating is obtained by means of a circulating bath (E306, Ecoline, Lauda GmbH), which pumps water in the cavity between the PMMA boxes. The feedback to a proportional-integral (PI) controller is given by a Pt100 thermoresistance inserted in a reference well. To maintain the pH of the medium in a physiological range (7.2-7.4), a 10% CO_2 gas cylinder is used; before introducing the air in the chamber, its moisture-content is enhanced by a commercial bubbling module (Okolab s.r.l., Italy). Besides, in order to prevent condensation, a tubing structure connected to the warming bath is placed over the top plate. The MEA housing is designed inside the chamber. Gold pins for the acquisition of electrical signals are in contact with the MEA pads. The signal is transmitted to the electronic circuitry, which is located outside the chamber, by means of three sealed connectors. The PMMA transparency and a cavity beneath the MEA housing allow cell optical

[2]A journal paper on this work has been submitted to *Biotechnology and Bioengineering* as **Biffi E**, Regalia G, Ghezzi D, Menegon A, De Ceglia R, Ferrigno G, Fiore GB, Pedrocchi A. A novel environmental chamber for long term neuronal network multisite recordings.

monitoring by a 5x objective of an inverted microscope.

The system was characterized in terms of heating control and gas flow rate. The temperature profile was comparable to the literature [Vukasinovic et al., 2009] and a gas flow of 70 ml/min maintained the pH of the medium between 7.38 and 7.57. Then, primary neuronal cultures, obtained from the dissociation of E17.5 mouse hippocampi, were plated on round glasses and on standard MEAs. Cell cultures were grown and maintained half in a humidified incubator, half in the chamber, previously sterilized, up to 21 days *in vitro* (DIV). The influence of the custom chamber on the cell vitality was quantitatively evaluated by propidium iodide/fluorescein diacetate staining at 7, 14 and 21 DIV. At each time point, 20x fluorescence images were taken from glass coverslips cultured both in the custom chamber ($n = 6$) and in the control incubator ($n = 6$). The vitality was computed as the percentage of cells expressing fluorescein diacetate (a healthy cells marker) on the total nuclei (marked with Hoechst-33342) and a one-way ANOVA test was performed to assess differences between the two culturing conditions. Figure 3A and 3B show the staining of a 7 DIV neuronal culture grown in the standard incubator and inside the custom chamber, respectively. No significant differences were found in cell viability (Figure 3C $p > 0.05$, one-way ANOVA, $n = 6$ in each group) under both culture conditions at different time points, indicating that the custom chamber alters neither the network development nor the neuronal viability over a long period of time.

Afterwards, electrophysiological recordings were performed by means of the standard setup and custom chamber, both connected to the analog to digital USB-ME64 board (MCS GmbH). The activity of three neuronal networks (13 DIV) grown on MEAs was analyzed in Matlab. The neuronal electrical activity recorded inside the chamber showed spiking organization qualitatively similar to standard recordings (Figure 3D and 3E). Additionally, the comparability of burst and network burst features in the two recording setups was confirmed by the analysis (Figure 3F, bottom). In contrast, a significant difference in spiking frequencies was detected (Wilcoxon test $p < 0.05$), due to the higher signal-to-noise ratio (SNR) in the standard recording setup (20 dB) compared to the customized one (18 dB) (channel activities in Figure 3F, top). The lower SNR was attributed to the lack of a decoupling and pre-amplification stage close to the signal source. For this reason, part of the amplification stage was later designed to be located inside the chamber and a single channel prototype (G: 900; bandwidth: 300 Hz-3 kHz) was implemented on breadboard. The printed circuit board (PCB) development is ongoing.

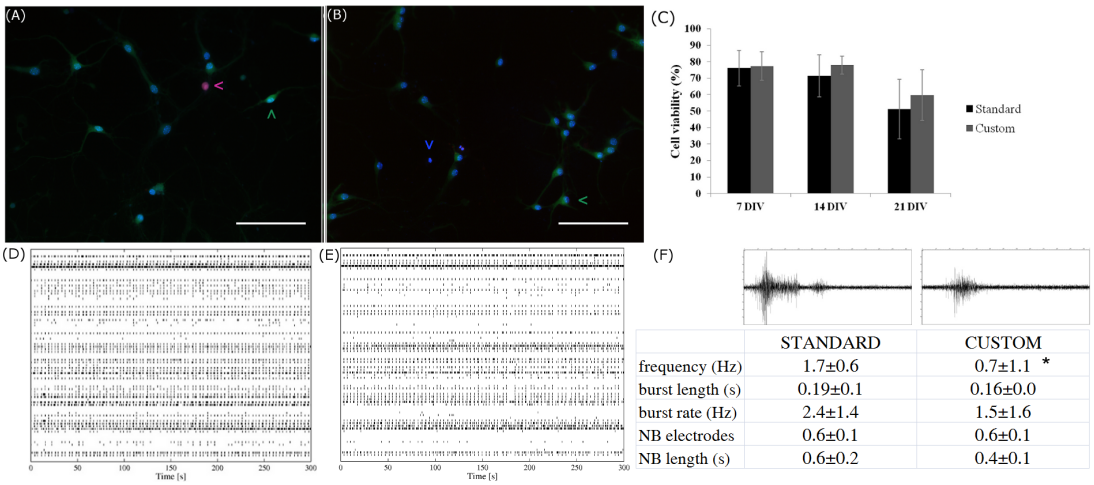

	STANDARD	CUSTOM
frequency (Hz)	1.7±0.6	0.7±1.1 *
burst length (s)	0.19±0.1	0.16±0.0
burst rate (Hz)	2.4±1.4	1.5±1.6
NB electrodes	0.6±0.1	0.6±0.1
NB length (s)	0.6±0.2	0.4±0.1

Figure 3: Viability test and recording ability of the custom chamber. Staining of a 7 DIV neuronal culture grown in the standard incubator (A) and inside the custom chamber (B). Scale bars 100 μm. Green, blue and violet arrowheads identify viable cells, necrotic/apoptotic cells and necrotic cells, respectively. Labels: red PI; green FDA; blue Hoechst-33342. (C) Statistical analysis of cell viability in a standard incubator (black) and in the custom chamber (gray) at 7, 14 and 21 DIV. Raster plots recorded by the standard setup (D) and the chamber (E). (F) Top: 1s activity of the same channel recorded with the two setups. Bottom: activity parameters median value ± the coefficient of variation ($n = 3$; $^* p < 0.05$).

S.5. Post-processing on hardware: a feasibility study[3]

When recording continuously for long periods of time using the chamber developed, a huge amount of data has to be handled. Hence, application-specific post-processing electronics is required. In this work, a spike detection and classification algorithm was developed in Matlab and the feasibility of its hardware implementation was investigated.

An amplitude threshold crossing technique was selected for spike detection. The threshold was computed as a multiple of basal noise level. Particularly, five noise estimation methods were developed in Matlab. Performances of these methods were statistically evaluated on simulated neuronal signal and on real electrical activity. The adaptability and sensitivity had priority when choosing the optimum spike detection method due to the noise level drift on a time-scale of hours and because of the non reversibility of the spike detection procedure (if implemented on hardware), respectively. The performance evaluation of noise estimation methods on simulated and real signals identified two of them as the adaptive algorithms with highest sensitivity. Then, the Big O notation was used to quantitatively evaluate

[3]The work has been published as **Biffi E**, Ghezzi D, Pedrocchi A, Ferrigno G. Development and validation of a spike detection and classification algorithm aimed at implementation on hardware devices. *Comput Intell Neurosci*, 2010, doi:10.1155/2010/659050.

their performances as a function of the number of their input data. It classified as the best algorithm AdaBandFlt, a quick adaptive noise estimation method, based on the evaluation of the signal root mean square (RMS) distribution. Subsequently, a feasibility study concerning the hardware implementation on a Field Programmable Gate Array (FPGA) of the selected thresholding method was done. The number of configurable logic blocks (CLBs), the memory occupation and timings were evaluated. Figure 4 shows the blocks architecture to compute the threshold value for 1 channel. To implement this design in a FPGA, taking into account all MEA channels, 64 differential input/output blocks, 64 dedicated multipliers, 4803 CLBs, 291 kbits of RAM and 1536 dedicated 2:1 multiplexers are required. Two feasible solutions were identified: the first one envisages the use of XC3S5000 (Xilinx Spartan-3) that satisfies hardware requirements for all channels. The second solution allows modular assembling using two smaller FPGAs (XC3S4000, Xilinx Spartan-3), each for 32 channels. The use of a FPGA would guarantee the real-time detection of spikes and the possibility of saving only their templates for the following classification.

After detection of spikes, a classification algorithm was developed in Matlab by using principal component analysis (PCA) and hierarchical classification to favour an automatic and reliable shape clustering. The algorithm was tested on simulated signal and real data and stated the quality of the clustering procedure.

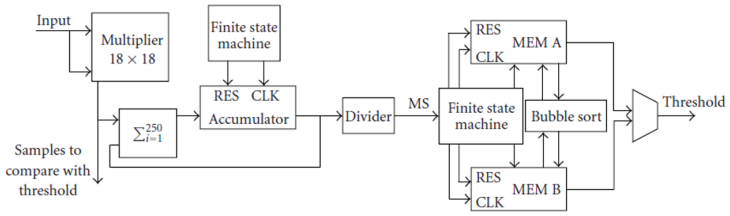

Figure 4: Architectural blocks to compute a threshold value.

To conclude, the developed algorithm has the highest performances in order to achieve recordings of neuronal activity over long period of time. Furthermore, it was demonstrated that the spike detection can be realized by using an FPGA. The hardware implementation is ongoing. Moreover, the PCA-hierarchical classifier may be implemented on a Digital Signal Processor (DSP), as already done in the literature [Han et al., 2004]. Hence, thanks to high speed hardware devices, the post-processing can be executed on-line, just keeping time stamps and waveforms and thus reducing data storage problems.

S.6. A new descriptor of neuronal connectivity[4]

The spike detection procedure is the necessary step which precedes the extraction of features that describe the network activity. Another important step in this framework is the definition of simple parameters able to take into account the behavior of integrated neuronal networks as a whole. To fulfill this aim, an intra network burst cross-correlation algorithm was developed and validated.

The algorithm divides the signal in 25 ms bins and computes the product of number of active sites and total spikes for each bin; network bursts (NBs) are identified when this product is bigger than nine, according to literature [van Pelt et al., 2005]. Then, the spike trains that belong to each NB are convoluted with a Gaussian function and the continuous cross correlation is computed. Finally, it is computed the mean value of Total Corr (MTC), which is the normalized integral of the correlation matrix for each NB. To evaluate the parameter sensitivity, ten cortical cultures (E17 mice) were treated with both submaximal (1 μM) and maximal (20 μM) bicuculline concentrations, a molecule that alters the neuronal network functional connectivity. The data were analyzed by the algorithm developed hereby and by two correlation-based methods described in the literature [Li et al., 2007a, Tateno and Jimbo, 1999]. The MTC was able to discriminate between the untreated and bicuculline-treated conditions, even at sub-maximal concentration ($p < 0.01$ Wilcoxon test). Furthermore, the comparison with established methods confirmed its high sensitivity. Indeed, the other algorithms revealed to be inadequate for the detection of small pharmacological compound concentrations [Tateno and Jimbo, 1999] or to be limited only to a local evaluation of the network activity [Li et al., 2007a]. Finally, in order to investigate the algorithm potential use in pharmacological studies, concentration–response experiments were performed with GABA, as a test molecule. The MTC concentration-response fitting was able to estimate, in a reliable way, the half maximal effective concentration (EC_{50}) values ranging from 2 μM to 8 μM, which is in agreement with the literature [Boldyreva, 2005].

[4]The work has been published as **Biffi E**, Menegon A, Regalia G, Maida S, Ferrigno G, Pedrocchi A. A new cross-correlation algorithm for the analysis of "*in vitro*" neuronal network activity aimed at pharmacological studies. *J Neurosci Methods*, 2011, 199(2): 321-327.

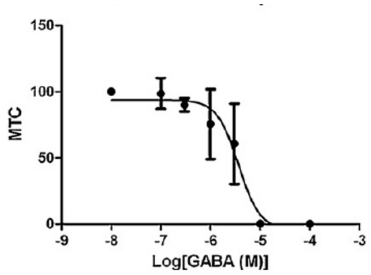

Figure 5: MTC concentration-response curve after GABA increasing concentrations addition ($R^2 = 0.7408$).

These results demonstrated the possibility of using MTC in classical pharmacological experiments (Figure 5). Thus, this approach is able to analyze and to detect changes in the correlation properties of neuronal networks condensing the information in a simple, reliable and highly sensitive parameter.

S.7. Local network stimulation using microfluidics. A feasibility study[5]

The pharmacological modulation of network electrophysiological activity is a topic of high interest in neuroscience. To solve the limitations of standard biochemical stimulation, a microfluidic device was developed by reversibly coupling a poly(dimethylsiloxane) (PDMS) closed chamber with a commercial flat MEA.

The PDMS chambers was obtained as previously described [Rasponi et al., 2011]. The device is characterized by 2 inlets, one outlet and a microchannel (100 μm in height) for cell culture. A 60-electrode flat MEA chip is interposed between the PDMS device and a neodymium magnet, which ensures the sealing. This configuration was used to assess the neuronal viability inside the device. Primary neuronal cultures were obtained from the dissociation of E17 mouse hippocampi and plated inside the microchamber. Activity was recorded with a commercial system (MCS GmbH) from 8 to 18 days *in vitro* (DIV). Single channel and network parameters were computed in Matlab and a statistical analysis (Wilcoxon test) was performed among different days of maturation. Neuronal networks were able to differentiate within a few days and their electrophysiological maturation was comparable with that of networks cultured in macro-environments. Accordingly, the Wilcoxon test highlighted significant differences ($p < 0.05$) among parameters at 10 DIV and at 12, 14, 16 and 18 DIV (Figure 6B shows MFR, for an instance). These results also

[5]The validation of the micro-chamber for neuronal growth and recording has been published as **Biffi E**, Menegon A, Piraino F, Pedrocchi A, Fiore GB, Rasponi M. Validation of long-term primary neuronal cultures and network activity through the integration of reversibly bonded microbioreactors and MEA substrates. *Biotechnol Bioeng*, 2012, 109(1): 166 - 175.

confirmed that the magnet has no effects on neuronal activity and development.

Then, an advanced version of the device, with a partial wall in the middle of the main channel, was developed (Figure 6A). The barrier divides seeded cells in two compartments, while still culturing them in the same environment. The activity of neurons grown in this configuration was recorded at 14 DIV, analyzed in Matlab and correlation values were computed [Biffi et al., 2011, Chapter 6] both inside and between compartments. These data confirmed that the two networks were comparable in channel and network parameters (e.g. for the left and the right side: MFR is 6.4 Hz and 5.5 Hz; burst length is 0.26 s and 0.28 s). Furthermore, correlation values proved that the two networks were not functionally connected, since the correlation in the same compartment was about ten times the correlation between different compartments. Hence, these two twin networks conceptually correspond to two MEAs. However, cells are grown in the same microenvironment, resulting in reduced experimental variation. Finally, the activity of neurons grown in this second configuration of the microfluidic device was recorded during local 0.5 μM tetrodotoxin (TTX) stimulation. The protocol required an untreated recording followed by a three minutes TTX and medium perfusion in the right and the left side of the channel, respectively, by means of a syringe pump. Subsequently, both channels were treated with fresh medium for ten minutes to enable the recovery of the activity. The experiment was repeated whereby the left and the right channel were reversed. The normalized mean firing rate (MFR) was evaluated on both sides for each step of the stimulation. Figure 6C shows the normalized MFR values during local TTX treatment, which was first performed on the right channel (black bar) and then on the left one (gray bar).

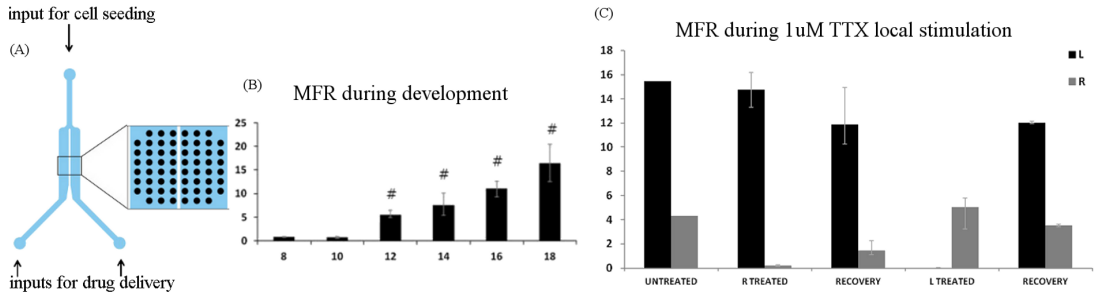

Figure 6: (A) Sketch of the channel layout. (B) Mean firing rate (Hz) during network development (x label: DIV; # $p < 0.05$ with respect to 10 DIV) (C) Normalized MFR during local TTX stimulation.

These experiments proved that the device developed here allows to successfully stimulate neuronal cultures in a selective way, without any interference between compartments.

S.8. Conclusions

My PhD work underlines the high impact of multisite electrophysiological studies on neurons towards brain disease research. Furthermore, it evidenced many weaknesses of the standard techniques. Therefore, the final outcome of this thesis is the development and assessment of systems which aim at progressing these technologies. The incubating and recording chamber developed hereby solves the problem of MEA long term acquisitions, growing cells and recording their activity since the beginning of their maturation. This reduces the thermal, osmotic and mechanic shocks, which neurons are usually subjected to, and it improves data reproducibility [Gross and Schwalm, 1994]. Another strength of the system is the possibility of housing multiple MEAs inside the chamber, which guarantee parallel tests in the same controlled environment. Besides, the microfluidic device for local drug stimulation allows to work with twin networks (i.e. two identical networks grown in the same microenvironment but not functionally connected), and to stimulate selectively only one of them. Once more, this reduces the variability which characterizes experiments with different MEAs and provides, on the same device, both the treated and the control trial.

Finally, these devices may be integrated in a compact system, configuring it for syringe pump lines insertion and replacing the standard MEA with the PDMS microfluidic chamber. As Figure 7 depicts, the system would permit long-term electrophysiological and optical examination of *in vitro* brain models during selective and controlled stimulation of cell electrophysiological activity, while maintaining environmental conditions. This integrated system could have a high impact on the screening of neuroactive molecules promoting a better understanding of brain pathologies and neurodegenerative diseases. To conclude, this thesis work provides the elements which establish an integrated electrophysiological and pharmacological workstation for brain studies and can offer great advantages in central nervous system research.

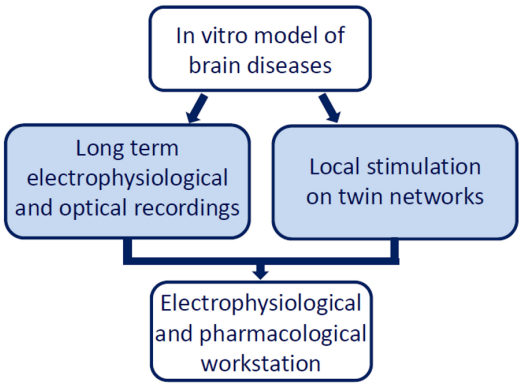

Figure 7: Hypothesis of the final integration of the developed devices.

Contents

Abbreviations

ADC:Analog-Digital Converter
AP: Action Potential
BIC: Bicuculline
BSA: Bovine Serum Albumin
CaB: Calbindin
CLB: Configurable Logic Block
CMOS: Complementary Metal-Oxide-Semiconductor
CNS: Central Nervous System
CO_2: Carbon dioxide
DIV: days *in vitro*
DSP: Digital Signal Processor
EAE: Experimental Autoimmune Encephalomyelitis
FEP: Fluorinated Ethylene-Propylene
FBS: Fetal Bovine Serum
FFT: Fast Fourier Transform
FPGA: Field Programmable Gate Array
GABA: γ-aminobutyric acid
GFAP: Glial Fibrillary Acid Protein
HBSS: Hank's Balanced Salt Solution
HEPES: 4-(2-hydroxyethyl)-1-piperazineethanesulfonic acid
IFN-γ: Interferon-γ
IL1-β: Interleukin1-β
IOB: Input/Output Block
ITO: Indium Tin Oxide
LUT: Look-Up Table
MCS: Multi Channel Systems
MEA: Micro Electrode Array
MFR: Mean Firing Rate
MOG: Myelin Oligodendrocytes Protein
MS: Multiple Sclerosis
MSN: Medium Spiny Neuron

NBM: Neurobasal Medium
NearLab: Neuroengineering and medical robotics Laboratory
OPamp: Operational Amplifier
PBS: Phosphate Buffered Saline
PCA: Principal Component Analysis
PCB: Printed Circuit Boards
PDMS: poly(dimethylsiloxane)
PGA: Programmable Gain Amplifier
PID: Proportional Integral Derivative
PMMA: Polymethylmethacrylate
P/S: Penicillin / Streptomycin
PV: Paravalbumin
RAM: Random-Access Memory
RMS: Root Mean Square
RT-PCR: Retro-Transcription Polymerase Chain Reaction
sIPSC: spontaneous Inhibitory PostsSynaptic Current
SNR: Signal-to-Noise Ratio
TTX: Tetrodotoxin
Th1: T helper 1
Tuj1: Neuron-specific class III β-tubulin
TNF-α: Tumor Necrosis Factor-α
UC: untreated culture

Chapter 1

Introduction

Diseases of the Central Nervous System (CNS) are a crucial topic in neuroscience. Among these, neurodegenerative diseases constitute a considerable portion. Neurodegenerative diseases are chronic pathologies of the CNS that cause brain functional derangement. Furthermore, they are growing in incidence due to increase in life expectancy, but still most of their causes and mechanisms are not well known. This raises the interest in studying brain alterations as well as developing and testing new molecules that could re-establish brain functionalities. Since the level of investigation is not ethical in human patients, researchers take advantage of using animal models which contribute to our understanding of disease mechanisms. The vast majority of experimental models have a genetic origin. Due to the ease of its genetic manipulation, the mouse has become the preferred system to pattern neurodegenerative diseases. Accordingly, several techniques for engineering the mouse genome, such as knock-in, conditional knockout and transgenics, can create specific gene-sequence alterations and thus manipulate the patterns of target-gene expression. Examples of neurodegenerative diseases that are investigated by means of genetic mice models are Alzheimer's disease [Chen and Zhang, 2011], Parkinson's disease [Dawson et al., 2010], Down syndrome [Bartesaghi et al., 2011], Amyotrophic Later Sclerosis [Gurney et al., 1994] and Epilepsy [Barclay and Rees, 1999]. In addition to genetic animal models, several human diseases, including Multiple Sclerosis [Brown and Sawchenko, 2007] and stroke [Durukan and Tatlisumak, 2009], are patterned on inducible experimental mouse models. In particular Multiple Sclerosis (MS), a widespread autoimmune disease of young adults, has been deeply investigated by using the experimental autoimmune encephalomyelitis (EAE) model.

Performing these researches at brain level introduces a very high degree of complexity due to the high degree of connectivity. Therefore, these studies take advantage of *in vitro* neuronal networks, which are widely used as a model for acquiring a basic understanding of network functionality. Thanks to *in vitro* studies it is possible to address directly effects of diseases and drugs at cellular and small network

level. A primary advantage of *in vitro* studies is that they offer a controlled environment which results in reduced experimental variation and assists in experimental replication. Others great advantages of tissue cultures are shortened experimental timescales and well-established experimental protocols [Polikov et al., 2008].

In vitro neuronal cultures are usually obtained by dissociating brain tissue mechanically and chemically. Then, neurons create connections and form a network. Since they have no pre-assigned tasks, they learn to interact only through their genetic program and external stimuli. It is precisely this neutrality of purpose that makes their study ideal for a precise and simple quantitative investigation of connectivity and communication processes [Eckmann et al., 2007]. Obviously, the brain does not leave the details of connection to chance. In contrast, connections are presumably determined according to functionality, with the view of enabling specific functions and processes. Therefore, the representation that *in vitro* cultures create is simplistic. However, this is not a disadvantage, but rather an opportunity to investigate capabilities of a culture and reasons which make the same neurons grown in the brain more capable [Eckmann et al., 2007].

During first weeks in culture, neurons extend many neurites, form synapses, and begin to develop spontaneous activity [Habets et al., 1987]. These activity patterns continue to develop over the course of a month *in vitro*. These changes are due to morphological changes of the neurons, as they grow, elaborate dendritic and axonal arbors and form numerous synaptic connections [Potter, 2001]. It is well-known that repeated cycles of a stimulation procedure could lead to a desired response and learning at network level. Indeed, for cultured neuronal networks, learning and development are processes that involve modulation between stimuli and responses. Specifically, either electrical stimulation [Shahaf and Marom, 2001] or pharmacological modulation [Li et al., 2007b] can be used to explore neuronal firing pattern features and development.

Since the focus lies on networks, Micro Electrode Arrays (MEAs) are valuable tools for these applications [Gross, 1979, Pine, 1980]. Indeed, they allow the investigation of learning processes and memory [Jimbo et al., 1999, Demarse et al., 2001, Segev et al., 2004, Baruchi and Ben-Jacob, 2007], of network development [van Pelt et al., 2004b, Chiappalone et al., 2006, 2007] and represent a widely recognized tool for pharmacological researches [Chiappalone et al., 2003, Morin et al., 2005, Boehler et al., 2007, Chen et al., 2008]. Recently, they have also been used to study *in vitro* models of brain malfunctions, such as epilepsy [Faingold, 2004] and neurodegeneration [Hakkoum et al., 2007].

In this perspective, it is of great interest to use MEA technology to characterize spontaneous electrophysiological activity of *in vitro* models of pathologies and to modulate it pharmacologically in order to regain a physiological network activity.

This goal gives rise to many technological challenges concerning the ability of studying the electrical activity during network maturation and of stimulating neurons locally with neuroactive molecules. Accordingly, it is required to control and maintain environmental parameters during electrophysiological tests due to the high degree of sensitivity of neuronal networks to changes in cell culture environment [Gross and Schwalm, 1994]. Indeed, instabilities in culture environment, which occur during experimental sessions, may induce electrophysiological activity changes and cell decline [Potter and DeMarse, 2001]. These issues get more crucial when the duration of the experiments is increased from hours to days. Besides, pharmacological stimulation is another crucial element. Currently, standard techniques make use of pipettes and require partial or complete change of the culture medium. Disadvantages of these protocols are the unknown kinetic of the interaction between molecules and cells and the rapid changes in the cellular environment, respectively. The latter may results in undesired neuronal response and electrode saturation. Finally, these stimulation protocols often lack of defined spatio-temporal control [Kothapalli et al., 2011] and are demanding in terms of reagents consumption and costs [Sung et al., 2010].

Aim of the work

Within this framework, this thesis aims at contributing to the aforementioned technological challenges and at improving the reproducibility and reliability of the neurophysiopathological data. In this work, the scientific importance of MEA technology in the neurodegenerative field was stressed by means of a study on EAE, the mice model of multiple sclerosis. During this project, MEAs were used, first, to deepen electrophysiological properties of cortical networks in physiological condition. Then, similar studies were performed on cultures which mimicked pathological conditions occurring in EAE. To do this, pro-inflammatory molecules were added to cell culture medium by means of standard pipettes and their effects on neuronal activity were evaluated at 12 and 24 hours after the treatment. Next, pathological neuronal activity was compared to the physiological one and was modulated by adding few neuroactive molecules. This investigation gave important results with possible outcomes for drug treatments on patients which suffer from Multiple Sclerosis. Furthermore, from a bioengineering point of view, this work allowed to settle cellular and MEA recording protocols and to arrange a group of standard algorithms for electrophysiological analysis.

During these steps, I evidenced few restrictions related to experimental equipments and techniques. First, it emerged the impossibility of recording neuronal activity continuously for many hours, because of the size of these data and the huge memory space required. This prevented from following the interaction kinetic of

pro-inflammatory molecules on neuronal functionalities. Furthermore, repeated acquisitions at 12 and 24 hours after treatments evidenced their limits since they were performed outside the incubator and this caused electrophysiological changes and cellular viability decline. Finally, drawbacks of the standard biochemical stimulation technique with pipettes came out. Indeed, it often caused neuronal response, which was uncontrolled in time and space, and electrode saturation.

For these reasons, I decided to tackle several technological challenges. First, a custom incubating chamber for neuronal growth and continuous neuronal activity recording was developed and tested. Its ability of maintaining constant environmental parameters was proved. Moreover, electrophysiological recordings were performed and limits, related to signal-to-noise ratio, were identified in the proposed approach. For this reason, a custom electronic board was further designed and a prototype was developed. Then, dedicated electronic boards for spike detection and classification were designed to handle the huge amount of data due to continuous acquisition. Indeed, when the goal lies on long term continuous recordings (as the ones performed by means of the chamber previously developed) application-specific post-processing electronics is required. Furthermore, on-line and real time analysis, optimization of memory use and data transmission rate improvement become necessary. Besides, another challenge that was tackled was related to the definition of a parameter which could characterize the effects of minimal concentrations of molecules and drugs on neuronal cells. Indeed, the identification of a single parameter able to represent the global level of network functionality still lacked in the neuropharmacological field. Thus, a cross-correlation algorithm was designed to provide a comprehensive functional evaluation of neuronal network communication properties. Afterward, challenges related to pharmacological stimulation techniques were faced. Specifically, it was developed a microfluidic device for culturing neuronal networks coupled to an array of microelectrodes for extracellular electrophysiology. Then, this device was validated for cell culturing. Furthermore, a thin wall was added in the middle of the main channel and this new configuration was used to grow two networks, which were similar but functionally uncorrelated. This resulted in reduced experimental variation. Finally, it was demonstrated the possibility of stimulate locally and selectively these twin networks.

To conclude, hese technologies, developed during my PhD, solve the problems concerning continuous and long term acquisitions and overcome the drawbacks of standard biochemical stimulation techniques.

Thesis organization

This thesis was carried on at NearLab (Bioengineering Dept, Politecnico di Milano, Milan) and it is organized in 8 chapters. After this **first chapter**, which provides a brief overview about the organization and the objectives of the work, the main chapters evolve.

The **second chapter** deals with the state of the art on *in vitro* neuronal networks, on their electrical features and on the dependency of electrophysiology on environmental characteristics. Then it describes typical data analysis methods and the standard technologies to study spontaneous and stimulated electrophysiological activity.

The **third chapter** describes a study on inhibitory transmission in striatal neurons of mice with induced EAE, and in cortical cultures, mimicking *in vitro* EAE inflammatory environment. This project was carried on in collaboration with the Neuroimmunology Unit, INSpe, Department of Neuroscience (San Raffaele Scientific Institute, Milan) and the Advanced Light and Electron Microscopy Bio-Imaging Center (San Raffaele Scientific Institute, Milan). First, it is presented an overview on EAE model and on features of this induced disease. Then, methods and results on neuronal networks, treated with a cocktail of pro-inflammatory cytokines, are described. These results represent the first methodological study on EAE carried out by means of MEAs. Finally, results obtained by other collaborators from Rome are presented and final conclusions of the work are discussed.

The **fourth chapter** describes the development and validation of a chamber that integrates incubating and recording functions. First, the state of the art about environmental chambers is investigated. Then, the chamber design and its temperature model are described. Tests to characterize performances of the system in terms of parameter stability are presented. Moreover, results of neuronal culture stainings, which were carried out to evaluate influences of the custom chamber on cell vitality, are described. Then, advantages and limits of neuronal activity recordings, which were performed inside the custom chamber, are discussed. Finally, the design of a custom pre-processing board for one MEA channel is described. This project was carried on in collaboration with the Advanced Light and Electron Microscopy Bio-Imaging Center (San Raffaele Scientific Institute, Milan) and with the Laboratory of Micro- and Bio-Fluid Dynamics (Biomechanics Research Group, Bioengineering Dept, Politecnico di Milano, Milan).

The **fifth chapter** presents the feasibility study and the design of post processing hardware for adaptive amplitude-threshold spike detection and classification. First, the state of the art about spike detection and classification method is investigated. Then, algorithm structure is described. Finally it is proposed the hardware design

for spike detection and automatic classification on Field Programmable Gate Arrays (FPGAs) and Digital Signal Processors (DSPs), respectively. The final goal is to execute on-line detection to reduce data storage problems for long term acquisitions in real-time mode.

Then, the **sixth chapter** presents the development and implementation of an intra network burst correlation analysis which aims at providing a method for the evaluation of neuronal network functionality during pharmacological modulation. In order to evaluate the sensitivity of the method, cortical cultures were processed in presence of bicuculline (BIC) and γ-aminobutyric acid (GABA), two molecules known to alter neuronal electrophysiology. Finally, it is discussed the opportunity to use this algorithm for the study of diseases and drugs able to alter network correlation properties (i.e. epilepsy, anxiety, neurodegenerative disorders) with respect to the physiological level. This project was carried on in collaboration with the Advanced Light and Electron Microscopy Bio-Imaging Center (San Raffaele Scientific Institute, Milan).

The **seventh chapter** deals with the validation of integrated microfluidic devices for long-term primary neuronal cell cultures and for spatially-controlled drug stimulation.These devices were developed by coupling a reversibly bonded PDMS microfluidic chamber with a commercial flat MEA. A single channel configuration was used to assess the neuronal viability inside this device. Results on network maturation and electrophysiology are shown. Then, a dual channel configuration was developed and twin networks, cultured in the same microenvironment but not functionally connected, were obtained. This configuration was used to stimulate these networks with tetrodotoxin (as proof of concept) in a spatially controlled manner. This project was carried on in collaboration with the Laboratory of Micro- and Bio-Fluid Dynamics (Biomechanics Research Group, Bioengineering Dept, Politecnico di Milano, Milan) and with the Advanced Light and Electron Microscopy Bio-Imaging Center (San Raffaele Scientific Institute, Milan).

Finally, a conclusive **eighth chapter** describes the benefits that the technologies developed hereby bring to the neuroscience field and discusses about the perspective of their eventual integration into one device.

Chapter 2

Background

2.1 Neurons and action potentials

The central nervous system (CNS) is composed of two kinds of specialized cells: neurons and glia. Neurons are the basic information processing structures in the CNS. Neuronal function is to receive input information from some neurons, process that information and send it as output to other neurons. Estimates indicate that there are around two hundred billion neurons in the brain and that each of these neurons is connected up to two hundred thousand other neurons. The other specialized cells are glia (or glial cells). These are the cells that maintain homeostasis, form myelin, and provide support and protection for neurons.

Briefly, a neuron consists of a cell body (or soma), an elongated projection (axon) and short branching fibers (dendrites). The soma contains the nucleus of the cell. Therefore, it is the metabolic control center and the location where most protein synthesis occurs. Axon and dendrites are processes through which signals flow to or away from the cell body. Typically, incoming signals from other neurons are received through dendrites. In contrast, the outgoing signal to other neurons flows along the axon. At the end of the axon, neurons make connections named synapses which are typically chemical synapses in the CNS. In that, axon terminals contain neurotransmitters which are the chemical messenger through which signals flow from one neuron to the next ones [Guyton and Hall, 2011].

Neuronal signals are called action potentials. An action potential is an electrical signal which occurs because ions move across neuronal membrane. Normally, the membrane potential of a neuron rests as $-70\,mV$. A transitory alteration of the membrane potential is caused by the acceptance and release of ions across the cell membrane through dedicated channels. This causes changes in the number of ions in the extracellular environment, and thus in the local charge density. Particularly, when the membrane potential becomes more positive and reaches a threshold value

the cell depolarizes rapidly, causing an action potential, followed by a repolarization back to baseline. Finally, the signal propagates along the axon until it reaches its axon terminals where communication with other neurons is achieved at synapses [Jones et al., 2011].

2.2 *In vitro* electrophysiology

Nowadays, nervous tissue can be cultured *in vitro* and kept alive for several months, while preserving their properties [Shahaf and Marom, 2001, Marom and Eytan, 2005]. Cultured neuronal networks can be either *ex vivo* animal brain slices or *in vitro* formed networks, composed of dissociated animal neurons. Particularly, dissociated neuronal cultures have the advantage of allowing the study of structural and functional evolution of a network in time and space [Morin et al., 2006]. In the field of *in vitro* dissociated neuronal cultures, there are two principal methods by which neuronal electrical activity can be measured: intracellular and extracellular. Intracellular electrophysiological activity of a cell is detected by patch clamp. Patch clamp devices feature an electrode that is inserted into the cell, and a second electrode that is sealed to a small region of the cell membrane. Thanks to this configuration, they measure the flux of ions across the membrane. Goals of patch clamp technique are mainly the study of single ion-channel currents and the investigation of related changes in cell membrane potentials. The advantage and interest of the patch clamp technique is that it allows to carry out accurate measurements of voltage changes in up to twelve neurons at the same time. On the other hand, it is highly invasive and time consuming [Eckmann et al., 2007, Jones et al., 2011].

In contrast, external micro-transducers are used to measure extracellular electrophysiological activity, which occurs outside the cell membrane [Morefield et al., 2000, Pancrazio et al., 2003, van Pelt et al., 2004b, Jones et al., 2011]. Micro-transducers measure the concentration of ions in their vicinity, which changes according to the activity of the cell. Indeed, upon the occurrence of an action potential, ions (mostly sodium and potassium ions) travel across the cell membrane in and out of the cell. This generates an electric field which can be recorded by means of metal microelectrodes [Gross, 1979, Pine, 1980, Heuschkel et al., 2002, Stett et al., 2003].

Additional methods that indirectly indicate the voltage change of a cell include optical measurements using voltage-sensitive or fluorescent dyes [Chien and Pine, 1991, Grinvald et al., 1982, Baker et al., 2005]. The principle of the technique is simple. The preparation is stained with a physiological solution containing voltage-sensitive dyes which bind externally to the neuronal membrane. These dye molecules serve as molecular transducers which transform changes in membrane potential into optical signals.

Aforementioned techniques are limited in measuring activity of many neurons with high spatial and temporal resolution [Thakur et al., 2007, Jones et al., 2011]. In contrast, one of the central concepts of contemporary neuroscience is that major brain functions are executed through the joint actions of neurons [Berdondini et al., 2009a]. Therefore, it is desirable to have the capability of measuring the behavior of many cells simultaneously. This level of analysis is very important because it has become clear that individual elements of information are encoded not by single cells, but rather by a population of cells [Nicolelis and Ribeiro, 2002]. However, the interplay between single cells and large population cell assemblies is still largely unknown [Engel et al., 2001]. In order to bridge the gap between single or few cell electrophysiology and neuronal population electrophysiology [Nicolelis and Ribeiro, 2002], new technologies are needed [Jones et al., 2011]. In this context microelectrode arrays (MEAs) represent a valuable and more suitable experimental tool.

2.2.1 Micro Electrode Arrays (MEAs)

MEAs are matrices of planar metallic electrodes and allow to record extracellular activity of neuronal preparations from multiple sites simultaneously in a non-destructive manner [Gross, 1979, Pine, 1980, Gross et al., 1982, Perelman and Ginosar, 2007]. From a practical point of view, MEA recordings offer many advantages. Indeed, they give a precise measurement of the electric signal with high temporal resolution, they do not need of micro-manipulators for electrode placement and they are less sensitive to mechanical vibrations than glass electrodes. Furthermore, they can be used several times when adequately cleaned after each recording session.

Several geometries are commercially available [MEA-Manual, 2010]. For *in vitro* research, most used MEAs are planar MEAs (pMEAs) in which passive electrodes are integrated on planar transparent glass substrates [Gross, 1979, Pine, 1980]. Standard planar MEAs have 60 microelectrodes (10-100 μm) arranged in a 8 x 8 squared layout grid with no corners (Figure 2.1). Microelectrodes are generally made of gold and often covered with platinum black to lower their impedance. Other materials that present a high nanoporosity are also used, such as titanium nitride (TiN) [Morin et al., 2005]. In particular, this material meets the challenge of manufacturing very small electrodes and at the same time keeping the impedance and the noise level down [MEA-Manual, 2010]. Interconnects are often made of indium-tin oxide, which is transparent and thus enables direct observation of the cells with an inverted microscope [Morin et al., 2005].

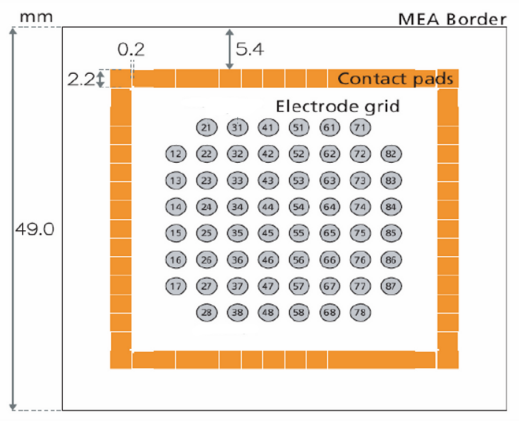

Figure 2.1: Electrode layout and sizes (adapted from [MEA-Manual, 2010]).

2.2.1.1 Cell-electrode interaction

When recording signals from cells cultured on MEA surface, those signals depend on the interaction between cells and electrodes. Figure 2.2 shows a cell body which covers partially the electrode surface. The free electrode area is in contact with the external saline and connected to ground. Therefore, the recorded potential is the sum of the potentials at the surface of the free electrode and the surface of the electrode covered by the membrane. Neglecting the low resistance R_b of the bath solution, the relation between the voltage at the contact pad V_{pad} and the voltage in the cleft between cell membrane and the electrode V_J is given by Equation 2.1:

$$\frac{V_{pad}}{V_J} = \frac{C_{JE}}{C_{FE} + C_{sh}} \approx \frac{a_{JE}}{a_{FE}} \tag{2.1}$$

where C_{JE} is the capacity of the covered electrode area of size A_{JE}, C_{FE} the capacity of the entire electrode area of size A_{FE}, and C_{sh} is the shunt capacity of the connecting lane (with $C_{sh} << C_{FE}$). Therefore, amplitude of the recorded signal depends linearly on the ratio of the covered electrode area and the entire electrode area [Fejtl et al., 2006].

2.2.1.2 Advantages

The first key feature of MEAs is the possibility of recording the activity of large neuronal networks in a non-invasive manner. Extracellular recordings through embedded electrodes, like those of MEAs, cause no effects on cultured cells, thus long-term monitoring of the activity can be achieved [Jimbo et al., 2006, Jones et al., 2011]. Furthermore, a MEA is a bi-directional interface between a network and a computer [Berdondini et al., 2009a]. Indeed, cells cultured on a MEA can be stimulated by electrical voltage or current injected through the electrodes. High temporal resolution of the recordings is another strength of this technology. Time resolution

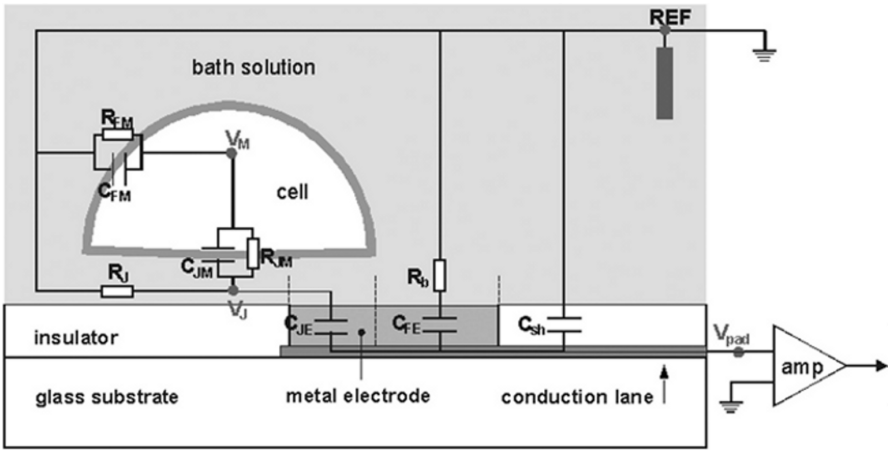

Figure 2.2: Extracellular recording of single-cell activity with planar electrodes (adapted from [Fejtl et al., 2006]).

is practically limited only by the sampling rate of the data acquisition system (50 kHz sampling has already been achieved). Finally, MEAs demonstrated to be suitable for integration with micro-structures for network patterning [Berdondini et al., 2006] and with microfluidics [Krause et al., 2006, Rowe et al., 2007, Dworak and Wheeler, 2009].

2.2.1.3 Limits

Low spatial resolution constitutes the major drawback of MEA technology. Indeed, the number of recording sites is limited because of the random distribution of cellular networks and the necessity of a good cell-electrode coupling [Berdondini et al., 2005]. A second disadvantage is that a single electrode may record signals from several neurons due to microelectrode size. As a result, the signal of each neuron has to be identified and sorted [Morin et al., 2005]. Therefore, it is difficult to establish a direct link between function and structure. Finally, the lack of selectivity of electrical stimulation is another important disadvantage [Ghezzi et al., 2008].

2.2.1.4 Applications

The aforementioned limits do not prevent MEAs from being considered standard tools in the field of drug discovery and basic research. Indeed, they offer a simple approach to examine the activities of neuronal cells on a large scale and provide an insight into the dynamics of *in vitro* networks. Accordingly, they allow the investigation of learning processes and memory [Jimbo et al., 1999, Demarse et al., 2001, Segev et al., 2004, Baruchi and Ben-Jacob, 2007], of network development [van Pelt et al., 2004b, Chiappalone et al., 2006, 2007] and of regulation of neuronal excitability [van Pelt et al., 2005]. Furthermore, they represent a widely recognized tool for pharmacological investigations [Chiappalone et al., 2003, Morin et al., 2005, Boehler

et al., 2007, Chen et al., 2008] and for neurotoxicology [Novellino et al., 2011]. Recently, they have also been used to study *in vitro* models of brain malfunctions, such as epilepsy [Faingold, 2004] and neurodegeneration [Hakkoum et al., 2007].

To conclude, MEA technology shows high impact on neuroscience field. Moreover, its relevance is underlined by the spread of commercial systems for spontaneous activity recordings and cell electrical stimulation (Multi Channel Systems GmbH, German; Panasonic Inc, Japan; Plexon Inc, USA).

2.3 Electrical signal features

Neurons *in vitro* spontaneously connect each other and maintain electrophysiological features typical of the brain [Brewer, 1997]. Their electrical activity is basically characterized by single action potentials whose onset mechanism was described in Section 2.1, and whose detection is influenced by cell-electrode interaction (see Section 2.2.1.1). Usually, frequency content of extracellular action potentials ranges from 500 Hz to 5 kHz [Bai and Wise, 2001, Pancrazio et al., 2003, Perelman and Ginosar, 2006, Rolston et al., 2009]. Furthermore, mature culture activity show high-frequency sequences of action potentials, called bursts. Generally, a consistent bursting activity is observed after 18 to 25 days *in vitro* [Gross and Kowalski, 1991]. During these episodes, neurons experience a rapid, transient (a few hundred milliseconds) increase of their firing rate, followed by a period of quiescence [Morin et al., 2005]. This periodic bursting represents a relatively simple and stable mode of activity in networks of neurons. Furthermore, it was found that periodic bursts are not controlled by specific pacemaker cells but rather are produced by spatial and temporal summation of a continuous random background of synaptic inputs. Finally, the frequency of spontaneous periodic bursting seems to be determined by the degree of connectivity of the network, and by the balance between the level of distributed excitation and recovery processes [Maeda et al., 1995].

Besides, when such episodes are synchronized and involve many recording channels, they are called network bursts (or network spikes) [Maeda et al., 1995, Eytan and Marom, 2006, Wagenaar et al., 2006b, O'Donovan, 1999]. Usually the generation of burst excitation in a part of the network is followed by propagation over the whole network. Since burst occur on many active electrodes, multiple regions in the network can act as the source of network bursts. Furthermore, neuronal interactions within connected networks become especially apparent during these periods of synchronized firing. In developing neurons in culture, such synchronized bursts occur spontaneously [van Pelt et al., 2005]. Moreover, their frequency is determined not only by the probability of burst generation but also by the probability of successful propagation over the network. These factors vary with the number of synapses per

cell, the synaptic density and maturation, the degree of process extension, and the cell excitability. When the probability of burst propagation is low there are only isolated action potentials. Such activity is typical of immature cultures. Then, during the second and third week, network bursts increase in number, length and frequency [van Pelt et al., 2005, Wagenaar et al., 2006b]. Furthermore, neuron recruitment follows an exponential process with a propagation velocity that is determined by the degree of connectivity [Eytan and Marom, 2006]. Gradual but significant changes of this recruitment were thus observed during network development [van Pelt et al., 2005].

During these events, many neurons cooperate through mutual interaction and build up these dynamic modes of network firing. The intense neuronal interaction during these network bursts is expected to provide special conditions for effectuating activity dependent mechanisms. Indeed, synchronous network activity was already implicated in synaptic transmission efficacy, learning and memory [van Pelt et al., 2005]. Furthermore, the same type of synchronized firing appears to occur *in vivo* in rat hippocampus [Buzsáki et al., 1992] and it was observed to be involved in plasticity of neuronal connections in both the rat hippocampus *in vivo* [Buzsáki et al., 1992] and in cultured cortical networks [Maeda et al., 1995].

2.4 Standard algorithms for signal analysis

There are no definitive theory of signal transduction available to interpret or predict signals recorded with MEAs [Morin et al., 2005]. Indeed, many parameters remain difficult to quantify and control in the course of standard experiments, such as the cell-electrode distances, the electrode area covered by the cell and the nature and density of ion channels in the cell membrane. Therefore, signals recorded with MEAs usually present strong variations from one electrode to another in terms of amplitude and waveform. As a result, most of the information available from these signals is contained in their time stamps. Time stamps series are obtained through spike detection, a process which discriminates spikes from background noise of an extracellular recording. Furthermore, since each electrode records signals coming from more than one neuron, spikes can be assigned to individual neurons. This process is called spike sorting.

Mathematically, a spike train (ST) is defined as follows (Equation 2.2):

$$ST(t) = \sum_{s=1}^{N_{spikes}} \delta(t - t_s) \tag{2.2}$$

where t_s is the timing of a spike, N_{spikes} is the number of recognized spikes and $\delta(t)$ is the Kronecker delta function [Bologna et al., 2010].

Spike detection of neuronal action potentials can be performed using supervised methods [Chandra and Optican, 1997, Lewicki, 1998] or using unsupervised ones [Watkins et al., 2004, Chan et al., 2008]. The simplest and most widely used unsupervised technique for spike detection is amplitude thresholding. This detects events when the signal crosses a user-specified amplitude threshold, which can be set manually by visual inspection or automatically [Guillory and Normann, 1999, Wagenaar et al., 2005]. Other methods involve principal components [Daffertshofer et al., 2004] and Haar transform [Yang and Shamma, 1988]. A more exhaustive analysis about spike detection methods can be found in Section 5.1. There, sorting methods are also discussed.

Before proceeding with further analysis, it is important to take into consideration the issue of stationarity. Therefore, signals have to be split in shorter spike trains which conserve it. Once spikes have been identified, the easiest and most direct way to characterize the level of activity of a cell is computing its firing rate. Dealing with MEAs, firing rate is computed for each active channel and then it is usually averaged among all of them, which results in the Mean Firing Rate (MFR) of the network [Bologna et al., 2010].

As aforementioned (Section 2.3), spontaneous bursting is observed in a wide range of *in vitro* neuronal preparations. Generally, a burst consists of a fast sequence of spikes with duration equal to the sum of inter-spike intervals (ISIs) within the burst itself and separated, from the following one, by an interval (Inter Burst Interval, IBI) relatively long compared to the burst duration. Accordingly, a burst train BT(t) of M bursts can be identified as in Equation 2.3:

$$BT(t) = \sum_{m-1}^{M} \Pi(\frac{t - t_m}{\tau_m}) \tag{2.3}$$

where τ_m is the burst duration and $\Pi(\frac{t}{\tau})$ is a rectangular function, centered at $t = 0$. Over the last ten years, different methodologies for burst definition and detection were developed [Tam, 2002, van Pelt et al., 2004b, Chiappalone et al., 2005, Selinger et al., 2007, Gourévitch and Eggermont, 2007, Sun et al., 2010, Bologna et al., 2010, Tokdar et al., 2010, Pasquale et al., 2010]. Particularly, a classical method requires to analyze the spike train using a shifting time window, sized as the minimum expected IBI. Then a threshold value of the maximum ISI (maxISI) within a burst is fixed. Furthermore, it is also established the minimum number of consecutive spikes belonging to a burst (minSpikes). Therefore, spike bursts are defined as sequences of spikes with ISI, each one smaller than the maxISI, and containing at least a number of spikes equal to minSpikes. Finally, spike bursts are represented as rectangular functions (as in Equation 2.3) with amplitude equal to the spike rate

within the burst [Chiappalone et al., 2005].

In Section 2.3, network bursts were also described. Few algorithms were implemented for the identification of these synchronized bursting events [van Pelt et al., 2004a,b, 2005, Pasquale et al., 2010]. A widely used method is based on the observation that both firing rates at individual sites and active site number increase during network bursts [van Pelt et al., 2004a, 2005]. Briefly, this method calculates the product of the number of active sites and the total number of spikes at these sites within 25 ms bins. This product is similar to the total spike number in case of uncorrelated firing. In contrast, during network bursts this product raises. The time point at which the product within a network burst has its maximal value is the time center of a network burst [van Pelt et al., 2005, Chiappalone et al., 2005].

After data analysis, descriptors of the electrophysiology can be extracted. Standard descriptors are [Chiappalone et al., 2005, Novellino et al., 2011]:

- *Number of spikes* summed over all the active channels within bins or in the whole spike train,

- *Network MFR* ($spikes/s$), summed over all the active channels,

- *Number of bursts* detected in the network within bins or in the whole spike train,

- *Mean bursting rate* ($bursts/min$),

- *Number of spikes in burst*,

- *Mean burst length* (s),

- *IBI* (s),

- *Spikes in burst/total spikes*,

- *Number of network bursts* detected in the network within bins or in the whole spike train,

- *Mean network bursting rate* ($bursts/min$),

- *Mean network burst length* (s).

Finally, more complex neuronal data analysis can be performed, such as cross-correlation and information theory [Garofalo et al., 2009, Bologna et al., 2010], spike pattern classification methods [Shadlen and Newsome, 1998, Brown et al., 2004], likelihood methods [Chornoboy et al., 1988], frequency-domain methods and neuronal spike train decoding [Brown et al., 2004].

2.5 Dependency of electrical signal on environmental parameters

Neuronal cultures require specific and controlled environmental features. Particularly, they mature and survive at 37°C, with a controlled pH at 7.4 and with a rela-

tive humidity close to 100% [Brewer, 1997]. Generally, the longevity and functional availability of cell cultures are mainly limited by contamination with pathogens, non-optimal medium composition and mechanical stress. Furthermore, fluctuations in temperature, pH or osmolality can lead to senescence or cell apoptosis [Blau et al., 2009]. Cell cultures grown in standard dishes are usually exposed to rather drastic changes in their microenvironment as soon as the door of the incubator is opened. Obviously, these phenomena are stressed during optical monitoring or electrophysiological sessions, which occur outside the incubator. Moreover, even when experiment duration is limited, these environmental changes are damaging since they can induce variations and instabilities in network electrophysiological activity.

2.5.1 Temperature

Changes in temperature produce marked changes in electrical behavior of excitable cells [Joyner, 1981], even if temperature variations within certain limits do not affect cellular viability [Pearce et al., 2005]. It was demonstrated by means of patch clamp that decreasing the temperature down to 15°C increases the membrane resistance. This means that membrane potential hyperpolarizes on decreasing temperature. Furthermore, low temperatures provoke a decrease in neurotransmitter release and a block of action potential transmission. Accordingly, it was observed that both synaptic activity and spontaneous bursting activity also decreases at low temperature [Forsythe and Coates, 1988]. Finally, it was proved that high temperatures are more dangerous than low ones and that changes in synaptic responses are reversible below 43°C [Fujii et al., 2002].

2.5.2 Medium acidity

Acidity of culture medium is a crucial parameter for neuron survival. Neural cell cultures are healthy when maintained at physiological pH, around 7.4. For this reason, most culture methods employ a buffering system similar to that found in blood, in which there is an equilibrium between dissolved CO_2 (bicarbonate anion) and a well-regulated 5% CO_2 atmosphere in the incubator. When brought into room atmosphere (0.05% CO_2), bicarbonate leaves the medium as gaseous CO_2 and the pH drifts. Particularly, when pH reaches values around 7.5, it effects cell physiology and thus limits neuronal activity recordings. Indeed, these can last only 10 minutes without experiencing detrimental pH drift in CO_2-buffered media (Figure 2.3). Finally, if the CO_2 balance is not re-establish, pH drift up to 8.5, a lethal alkaline value, in about one hour [Potter and DeMarse, 2001].

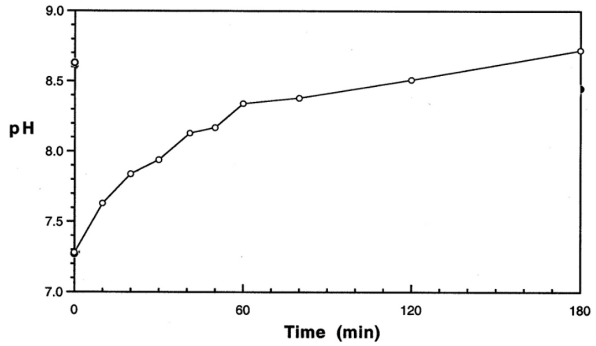

Figure 2.3: Values off medium pH of cultures maintained on a lab bench in room air (adapted from [Potter and DeMarse, 2001]).

2.5.3 Osmolality

Studies have shown that reduction of water evaporation and stabilization of osmolality has beneficial effects on the longevity of neurons in culture [Potter and DeMarse, 2001, Blau et al., 2009]. Standard culture chambers have problems with evaporation of water from the medium. This results in hyperosmotic conditions that are responsible for the slow death of many neuronal cultures after a few weeks [Potter and DeMarse, 2001]. Indeed, it was measured that osmolality of the medium increased 10.5 mOsm/day in a humidified incubator. Furthermore, it was proved that a rise of 50 mOsm is lethal to neuronal cultures [Potter and DeMarse, 2001] and that hyperosmotic stress influences the expression of genes in many cells [Arimochi and Morita, 2005]. Concerning direct effects on signaling, high osmolality might cause voltage changes in amplitude or time course. Furthermore, it was demonstrated that it affects uptake of γ-aminobutyric acid (GABA), which is the major inhibitory neurotransmitter in the CNS [Olsen et al., 2005].

To conclude, changes in neuronal electrical activity due to variations in temperature, medium acidity and osmolality can be traced back to a unique mechanism, which is the imbalance in medium salt-content. Indeed, as discussed in Section 2.1, each neuron has a concentration gradient of ions across its membrane that creates an electrochemical potential difference [Jones et al., 2011]. Therefore, modifications in ion concentrations induce changes in membrane potential and thus in neuronal excitability. Hence, the aforementioned environmental changes act exactly in this manner. Accordingly, temperature oscillations can induce variation in salt solubility [Forsythe and Coates, 1988], pH increase causes a reduction in proton number as well as hyperosmolality, due to water-content evaporation, provokes an increase in salt concentration. These changes have effect on neuronal activity in about thirty minutes and provoke cell culture decline in less than two hours [Potter and DeMarse, 2001].

2.6 Features and limits of standard techniques

Keeping neuronal networks in long-term culture is a desirable but challenging task [Blau et al., 2009]. As aforementioned (see Section 2.5), both cell viability and electrical activity depend on environmental features. Furthermore, mechanical perturbations due to culture movements, medium changes and drug stimulations, can affect activity patterns. Therefore, electrophysiological sessions and pharmacological experiments can typically provoke instability in neuronal spontaneous activity and decrease in cell vitality.

2.6.1 MEA recording setup

A widely used commercial system for electrophysiological multisite recordings is the MEA60 system. It was originally introduced in 1996 by Multi Channel Systems (MCS GmbH). The 60-channel amplifier (x 1200, 12-bit resolution, bandwidth 0.02 Hz - 8.5 kHz) and electronic circuitries are organized into three compact housings. This ensures optimal signal-to-noise ratio of the recording and results in an overall low noise level of the complete amplifier chain smaller than noise level of a MEA TiN electrode. Therefore, single unit activity can be readily detected [Fejtl et al., 2006]. Furthermore, the data acquisition card allows the simultaneous sampling of up to 128 channels at a sampling rate of 50 kHz per channel. Besides, MEA amplifiers have an integrated heating system for controlling MEA temperature during electrophysiological experiments [MEA1060-Manual, 2011]. In contrast, activity is perturbed by culture transfer from incubator to the recording equipment. Furthermore, MEA chips are maintained in room atmosphere (0.05% CO_2) which provokes drift of pH values [Potter and DeMarse, 2001, Lin et al., 2010]. Finally, the difference between MEA surface temperature (heated up by the heating system) and air temperature causes evaporation and thus hyperosmolality. Therefore, electrophysiological sessions in room air are limited to approximately 120 minutes [Potter and DeMarse, 2001].

2.6.2 Drug stimulation techniques

Important results in neurobiology were obtained thanks to pharmacological neuronal activity modulation. Indeed, drug stimulation of neuronal network grown on MEAs allowed investigating the nervous system [Jimbo et al., 2000, Boehler et al., 2007, Chiappalone et al., 2003]. Furthermore, it was possible to use this platform in toxicology and for neuroactive substance identification [Morin et al., 2005, Novellino et al., 2011].

Standard techniques for adding certain concentration of molecules to the culture

medium make use of graduated pipettes. Specifically, it is possible to distinguish two protocols: the partial change and the complete change of culture medium. The former method is characterized by the suction of a part (usually half) of the medium. Then, this part is replaced with the same amount of medium mixed with a 2 x concentrated drug to reach a final and desired concentration [Boehler et al., 2007]. The first source of error is that the molecule has a concentration value based on the estimation of the total volume inside the culturing well. This problem is enhanced by medium water-content evaporation which occurs inside incubators. Furthermore, this method has the huge disadvantage that the kinetic of interaction between the molecule and the cells is unknown. In addition, it could induce a concentration gradient and the consequent premature inactivation of channels under study.

The second technique requires the complete suction of the medium and its complete replacement with fresh 1 x concentrated drug in medium. Strength points of this approach are the exact knowledge of drug concentration and the absence of gradients. In contrast, rapid changes in the chemical environment and shear stress which can occur during the instant medium replacement, usually provoke electrode saturation and neuronal spiking response, respectively.

In addition to those drawbacks, these standard protocols make drug testing a demanding process in terms of cost [Sung et al., 2010] and prevent from obtaining sharp temporal and spatial controls during pharmacological stimulation [Kothapalli et al., 2011].

Chapter 3

Study of GABA transmission in Th1-treated neuronal cultures [1]

Multiple sclerosis (MS) is a chronic debilitating disease generally thought to be immune mediated, which involves a polygenic predisposition and is worsen by environmental toxicity [Brown and Sawchenko, 2007]. It is characterized by demyelination, that underlies potentially reversible neuronal dysfunction early in disease, and by neurodegeneration, which results in permanent neurological deficits [Bjartmar et al., 2003]. Although neurodegeneration is traditionally viewed as occurring late in the course of MS, recent evidence supports an early onset of progressive neuronal loss [Bjartmar et al., 2003]. To clarify these mechanisms, it is usually studied an animal model of neurodegeneration called experimental autoimmune encephalomyelitis (EAE) model. Analysis of disease progression on this model suggested similarities between induced EAE and MS which may be indicative of a similar etiology. Additionally, subsequent neurodegeneration affecting multiple brain levels is consistent with typical signs in MS patients and is suggestive of common bases in neuropathology. Therefore, characterization of inflammatory events in EAE might provide insights into strategies to prevent disease progression in patients [Brown and Sawchenko, 2007].

This chapter deals with the the investigation of the effects of inflammatory events on γ-Aminobutyric acid (GABA) signaling. Specifically, possible changes were evaluated in EAE mice and in neuronal cultures, which were treated to mimic typical inflammatory milieu of active neuro-inflammation. Particularly, I worked on the *in vitro* part in collaboration with the Neuroimmunology Unit, INSpe, Department of Neuroscience (San Raffaele Scientific Institute, Milan) and with the Advanced Light

[1] The work has been published as Rossi S, Muzio L, De Chiara V, Grasselli G, Musella A, Musumeci G, Mandolesi G, De Ceglia R, Maida S, **Biffi E**, Pedrocchi A, Menegon A, Bernardi G, Furlan R, Martino G, Centonze D. Impaired striatal GABA transmission in experimental autoimmune encephalomyelitis. *Brain Behav Immun*, 2011, 25(5):947-56.

and Electron Microscopy Bio-Imaging Center (San Raffaele Scientific Institute, Milan). This study was based on the increasing evidence that a functional interaction existed between pro-inflammatory molecules and synaptic strength [Beattie et al., 2002, Stellwagen and Malenka, 2006, Zhang et al., 2008]. Therefore, the aim was to determine whether such inflammatory signals can alter complex network functions including communication and integrative properties. Concerning the *ex vivo* study, it was mainly investigated by the Neuroimmunology Unit, INSpe, Department of Neuroscience (San Raffaele Scientific Institute, Milan), the Neuroscience Department (Università Tor Vergata, Rome) and the CERC (Fondazione Santa Lucia, Rome). They carried on an investigation on striatal slices obtained from brains of EAE mice. In this chapter, first the state of the art on the EAE model and on its electrophysiological features is briefly described. Then, methods and results on Multi Electrode Array (MEA) recordings of *in vitro* inflamed neuronal networks are presented. Finally, results from our collaborators in Rome are briefly described before discussing about the high impact of this multicenter work.

3.1 The EAE model: state of the art.

This model was born in the early 1930s, when Rivers observed that normal brain extracts from rabbits injected into macaques caused acute Central Nervous System (CNS) disease with immune cell infiltration and demyelinating lesions [Rivers et al., 1933, Rivers and Schwentker, 1935]. Substantial progresses in reproducing the pathology and clinical course of MS in EAE followed the identification of myelin oligodendrocytes protein (MOG) which is generally deliver to mice by subcutaneous injection. MOG and in particular its specific peptide MOG_{35-55}, is considered the only CNS autoantigen known to induce both an encephalitogenic T-cell response and a demyelinating autoantibody response in EAE [Lebar et al., 1986]. This combination acts to reproduce the complex range of pathological and clinical MS phenotypes. Particularly, MOG_{35-55}-EAE mice develop a chronic progressive demyelinating non remitting EAE which evolves in a manner consistent with an ascending myelopathy [von Büdingen et al., 2001, 2006]. The T cell response plays a critical role in the initial stage of the MOG_{35-55}-EAE disease since it is required to initiate CNS inflammation [Iglesias et al., 2001]. Indeed, only after its activation MOG_{35-55} specific antibodies can penetrate into the CNS and bind to the myelin surface. Moreover, T cell-mediated response also recruits and activates phagocytes (macrophages and microglia) within the CNS, which provides the progress of demyelination [Mendel et al., 1995].

Therefore, inflammation and the subsequent neurodegeneration are hallmarks of the EAE pathogenesis. Local immune response, resulted from infiltrating blood

derived cells, i.e. T helper 1 (Th1) lymphocytes, is characterized by a broad spectrum of pro-inflammatory cytokines. These act on oligodendrocytes, astrocytes, resident microglia and neurons and thus elicit CNS derangement. Indeed, the complex inflammatory milieu secreted by these cells spreads through the CNS. Thus, it is possible that some detrimental effects occurring to the neuronal component may arise from a direct interaction between these cues and neurons. Indeed, neurons express on their cell surface chemokine and cytokine receptors and it is reasonable to think that once these receptors are engaged they can modulate neuronal functions [Stellwagen et al., 2005].

Specifically, Interferon-γ (IFN-γ), Tumor Necrosis Factor-α (TNF-α) and Interleukin1-β (IL1-β) represent key molecules of adaptive immunity and are secreted by Th1 cells infiltrating CNS of both EAE and MS active lesions. In addition, these pro-inflammatory molecules can also alter neuronal functioning. Indeed, TNF-α enhances synaptic efficacy of cultured neurons [Beattie et al., 2002], IL1-β increases neuronal excitability [Zhang et al., 2008] and IFN-γ causes long term modifications of synaptic activity and neuronal damages [Vikman et al., 2001, Mizuno et al., 2008].

Glutamate and GABA are, respectively, the main excitatory and inhibitory neurotransmitters in the CNS, whose activities are normally balanced in neurons. To date, glutamate transmission has been studied in neurophysiological investigations in EAE mice [Centonze et al., 2009]. This evidenced that inflammation and abnormal expression of glutamate receptors promote synaptic degeneration and dendritic spine loss. In contrast, possible changes of GABA signaling in this model of MS have been inferred on the basis of biochemical [Gottesfeld et al., 1976], molecular [Wang et al., 2008], and morphological studies [Ziehn et al., 2010], but never addressed through direct recordings of synaptic activity.

Finally, both glutamatergic and GABAergic synaptic activity can be studied in the striatum by means of whole-cell patch clamp recordings from single neurons in slices. The striatum is a sub-cortical gray matter structure whose activity is finely regulated by both glutamate and GABA inputs [Fisone et al., 2007, Tepper et al., 2007]. It is highly sensitive to the neurodegenerative process associated with MS [Henry et al., 2008, Tao et al., 2009, Ceccarelli et al., 2010], and undergoes complex alterations of glutamate transmission and dendritic damage during EAE [Centonze et al., 2009]. Importantly, these synaptic alterations occur in the absence of overt demyelinating lesions, and even before the appearance of the EAE-associated neurological deficits, indicating that they are not a mere consequence of axonal damage [Centonze et al., 2009].

To conclude, up to now there is no electrophysiological evidence concerning the alteration of inhibitory transmission in the brain of EAE mice. Therefore, it would be important to assess whether pro-inflammatoy molecules can trigger alterations

of synaptic inhibition occurring in these models, and to explore further synaptic mechanisms which possibly contribute to neuronal damage occurring during neuro-inflammation.

3.2 Methods

3.2.1 Cell cultures

Primary neuronal cell cultures were obtained from CD1 mice. Mice were sacrificed by inhalation of CO_2, and E17.5 embryos were removed immediately by cesarean section. Brains were carefully dissected in cold Hank's Balanced Salt Solution (HBSS, Gibco) supplemented with glucose 0.6% and 5 mM HEPES pH 7.4 (Sigma). The cerebral cortices of embryos were rapidly removed, chopped with a fine scissor and subsequently mechanically dissociated in single cells by using fire-polished Pasteur pipettes. Then, cells were re-suspended in culture medium containing 50% D-MEM (Gibco); 50% Ham's F12 (Gibco); 5 mM HEPES pH 7.4; 0.6% glucose; 1% Glutamax (Invitrogen); 30 nM Na-Selenite (Sigma); 20 nM Progesterone (Sigma); 60 nM Putrescine (Sigma); 100 μg/ml Transferine (Sigma) and 5 μM Insulin (Sigma). No antimitotic and antibiotic drugs were added to cultures. Neurons were plated onto poly-lysine (2 mg/ml; Sigma) and laminin (10 μg/ml; Sigma) coated 60-electrode MEAs (Multi Channel Systems, MCS, GmbH) at a final density of 700 cells/mm^2 per chip. Cells were also plated on dishes for immunofluorescence and retro-transcription polymerase chain reaction (RT-PCR) experiments at the concentration of 400 cells/mm^2. Finally, both MEAs and dishes were incubated in a humidified 5% CO_2 atmosphere at 37°C.

3.2.2 Immunofluorescence

Neuronal cultures at 12 days *in vitro* (DIV) were fixed in paraformaldehyde 4% for 5 minutes, washed three times in Phosphate Buffered Saline (PBS) 1x, then blocked in PBS 1x, Fetal Bovine Serum (FBS) 10%, Bovine Serum Albumin (BSA) 1 mg/ml for 1 hour. Primary antibodies were applied in the same buffer overnight at 4°C. The next day, slides were washed three times in PBS 1x before applying Alexafluor conjugated secondary antibodies. Nuclei were stained with Hoechst-33342 (1:10000, Invitrogen). The following primary antibodies were used: mouse anti-Tubulin β-III (Tuj1, 1:1000, Millipore); Rabbit anti-Calbindin (CaB, 1:500, Swant); rabbit-anti-(glial fibrillary acid protein) (GFAP, 1:2000, Dako). These are a tubulin neuronal marker, a GABAergic marker and an astrocyte marker, respectively. Images were acquired with a Leica TCR SP5 confocal imaging system (Leica Microsystem, Germany) and labeled cells were manually counted.

3.2.3 MEA recordings and cytokine treatments

Extracellular 5 minute recordings of neuronal activity at 12 DIV were made by using a MEA1060 signal amplification and data acquisitions system (Multi Channel Systems, MCS GmbH). The signals collected from the microelectrodes were amplified 1100x, digitalized at 25 kHz and subsequently processed off-line. Spikes were detected using MCRack Software (MCS GmbH): the threshold was set, for each channel, to seven times the standard deviation of average noise amplitude computed at the beginning of each measurement. Each culture was recorded at time zero (t0), then randomized MEAs were treated either with a cocktail of pro-inflammatory cytokines or with a vehicle. Pro-inflammatory cocktail contained: 20 ng/ml IFN-γ (Peprotec) [Butovsky et al., 2006]; 100 ng/ml IL1-β (Euroclone) [Zhang et al., 2008] and 100 ng/ml TNF-α (Peprotec) [Beattie et al., 2002], which mimicked the typical EAE inflammatory milieu. Then, their activity was recorded after 12 (t12) and 24 h (t24). Control MEAs received saline as sham treatment. Then, some cultures were treated with increasing amount of GABA (in μM: 0.01, 0.1, 0.3, 1, 3, 10 and 100; Sigma) and subsequently recorded.

3.2.4 Algorithms for MEA data analysis

The off-line standard analysis was implemented in Matlab (The Mathworks, Natick, USA) as described in Section 2.4. The median number of active channels and the total number of spikes were extracted for each culture. Successively, a burst analysis was implemented as described in the literature [Chiappalone et al., 2005, 2006]. Specifically, bursts were detected when the minimum number of spikes was equal to 10 and the maximum Inter Spike Interval (ISI) was 100 ms. Finally, network bursts were identified when the product of the number of active channels and the number of spikes, evaluated in 25 ms bins, was bigger than 9 [van Pelt et al., 2005, Chiappalone et al., 2005] using a minimum Inter Network Burst Interval (INBI) of 100 ms. These algorithms allow to extract many standard descriptors of the neuronal electrophysiological activity. However, in this work only few of them were considered. Specifically, the median number of burst, the burst duration and the percentage of active channels which displayed burst activity were evaluated. Furthermore, the network activity was assessed by means of network burst length.

Statistical analysis on these data was performed using non-parametric tests. Specifically, a Wilcoxon matched pair test was developed for paired data analysis (inside groups) and a Mann-Whitney test was performed between treated and untreated cultures at 24 hours. For GABA concentration-response curves, a non-linear regression was used to fit data in a variable slope sigmoidal model. The goodness-of-fit was assessed using the Coefficient of Determination R^2. The significance was

established at $p < 0.05$.

3.2.5 RT-PCR

The expression levels of parvalbumin (PV), a calcium-binding protein which is present in GABAergic interneurons, were examined both in Th1- and sham-treated cell cultures at 12 and 24 hours after the treatment ($n = 3$ for each group). Neurons were collected as previously reported [Muzio et al., 2010]. Briefly, total RNA was extracted from neuronal cultures ($n = 3$ independent cultures for each group) by using RNeasy Mini Kit (Qiagen). The LightCycler R480 System (Roche) and SYBRR GreencJumpStart™ Taq ReadyMix™ (Sigma) were used together with adequate PV and Histone H3 primers [Rossi et al., 2011]. Each RNA extract was normalized on the expression of the housekeeping gene Histone H3.

3.3 Results

Primary neuronal cultures were characterized for the presence of GABAergic neurons (Figure 3.1A) and glial cells (Figure 3.1B) by immunofluorescence images at 12 DIV. 13% (±5.13) of plated cells expressed the GABAergic marker CaB (Figure 3.1C, black bar, $n = 3$) and GFAP expression was observed on 7.04% (±2.24) of total plated cells (Figure 3.1C, white bar, $n = 3$). Then, possible stable alterations induced by inflammatory cues were investigated. Pro-inflammatory cytokines did not affect the median number of active electrodes in treated and control networks (Figure 3.1D, $n = 14$), as well as the total number of spikes recorded in each group (Figure 3.1E, $n = 14$). The percentage of active electrodes that displayed bursting activity and the median number of bursts were not altered in the presence of pro-inflammatory milieu (Figure 3.1F and 3.1G, $n = 9$). Also duration of bursts did not show differences between treated and control groups (Figure 3.1H, $n = 9$). In contrast, pro-inflammatory cytokines significantly increased the network burst length, that was approximately doubled in cultures treated for 24 hours with Th1 cytokines (Figure 3.1I, $n = 14$, $p < 0.01$ inside groups, $p < 0.05$ between treated and untreated cell cultures at 24 hours).

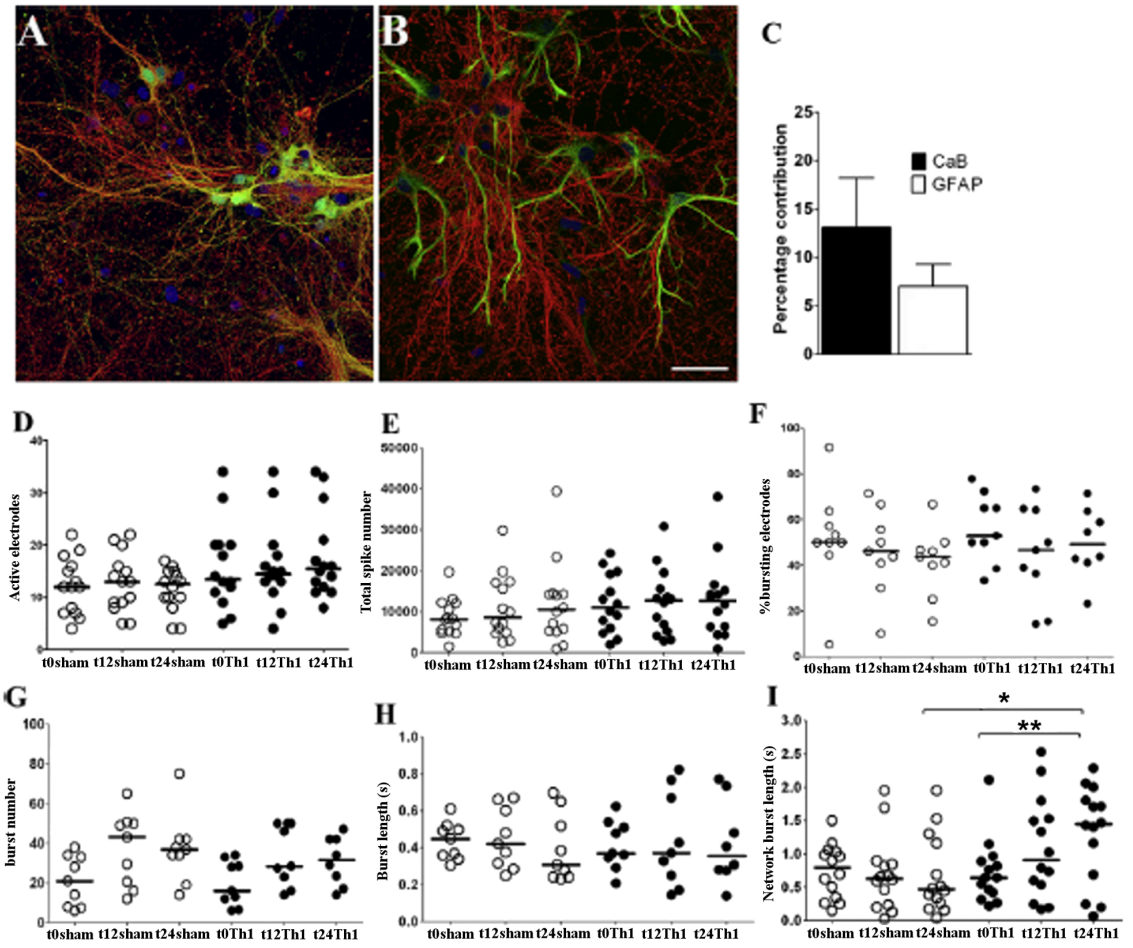

Figure 3.1: Effect of pro-inflammatory cytokines on neuronal network homeostasis. Immunofluorescence of 12 DIV primary neuronal cultures for (A) Tuj1 (red) and CaB (green) and (B) Tuj1 (red) and GFAP (green). Scale bar: 50 μm. (C) Percentages of CaB and GFAP expressing cells over total cell number. (D-I) Single experiments (solid circles: Th1-treated cell cultures; dashed circles: sham-treated cell cultures) and median values (lines) before the treatment (1st time point, t0) and after 12 and 24 hours (2nd and 3rd time points, t12 and t24) for the following parameters: (D) active electrodes, (E) total spike number, (F) percentages of electrodes displaying burst activity, (G) burst number per electrode, (H) burst length and (I) network burst length. Significant differences were only identified in the network burst length: Wilcoxon test (inside Th1-treated group) showed differences between the 1st and the 3rd time point. Mann-Whitney test (between untreated and Th1-treated group) showed differences after 24 hour treatments.

In normal circumstances, network bursts are sensitive to synaptic connectivity and are involved in plasticity [Maeda et al., 1998]. Since this parameter might be modulated by GABAergic signaling, it was studied whether the alteration elicited by Th1 cues depends on alteration of GABAergic signaling. Therefore, cultures were subsequently treated with increasing amount of GABA, which normally causes a significant reduction of recorded spikes (as verified in Figure 3.2A). GABA addition on Th1-treated cultures induced a dramatic reduction of network burst length

which became comparable to those of control neuronal cultures after 10 μM GABA treatment (Figure 3.2B, $p < 0.05$ between treated and untreated cell cultures after 0.3 μM GABA treatment).

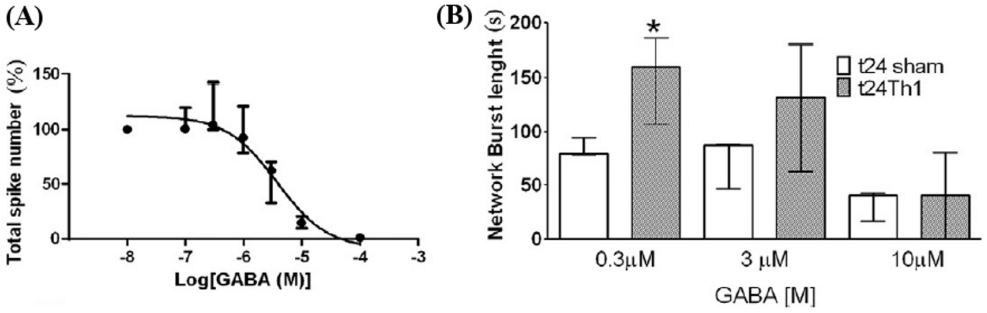

Figure 3.2: (A) Total spike number of untreated networks after the addition of increasing concentration of GABA. $R^2 = 0.8872$ and EC_{50} (95% confidence) comprised between 1.8 and 7.8 μM. (K) Network burst length of sham-treated (white bars) and Th1-treated (gray bars) cultures, after GABA increasing additions. Mann-Whitney test evidenced $p < 0.05$ between treated and untreated cell cultures after 0.3 μM GABA treatment, while it identified no differences after 10 μM GABA treatment.

Finally, the treatment with pro-inflammatory cytokines significantly reduced the expression levels of PV after 12 and 24 hours. Figure 3.3 shows the RT-PCR results about Histone H3 primers (top) and PV primers (bottom) at time zero ($T0_{sh}$) and after the cytokine treatment ($T12_{Th1}$ and $T24_{Th1}$)

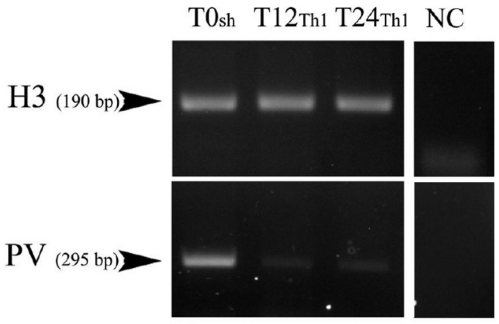

Figure 3.3: Significant reduction of the expression levels of PV after 12 and 24 hours the cytokine addition. RT-PCR results about Histone H3 primers (top) and PV primers (bottom) at time zero ($T0_{sh}$) and after the cytokines treatment ($T12_{Th1}$ and $T24_{Th1}$). NC is the negative control.

3.4 Brief overview on *ex vivo* results

Spontaneous inhibitory postsynaptic currents (sIPSCs) were measured in striatal slices as an indicator of the physiological activity of GABA signaling. Electrophysiological recordings showed a reduction of sIPSCs recorded from striatal pro-

jection neurons of mice with MOG_{35-55}-induced EAE compared to control mice. GABAergic sIPSC deficits started in the acute phase of the disease (20–25 days post immunization, dpi; $n = 18$; $p < 0.01$ for frequency), and were exacerbated at later (chronic) time-points (35, 50, 70 and 90 dpi; $n \geq 10$ for each time point and experimental group; $p < 0.01$ for both frequency and amplitude).

Acute (3 hours) incubation of striatal slices from control mice with activated BV2 immortalized microglia failed to affect sIPSC frequency and amplitude ($n = 12$; $p > 0.05$ for both parameters). Accordingly, acute incubation of striatal slices with TNF-α (3 hours) also caused negligible effects on both frequency and amplitude of sIPSCs ($n = 10$; $p > 0.05$ for both parameters). These data indicated that acute treatments with pro-inflammatory molecules released by microglia can not alter GABA transmission.

Furthermore, in this study the differential involvement of GABA inputs to Medium Spiny Neurons (MSNs) in EAE was investigated. MSNs are the principal striatal neurons and they receive GABA inputs by axon collaterals from MSNs themselves and by GABAergic interneurons. This two inputs differentially influence the activity of MSNs. Particularly, inhibition from GABAergic interneurons predominantly targets MSN somatic regions and these contacts give rise to sIPSCs of higher amplitude than contacts to distant dendrites [Koos et al., 2004]. Since EAE preferentially reduced sIPSCs of high amplitude, it resulted that sIPSC inhibition likely involved synaptic inputs arising from GABAergic interneurons. Furthermore, sIPSC inhibition was associated with a selective loss of striatal parvalbumin (PV)-positive GABAergic interneurons. Specifically, PV+ interneurons were significantly reduced in EAE mice (at 20 dpi) down to 74% of the controls (EAE = 24.6 neurons/ mm^2; control = 33.5 neurons/mm^2; $p < 0.001$), accordingly with RT-PCR data obtained on *in vitro* cultures. These immunohistochemical data were confirmed by western blots of the PV expression levels in the striatum of both pre-symptomatic and acute EAE mice.

3.5 Discussion

Previous studies have postulated impaired GABA transmission in MS and in EAE. GABA is reduced in the cerebrospinal fluid of MS subjects [Qureshi and Baig, 1988], and protein and mRNA expressions of the GABA transporter-1 (GAT-1) are dramatically decreased in the spinal cord of EAE mice [Wang et al., 2008]. Furthermore, potentiation of GABA signaling significantly ameliorates EAE clinical course, through a mechanism likely involving a direct neuroprotective effect and an inhibitory action both on antigen-presenting cells and on the resulting inflammatory response [Bhat et al., 2010].

The present study is the first combined neurophysiological and morphological investigation of inhibitory transmission in the brain of EAE mice and in network of neurons. These data demonstrate irreversible alterations of GABA transmission in the striatum of EAE mice, providing further evidence that gray matter structures of the nervous system undergo profound rearrangements of synaptic transmission during immune-mediated attack of the central myelin. Exacerbated glutamate-mediated transmission had been previously reported in EAE striata, in the absence of overt demyelinating foci, but in association with microglial activation and TNF-α release [Centonze et al., 2009]. However, the mechanisms at the basis of enhanced glutamate and reduced GABA transmission do not seem to overlap and the kinetic of glutamate transmission up-regulation and GABA down-regulation were different during EAE. In fact, glutamate transmission hyperfunctioning was evident in the pre-symptomatic and acute phases (when the activation of resident microglia was maximal), while GABAergic hypofunctioning was especially marked in the chronic phases of the disease (when microglial cells return to the resting state [Centonze et al., 2009]).

In this work, it was showed that a cocktail of pro-inflammatory cytokines can perturb the GABAergic system *in vitro*, when chronically administered for 24 hours. In line with this evidence, it was impossible to replicate the neurophysiological abnormalities of GABAergic sIPSCs following short incubation of striatal slices with either activated BV2 microglia or TNF-α. Altogether, these data suggest that chronic stimulation of neuronal networks, that is possible *in vitro* by using neuronal cultures, determines profound alteration of GABA transmission. Based on these considerations, it is conceivable that microglia and pro-inflammatory molecules, released by microglia, contribute to alter GABAergic transmission in the intact brain during EAE. These results are in agreement with other reports which show that prolonged treatments with TNF-α induce severe derangement of neuronal morphology by altering the dendritic branching [Neumann et al., 2002] and perturbing spatial learning [Aloe et al., 1999, Golan et al., 2004].

These data might suggest different neuroprotective strategies in the early and late stages of MS. Indeed, the unbalance towards neuronal excitation, which characterizes the entire course of EAE since its pre-symptomatic phase, likely primes excitotoxic damage by increasing neuronal vulnerability to MS-specific mitochondrial dysfunction [Vyshkina et al., 2005], or to the neurotoxic effects of inflammation [Xiong and McNamara, 2002, Zhu et al., 2003].

Furthermore, data presented in this chapter seem to indicate that the feedback and feed-forward GABAergic control over striatal output is differentially affected in EAE, because sIPSCs of larger amplitude were predominantly reduced in these mice, as expected for a preferential involvement of inhibitory interneuronal activity [Ben-

nett and Bolam, 1994, Kubota and Kawaguchi, 2000, Koos et al., 2004, Gustafson et al., 2006]. In line with this hypothesis, the total number of striatal neurons, largely composed of projection MSNs [Kawaguchi et al., 1995, Wilson and Kawaguchi, 1996, Tepper et al., 2004], is not reduced in EAE [Centonze et al., 2009], while it was found that GABAergic interneurons (PV-positive) are markedly underrepresented in the striatum. Indeed, a significant reduction in the number of PV-positive striatal cells accompanied impaired GABA signaling seen in electrophysiological, morphological and western blot experiments. Furthermore, PV expression was also severely reduced in neuronal cultures treated with of pro-inflammatory cytokines. These data point to GABAergic interneurons as the primary cell-type population compromised by EAE, and are in good agreement with previous findings showing selective loss of PV interneurons, and reduced extension of PV-positive neurites in the normal appearing gray matter and in the motor cortex of MS patients [Dutta et al., 2006, Clements et al., 2008]. Defective GABAergic transmission within the motor cortex has also been postulated in MS patients on the basis of neurophysiological findings with paired-pulse transcranial magnetic stimulation [Caramia et al., 2004]. Furthermore, loss of PV-positive interneurons was also observed in the hippocampus of EAE mice, in association with significant defects of hippocampus-related memory abilities [Ziehn et al., 2010]. Finally, the reasons of the selective susceptibility of PV interneurons to degenerate in MS and in EAE has to be further investigated. The evidence, however, that cytokines signaling, *per se*, is able to alter GABAergic transmission and consequently circuit functioning, as demonstrated by *in vitro* experiments, gives additional interest to the possibility that this mechanism is at the base of late stages of MS pathogenesis. The general GABAergic down-regulation induced by cytokines chronic treatment that emerges from this study, is of impulse for the search of drugs able to control this alteration. Furthermore, the *in vitro* model of cortical neurons treatment with cytokines and the paradigm for GABAergic alteration study could turn to be helpful for future drug screening studies.

In conclusion, the results of the present investigation indicate defective GABA transmission in a reliable mouse model of MS and in neuronal networks *in vitro*, and suggest that pharmacological agents potentiating GABA signaling might be considered an alternative valuable therapeutic option to limit neuronal damage in MS patients.

Chapter 4

Development of a chamber for long term MEA recordings[1]

Spontaneously active neuronal networks show a high degree of sensitivity to slight changes in the physical and chemical environment of cell cultures [Gross and Schwalm, 1994] (see Section 2.5). For these reasons, the ability of controlling and maintaining the environmental parameters during optical and electrophysiological measurements is an important requirement in the experimental design. Particularly, applications involving Micro Electrode Arrays (MEAs) [Gross, 1979, Pine, 1980, Morin et al., 2005, Johnstone et al., 2010] suffer from some limits imposed by the standard experimental equipment. This is usually composed of an incubator, where cell cultures are grown, and of the freestanding electronics for neuronal activity recording. Thus, during experimental sessions, the MEA chip has to be moved from the incubator to the recording stage and this may induce changes in the temperature, contamination of the cellular environment and mechanical disturbances. Moreover, the content of CO_2 in the environmental air, lower than the peculiar percentage of an incubator, rapidly results in elevation of the cell culture medium pH, even accentuated by the medium evaporation effect, which may also induce hyperosmolarity. These issues get worse when the duration of the experiments increases from hours to days, which is the time extent required in order to study network functional plasticity [Shahaf and Marom, 2001, Chiappalone et al., 2008], long-term neuronal network phenomena [van Pelt et al., 2004a,b, Hofmann and Bading, 2006] and chronic treatment effects [Morefield et al., 2000, Xiang et al., 2008, Howell et al., 2011]. The shortcomings of the aforementioned setup cause a gradual decline in the health of these cell cultures and a decrease of data reproducibility, for which the environmental stability is critical [Gross and Schwalm, 1994]. Accordingly, the insertion of instruments,

[1] A journal paper on this work has been submitted to *Biotechnology and Bioengineering* as **Biffi E**, Regalia G, Ghezzi D, Menegon A, De Ceglia R, Ferrigno G, Fiore GB, Pedrocchi A. A novel environmental chamber for long term neuronal network multisite recordings.

which are used during the experiments (e.g. a microscope), inside a standard incubator avoids cell culture contamination and mechanical stress [Slocum et al., 2000]. In contrast, this method significantly reduces physical accessibility to those instruments and thus, it requires remote controls and handling tools [Petronis et al., 2006]. Therefore, miniaturized cell culture incubators, which can be integrated with sensors to control environmental parameters, are a convenient solution for long term experiments.

This chapter deals with the technological development of a novel environmental chamber which measures the electrical activity of neuronal networks grown on MEAs. First, the state of the art about environmental chambers is investigated. Then, the chamber design and its temperature model are described. Tests to characterize performances of the system in terms of heating control and CO_2 flow rate are presented. Moreover, results of neuronal culture stainings, which were carried out to evaluate influences of the custom chamber on the cell vitality, are described. Finally, advantages and limits of neuronal activity recordings, which were performed inside the chamber, are discussed and the design of a custom single-channel preprocessing board is presented. The project was carried out in collaboration with the Laboratory of Micro- and Bio-Fluid Dynamics (Biomechanics Research Group, Bioengineering Dept, Politecnico di Milano, Milan) and with the Advanced Light and Electron Microscopy Bio-Imaging Center (San Raffaele Scientific Institute, Milan).

4.1 Environmental chambers for long term experiments: state of the art.

Prototypes of environmental chambers appeared in the 1950s [Christiansen et al., 1953, Rose, 1967, Sykes and Moore, 1959] and during the '80s several systems improving cell survival were developed. Temperature controlled bath chambers were designed to provide an accurate and uniform heating during live cell imaging [Heidemann et al., 2003, Ho et al., 2005] and patch clamp experiments [Forsythe and Coates, 1988, Toyotomi and Momose, 1989], which is required because of the temperature dependence of neuronal properties (Section 2.5). The temperature required for cell growth is usually maintained by a heated airstream or water flow directed inside or around the chamber [Lanzaro et al., 2005], or by integrated electric heaters, which consist of indium tin oxide (ITO) thin films [Toyotomi and Momose, 1989], or Peltier elements [Forsythe and Coates, 1988, Picard et al., 2010]. Particularly, Forsythe and Coates developed an open round chamber for electrophysiological studies on acutely dissociated neurons. The chamber temperature was controlled by a Peltier driven heat exchanger, which warmed up the dish surface. A similar chamber was devel-

oped by Toyotomi and collaborators. In their device, a transparent conducting film of ITO was the heating element, which was used both to heat directly the bath chamber and to preheat the perfusion solution. The system showed an accuracy in temperature control equal to ±0.8°C. Then, these heating elements were optimized by other groups and allowed to reach accuracy values lower than ±0.2°C, which are typical values for standard incubators [Petronis et al., 2006, Vukasinovic et al., 2009, Picard et al., 2010]. Meanwhile, devices to control the gaseous environment and to improve bicarbonate-carbon dioxide buffer system aiming at pH maintenance were also proposed [Fantini et al., 1987, Bavister, 1988, Vukasinovic et al., 2009]. Some authors controlled the gaseous environment by filling a cell culture chamber with a gas mixture and sealing it [Mohler et al., 1987, Morrison et al., 2000]. However, these systems were stable only for few days. Other groups used a continuous air flow to maintain a suitable CO_2 concentration [Fantini et al., 1987, Bavister, 1988]. Recently, Ho and collaborators developed a micro-chamber independent from a standard incubator, that was able to perform imaging experiments for up to twenty days [Ho et al., 2005]. The system consisted of a closed mini chamber and an ITO thin film that provided the heating. A perfusion pump and a gas pump were used for cell culture medium deliver and for humid 5% CO_2 air supply, respectively.

In the aforementioned systems, the humidity level hardly reached high values, which caused medium evaporation. For this reason, medium-filled closed chambers were considered as a good option [Gross and Schwalm, 1994, Petronis et al., 2006]. In these systems, a physiological pH was maintained by the perfusion of cell culture medium previously enriched of CO_2. A disadvantage of these chambers was the frequent presence of air bubbles that can damage cells [Gross and Schwalm, 1994]. To avoid gas perfusion and the consequent formation of bubbles, other researchers enriched the medium with Hepes, a buffering agent that helps in maintaining physiological pH despite changes in CO_2 concentration [Lin et al., 2010]. However, Hepes is phototoxic [Potter and DeMarse, 2001] and can alter neuronal network dynamics at high concentration [Gross and Schwalm, 1994]. The importance of these environmental chambers is underlined by the availability of similar commercial systems that maintain temperature, pH and humidity during long term optical experiments, independently from a standard incubator (Microscope Incubator, Cambridge Analytical Instruments; POC-R2 Chamber System, Pencon; CO_2 microscope stage incubator, Okolab srl; CSMI Chambered Slide Micro-Incubator, Harvard Apparatus).

Many efforts were also done to improve the reliability of Multi Electrode Array (MEA) recordings. Over the last years, few groups have developed devices to limit osmotic changes and medium acidification during neuronal activity recording with the standard setup [Potter and DeMarse, 2001, Blau et al., 2009]. Others have introduced recording and perfusion equipments inside an incubator [Potter and DeMarse,

2001, Mukai et al., 2003]. Finally, few groups have coupled small flow chambers to MEA chips [Gross and Schwalm, 1994, Blau and Ziegler, 2001, Pancrazio et al., 2003]. The first prototype of a culturing device for MEA experiments was described by Gross and Schwalm [Gross and Schwalm, 1994]. This medium-filled closed chamber housed a matrix of 64 ITO microelectrodes and it was completely transparent for microscope observation. The heating of the chamber was assured by resistive elements and a peristaltic pump guaranteed the medium circulation. The medium was previously mixed to a 10% CO_2 airflow, which preserved a physiological pH. This prototype allowed to monitor the neuronal activity for eight days. Its main disadvantages concerned flow discontinuities and accumulation over the recording matrix of bubbles, which could damage cells and obstruct imaging experiments. Moreover, this system did not allow modular assembling and, thus, parallel electrophysiological measurements. Then, a similar perfusion chamber was developed by Blau and Ziegler [Blau and Ziegler, 2001]. The temperature of the chamber was controlled by a feedback loop made of a temperature sensor and a controller, which provided the heating current back to an ITO resistive layer. The medium flow was maintained constant through the chamber by a miniaturized peristaltic pump. A drawback of this system was the use of 20 mM Hepes for pH stabilization [Gross and Schwalm, 1994, Potter and DeMarse, 2001]. Other disadvantages were the difficulty of maintaining a stable environment because of the chamber small size, and the dependency of cell survival on perfusion parameters. In the same year, Potter and DeMarse described a culture dish lid made of fluorinated ethylene-propylene (FEP), a transparent hydrophobic membrane, which was selectively permeable to O_2 and CO_2, and relatively impermeable to water vapor. This sealing membrane was able to prevent infections, hyperosmolarity and to limit pH increase in room air [Potter and DeMarse, 2001]. This was beneficial for electrophysiological sessions, since it allowed recording for 30 minutes, before the upward drift of pH affects cell physiology ([Potter and DeMarse, 2001], Section 2.5). Moreover, the evaporation decrease allowed to introduce the standard MEA recording equipment inside a dry incubator. Indeed, the electronics of the recording systems would have been quickly damaged by a standard humid incubator with a moisture content higher than 65% [Hales et al., 2010]. The main disadvantage of this integrated device was the requirement of a dedicated incubator for each cell culture. A similar lid was described by Blau and collaborators [Blau et al., 2009]. Their poly(dimethylsiloxane) (PDMS) lid performed better in reducing evaporation than FEP membranes. Therefore, they obtained a higher viability of cultured cells and significantly longer survival *in vitro*. However, they could not perform continuous recordings of neuronal activity. In contrast, Mukai and collaborators described a system which coupled an incubator with a perfusion equipment for medium changes and a recording setup for electrical signal acquisition

[Mukai et al., 2003]. Their system recorded 150 s of neuronal activity every thirty minutes and allowed monitoring neuronal networks for one month. Disadvantages of this method concerned the reduced accessibility for cell culture optical monitoring, the necessity of a dedicated incubator and the system encumbrance. Finally, in the same year, Pancrazio and collaborators described a small perfusion chamber that incorporated a microelectrode array and low noise amplifier and filter boards [Pancrazio et al., 2003]. Its main advantage was the portability that is a suitable feature for autonomous culturing and recording systems. In contrast, its main drawback was the fluidic system configuration which did not accommodate more than one neuronal network.

Hence, compactness is another important requirement for multi-channel recording systems [Charvet et al., 2010]. To achieve portability, it is useful to develop compact electronic circuits for extracellular neuronal signal recordings. In the literature, electronic systems for *in vitro* neuronal signal multi-channel amplification and filtering have been proposed [Obeid et al., 2004, Rolston et al., 2009]. The common goal was to replace cumbersome commercial acquisition systems and thus to realize multiple modular printed circuit boards (PCBs) with discrete components. Rolston and co-workers [Rolston et al., 2009] designed a front-end board composed of four 15.2 x 8.9 cm PCBs, each one dedicated to 16 MEA channels. Obeid and collaborators [Obeid et al., 2004] proposed a similar system, which also included a multiplexing system to reduce connection number to the following analog-to-digital converter. Besides, active and passive components were integrated in the same substrate realized by means of Complementary Metal-Oxide-Semiconductor (CMOS) technology, to further reduce board dimensions [Bai and Wise, 2001, Mohseni and Najafi, 2004, Dabrowski et al., 2004, Olsson et al., 2005, Borghi et al., 2007, Frey et al., 2009, Charvet et al., 2010]. Indeed, CMOS technology allowed the integration of a large number of channels and enabled high quality electrical recordings. For example, Charvet and collaborators [Charvet et al., 2010] realized 64 recording and stimulation channels embedded in a 2.4 x 11.2 mm chip and created a compact system by locating four of these chips on a culture platform. In spite of the clear advantage provided by miniaturization capability, CMOS technology requires specialized machinery and thus it is difficult and expensive to replicate the systems by other laboratories [Rolston et al., 2009].

Therefore, so far there are no integrated and compact devices able to grow neuronal cultures since the beginning of their maturation for a long period and to provide long term multichannel recordings while controlling all the environmental parameters at the same time without the need of an external cumbersome incubator.

4.2 Methods

4.2.1 System design

The device described here has to exhibit the following requirements: 1) temperature control, 2) humidity maintenance, 3) pH stabilization, 4) sterility preservation, 5) optical transparency, 6) external accesses for medium change and pharmacological stimulation, 7) integrated acquisition card to acquire neuronal signals. Furthermore, the incubating chamber was designed to be suitable for cell monitoring on an inverted microscope.

A schematic representation of the chamber and the whole system is shown in Figure 4.1. The chamber is formed by an outer and an inner box, which are separated by a cavity filled with water (Figure 4.1A) and covered by a top plate. The size of the outer box is 180 mm x 180 mm, with a height of 45 mm. The inner box, leant on the outer one by means of four small backings, is formed by a 150 mm x 150 mm base with a height equal to 30 mm; a 50 x 50 mm MEA housing is provided inside. A silicone membrane is located between the top plate and the boxes beneath, to guarantee the sealing of the closure, which is provided by means of eight small Rolez clamps. Proper openings for medium and pharmacological agents addition are designed into the top, assuring sterility with pierce silicone membranes for needles insertion. Moreover, joins for air inlet and outlet are provided as shown in Figure 4.1A. The chamber heating is obtained by means of a circulating bath (E306, Ecoline, Lauda GmbH) which pumps water in the space surrounding the inner box of the incubating chamber by means of two metal joins (Figure 4.1B and 4.1C). A PT100 thermo-resistance is inserted in a reference well, filled with water, through a sealed opening in the top plate. The probe provides the feedback loop for the temperature. The MEA housing and the reference well are designed symmetrically to guarantee a better temperature control (Figure 4.1A). To maintain the pH of the medium in a physiological range (7.4), it is used a gas cylinder containing 20% O_2, 70% N_2 and 10% CO_2. A percentage of humidity higher than 95% is maintained using a commercial bubbling module (Okolab s.r.l., Italy), which enhances the air moisture-content before introducing it into the chamber through the top plate. In order to prevent condensation, a tubing structure connected to the warming bath is placed over the top plate (Figure 4.1C). Gold pins for electrical signal acquisition are located inside the chamber, in contact with MEA pads. The signal is carried outside to an external custom board (76 mm x 115 mm) placed on the top plate (Figure 4.1B), which arranges signals in a single 68-pin socket that matches the standard Multi Channel Systems cable (MCS GmbH). The electrical connection between gold pins and the external circuitry is allowed by means of three connectors, which pass through the top of the chamber. For this purpose, three openings were designed with

Pro-Engineer Wildfire, manufactured using subtractive rapid prototyping (Roland Modela MDX-40) and sealed by means of a silicone glue (Elastosil E43, Wacker Chemie AG). The same milling machine was used to realize openings for the introduction of inverted microscope objectives beneath both the MEA housing and the reference well. The chamber is made of polymethylmethacrylate (PMMA) plates, glued by means of an acrylic adhesive. This material was selected due to its optical transparency. The whole system can be sterilized with Ultra Violet rays or with Ethylene Oxide (EtO).

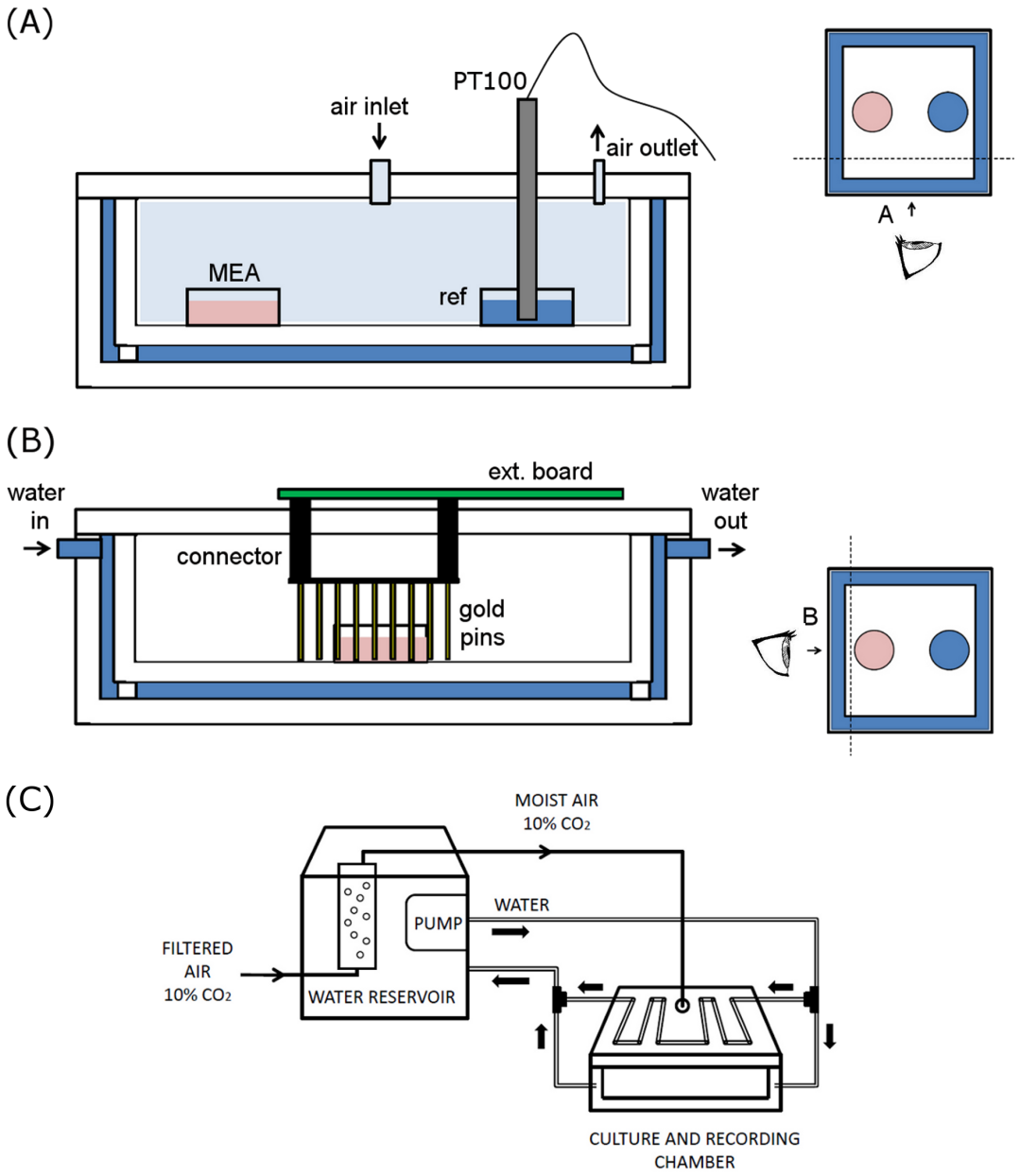

Figure 4.1: (A) and (B) are schematic illustrations of two different sections of the chamber. Simple schemes that represent the point of observation of the two pictures on the left are illustrated on the right. (C) Configuration of the whole system.

4.2.2 Lumped parameters thermal model

A lumped parameter thermal model was realized to confirm the goodness of the chamber design and to choose (1) the wall thickness of inner and outer boxes and (2) the controller characteristics. The electrical circuit that represents the "analogue model" of the system is shown in Figure 4.2A. Features of each block are condensed in one resistor and one capacitor, whose values are determined by its size and material (Figure 4.2A, dashed box). Accordingly, the MEA and the reference well are modeled with the same components due to their symmetry. Then, the transfer function between the temperature of the water (*Th2o*), forced by the current generator Q, and the temperature inside the medium (*Tm*) was computed. This block was introduced into the model of the whole system, designed in Matlab (Simulink). The input is composed by a ramp block, whose slope models the experimental heating curve of the commercial bath, and a saturation block limited to 37, which is the temperature set point. The chamber is described by the transfer function block, which is connected to the Proportional Integral controller (PI). A saturation block, whose lower limit is equal to 20 (i.e. the average environmental temperature), is interposed between them. This simulates the circulating thermostat controller which does not have the cooling function (Figure 4.2B).

4.2.3 Temperature tests and pH stabilization

The system (described in Section 4.2.1) was tested in terms of temperature profile and gas flow rate, crucial for the cell culture medium pH preservation. Concerning the temperature, the time to reach the set point (37°C), the overshoot peak and the amplitude of the oscillations around 37°C were evaluated. The experiments were performed with the following protocol: 3 ml room-temperature water were inserted into the reference well, the PT100 probe was placed in it and the chamber was closed. After connecting a computer to the bath, the pump for water circulation was switched on and bath and PT100 temperature values were acquired and visualized with Wintherm® Plus software (Lauda GmbH). Concerning the flow control, a flow meter (60 ml/min - 600 ml/min, Platon NG series, CT Platon SaS) was interposed between the air cylinder and the bubbling module. The flow meter full scale range was chosen accordingly to typical value for commercial gas mixer (DGTC02BX, Okolab srl). The flow was initially set to 400 ml/min. This value is an average of flow values used for both commercial (CO_2 microscope stage incubator, Okolab srl, Lanzaro et al., 2005) and custom-made [Wright, 1964] incubators, normalized on the chamber volume. Tests to determine the flow value able to maintain the pH in a physiological range (7.4) were then performed. Ten Petri dishes filled with medium (2 ml) were kept half in the chamber and half inside a standard incubator. The air

flow in the chamber was varied around 400 ml/min from 60 ml/min to 600 ml/min. Each flow value was maintained for 24 hours; after this period, the pH of the medium kept inside the chamber or in the standard incubator was measured by a Beckman 350 pH meter (Beckman Coulter S.p.A). Besides, during all the experiments, changes in pH values were evaluated by monitoring phenol red, a wide used pH indicator, contained in the cell culture medium. Finally, to monitor the pressure that the chamber was subjected to, a pressure gauge was connected before the air inlet into the chamber.

4.2.4 Substrate preparation

Two different types of surfaces were used as substrate for cell plating: round glass coverslips (diameter 24 mm) and standard 60 electrodes MEA biochips (electrode spacing 200 μm, electrode diameter 30 μm; Multi Channel Systems, MCS GmbH, Reutlingen, Germany). All the used reagents and materials were provided by Invitrogen, if it is not differently specified.

Coverslips were bathed 12 hours in HNO_3, thoroughly cleaned in MilliQ water and autoclaved. After the sterilization procedure, each coverslip was located in a small Petri dish, treated with poly-L-lysine (1 mg/ml, Sigma-Aldrich) in 100 mM borate buffer pH 8.5 and placed overnight in a humidified incubator at 37°C. Then, coverslips were carefully rinsed with sterile Phosphate Buffered Saline (PBS) to remove residues and finally incubated overnight with plating medium (Neurobasal medium (NBM) supplemented with 10% Fetal bovine serum (FBS; Lonza) and 1% Penicillin / Streptomycin (P / S)) the day before the dissection.

MEA biochips were sterilized by means of an overnight treatment in oven at 110°C and filled with plating medium 4 hours to increase their hydrophilicity. Afterward, they were treated overnight with poly-L-lysine (2 mg/ml) in a humidified incubator. After careful washings in PBS, MEAs were filled and incubated with plating medium (NBM, 10% FBS, 1% P / S).

4.2.5 Neuronal culture preparation

Primary neuronal cultures were obtained from CD1 mice at E17.5. Hippocampi were extracted, rinsed with Hank's Balanced Salt Solution (HBSS) and treated with Trypsin (0.25%; Sigma-Aldrich) for 15 minutes at 37°C. Then, cells were resuspended in plating medium (NBM, 10% FBS, 1% P / S) and mechanically dissociated using glass pipettes. Dissociated cells were plated at 200 cells/mm^2 and 800 cells/mm^2 for each coverslip and MEA, respectively. To allow cell adhesion, they were incubated for 4 hours in a humidified incubator at 37°C; successively, the plating medium was replaced with the cell culture medium (NBM, B-27 1x, 1% P / S,

Glutamax 1 mM and 10 mM Hepes pH 7.4 (Lonza)), 2 ml for each coverslip, 1 ml for each MEA. The 30% of the total amount of medium was changed the first day after plating and every 2 days until the end of the experiments. Neuronal cultures were split in two equal groups. One group was grown and maintained in a humidified incubator, while the other in the custom chamber, previously sterilized, up to 21 days *in vitro* (DIV).

4.2.6 Immunostainings

14 DIV neuronal cultures were fixed for 5 minutes in 4% paraformaldehyde, 4% sucrose, phosphate buffer 120 mM at pH 7.4 and 37°C. Cells were rinsed in PBS 1X three times after fixing. Non-specific sites were blocked and cells were permeabilized for 1 hour in 16.6% normal goat serum, 0.3% Triton X-100 in PBS. Cells were incubated in the same buffer with primary antibodies overnight at 4°C as follows: rabbit-anti-(glial fibrillary acid protein) (GFAP, 1:2000, Dako); mouse-anti-tubulin β-III (Tuj-1 clone, 1:1000, Millipore). After rinsing five times with phosphate buffer at room temperature, cells were incubated for 2 hours at room temperature with either Alexa-fluor 546 goat anti-mouse IgG (1:1000) together with conjugated Alexa-fluor 488 goat anti-rabbit IgG (1:1000). After rinsing four times in phosphate buffer with decreasing NaCl molarity, the nuclei of cells were stained for 5 minutes at room temperature with Hoechst-33342 diluted in phosphate buffer to a final concentration of 1:10000. After one final rinse, coverslips were mounted with fluorescent mounting medium (Dako) and imaged through a epifluorescence microscope (Axiovert 135 TV, Zeiss). Standard 4´-6-diamidino-2-phenylindole (ex: 365/10, em: LP397, dic: 395dclp), green fluorescent protein (ex: 450/40, em: 535/50, dic: 505dclp) and tetramethylrhodamine isothiocyanate (ex: 546/10, em: 575-640, dic: 560dclp) filter set was used to image Hoechst-33342, Alexa-fluor 488 and Alexa-fluor 546, respectively.

4.2.7 Cell viability assays

Cell viability was verified by propidium iodide/fluorescein diacetate staining at 7 DIV, 14 DIV and 21 DIV. Cells grown on glass coverslips were rinsed twice with ringer solution (in mM: NaCl 130; KCl 5; KH_2PO_4 1.2; $MgSO_4$ 1.2; $CaCl_2$ 2; Hepes 25, Glucose 6). Then, they were incubated for 4 minutes in ringer solution containing 15 μg·ml^{-1} of Fluorescein diacetate (Sigma-Aldrich), 5 μg·ml^{-1} of Propidium iodine and 3 μg·ml^{-1} of Hoechst-33342. Then, cells were washed with ringer and multiple images were taken by a CCD Camera (Exi-Blue Fluorescence microscopy camera, QImaging) mounted on an epifluorescence microscope (Axiovert 135 TV, Zeiss). Standard 4´-6-diamidino-2-phenylindole (ex: 365/10, em: LP397, dic: 395dclp),

fluorescein isothiocyanate (ex: 450-490, em: 515-565, dic: 510dclp) and rhodamine (ex: 546/10, em: 575-640, dic: 560dclp) filter set was used to image Hoechst-33342, fluorescein diacetate and propidium iodide, respectively. Then, images were acquired and visualized with Volocity software (Perkin Elmer). At each time point, 20x images were taken from glass coverslips cultured in the custom chamber ($n = 6$) and in the control incubator ($n = 6$). Four fields per coverslip were imaged and the percentage of living cells per field was counted and averaged. The percentage of healthy cells was calculated as the percentage of cells expressing fluorescein diacetate on the total nuclei expressing Hoechst-33342. Percentage of living cells was reported at every time point as mean ± SD of six independent plates and a one-way ANOVA test was performed with Statistica (StatSoft Inc). The significance level was established at $p < 0.05$.

4.2.8 Electrophysiological recordings

Recordings with the standard system were performed with a USB-ME64 system (MCS GmbH) and a Programmable Gain Amplifier (PGA64, MCS GmbH). Specifically, the preamplifier stage (MEA-1060-Inv-BC-Standard, gain: 55, bandwidth: 0.02 Hz - 8.5 kHz, MCS GmbH), was connected to the PGA (gain: 50, bandwidth: 1 Hz - 5 kHz). The PGA, in turn, was connected to the data acquisition and analog-digital converter (ADC, sampling frequency 20 kHz) and to the computer. Recordings with the custom system were performed with the same equipment but the commercial preamplifier was replaced with the custom chamber and the 68-pin socket placed on the customized external board was connected to the PGA (gain: 1000, bandwidth: 1 Hz - 5 kHz).

To assess the recording feasibility inside the chamber, the spontaneous electrical activity of 3 hippocampal neuronal networks (13 DIV) grown on MEAs was recorded repeatedly for 5 minutes by both the standard and the custom setup. In both configurations, single recording started right after the stabilization of the electrical signals to minimize mechanical stress on cells. On average, the time to reach stability was 10 minutes. The signal to noise ratio (SNR) was computed for each setup. Then, spikes were detected from raw data with MCRack Software (MCS GmbH), using for each channel a fixed threshold equal to five times the standard deviation of average noise amplitude in the first 500 ms of signal. Furthermore, the signal acquired with the standard system was defined as the gold standard and the sensitivity (SE) of the detection with the custom setup was computed as follows (Equation 4.1)

$$\frac{TP}{TP + FN} \tag{4.1}$$

where TP is the number of true positive and FN is the number of false negative.

Afterward, off-line analysis was implemented in Matlab (The Mathworks, Natick, USA) as previously described (Section 2.4 and 3.2.4). The mean firing rate (MFR) was extracted for each recording as a general evaluation of the state of the cell cultures. Then, the parameters extracted as descriptors of the spontaneous electrophysiology were

(i) the bursting rate (number of bursts per minute),

(ii) the burst duration (s),

(iii) the number of electrodes involved in network bursts,

(iv) the network burst duration (s).

These parameters were analyzed for each recording and median values of the 3 repeated data sets were computed. A non-parametric statistical analysis (Wilcoxon matched pair test) was performed to identify differences between the two recording setups. Data are given as median value and coefficient of variation, which is the ratio between the interquartile range and the median value. Statistical analyses were performed with the commercial tool Statistica (StatSoft Inc). The significance level was established at $p < 0.05$.

Subsequently, recordings of spontaneous electrical activity of two 18 DIV neuronal networks, identical for cell type, density and treatments, were performed. Specifically, one MEA was acquired for 3 hours by the standard setup while the other one was recorded directly inside the custom chamber. Spikes were detected with MCRack. Then, the time course of the recordings was evaluated in terms of MFR. The frequency values were computed for each 1 min bin in Matlab and normalized on the value of the first minute.

4.2.9 Single-channel dedicated board

Design of the single-channel front-end circuit planned the presence of a decoupling stage (see Section 4.3.5). On the basis of *in vitro* MEA signal features, the following project requirements were defined:

- Band-pass filtering within the frequency range of neuronal spikes (100 Hz - 5 kHz), to improve the SNR,

- Maximally flat frequency response and linear phase, in order not to alter signal morphology,

- Input offset tolerance, in order not to saturate the first stage [Bai and Wise, 2001, Dabrowski et al., 2004, Borghi et al., 2007, Rieger et al., 2007, Rieger and Taylor, 2009],

- 50 Hz interference attenuation,

- Input referred noise lower than 20 μV peak-to-peak, which is the electrode noise mean value [Bai and Wise, 2001],

- Minimum number of circuit components for further integration within the incubating chamber.

Circuit bandwidth was fixed to 300 Hz - 3 kHz as suggested by the literature [Gray et al., 2001, DeBusschere and Kovacs, 2001, Pancrazio et al., 2003, Rolston et al., 2009, Charvet et al., 2010]. These values were also confirmed by spectrogram analysis of broadband MEA signals. Then, the circuit topology and the component values were defined. Furthermore, assessments of circuitry performances were made by means of Spice simulations (LTSpice, Linear Technology). Specifically, simulations were performed to analyze the frequency response gain and phase, the 50 Hz amplification and the input referred electronic noise, which was computed by integrating output noise power spectral density within the passband. Moreover, it was evaluated circuit output in response to sinusoidal waves and real MEA signals.

Afterward, a prototype of the circuit was realized on a breadboard with discrete through hole mounting components. Performances of this prototype were tested in terms of gain and bandwidth by means of a sinusoidal wave generator (GFG-8210, Instek), a bench-top power supply (GPS-4303, Instek) and an ADC board (NI USB-6009, National Instruments, 14 bit, 48 kHz). Specifically, sinusoidal waves with amplitude 22 mV peak-to-peak and variable frequency (from 0.5 Hz to 12 kHz) were used as input. Power supply was set to ± 10V and both input and output signals were acquired by means of NI USB-6009. Then, the estimated gain was obtained by processing input and output signals in Matlab environment. Particularly, fast Fourier Transform (FFT) of input and output signals was computed over 100 periods. Then, gain was computed as the ratio between the FFT modulus of the output and the input.

Finally, it was carried out a feasibility study of the front-end PCB for 60 channels. Its integration with the custom chamber was evaluated in terms of area, thermal heating and battery power supply duration.

4.3 Results

4.3.1 The thermal model

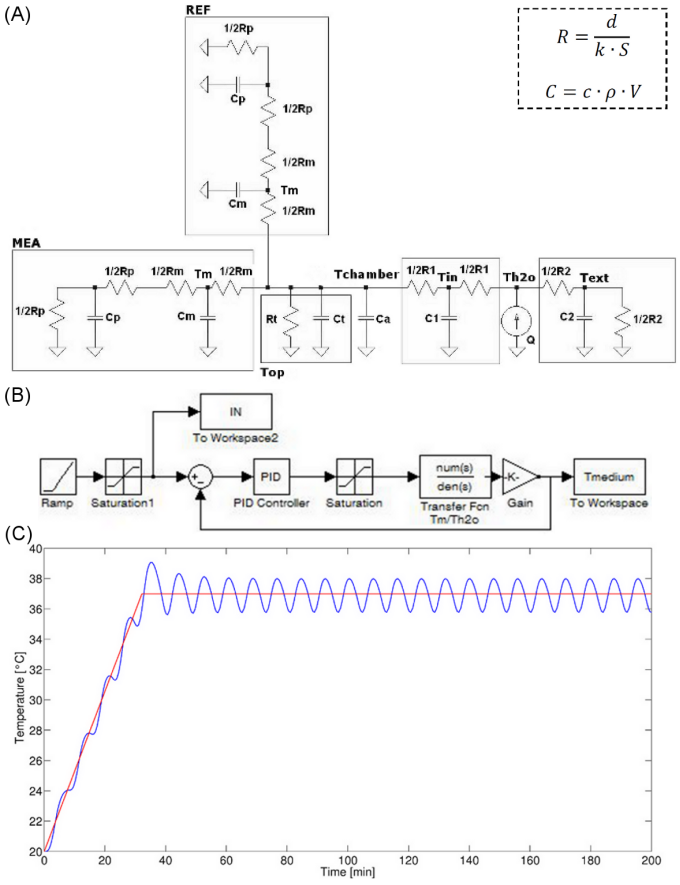

Figure 4.2: (A) Circuitry representing the lumped parameter thermal model of the chamber. Q: current generator. R1, C1: inner walls resistance and capacitance; R2, C2: outer walls resistance and capacitance; Ca: Capacitance of the air inside the chamber; Rt, Ct: top plate resistance and capacitance; Rm, Cm: resistance and capacitance of both cell culture medium (MEA well) and water (reference well); Rp, Cp: resistance and capacitance of the walls beneath the medium and the reference water. Dashed box: R and C are determined by the size and material of each block. d is the wall length [m]; k is the thermal conductivity [$W \cdot m^{-1} \cdot K^{-1}$]; S is the wall surface [m^2]; c is the specific heat capacity [$J \cdot g^{-1} \cdot K^{-1}$]; ρ is the density [$g \cdot m^{-3}$] and V is the wall volume [m^3]. (B) Blocks of the Simulink model. (C) Result of a thermal simulation with outer wall thickness = 10 mm and inner walls thickness = 5 mm (simulating time of 200 minutes, P = 10 and I = 0.1). The blue line is Tm; the red one is the controlled driving temperature.

The outcome of an acceptable simulation (simulating time of 200 min) is depicted in Figure 4.2C. The picture shows that Tm takes about 30 min to grow from 20°C (external environmental average temperature of the laboratory) to 37°C and that, after a small overshoot at 39°C, it starts to oscillate around the set point. This result was obtained defining the wall thicknesses equal to 10 mm for the outer wall and

5 mm for the inner one. Furthermore, the controller parameters P and I were set to 10 and 0.1, respectively. Then, these thickness values and the PI characteristics were chosen for the chamber production and the PID programming. Values of all parameters used in this simulation are listed in Table 4.1.

Parameter	R1	C1	R2	C2	Ca	Rt	Ct	Rm	Cm	Rp	Cp
Value	2.63	354.23	4.41	839.66	16.18	2.69	342.86	20.57	4.15	116.96	1.30

Table 4.1: Values of components of the electric analogue model used during temperature simulations. R values are in $K \cdot W^{-1}$. C values are in $J \cdot K^{-1}$.

4.3.2 The system assembly

The system was assembled as shown in Figure 4.3A and then connected to a 50 L / 150 bar gas cylinder (10% CO_2) by means of an air tube (white arrow). Figure 4.3B depicts the chamber from the top. On the left it shows the PT100 probe and two 1 ml syringes for medium change and pharmacological stimulation. Next, there are the air inlet (yellow tube) and the air outlet, connected to a 0.2 μm filter to maintain sterility inside the chamber. On the right, the acquisition board that gets the 60 signals from MEA electrodes through the top slide is shown. Furthermore, Figure 4.3C is a bottom view of the chamber and displays the opening for an inverted microscope objective. Finally, Figure 4.3D shows the inside of the chamber, which accommodates the MEA and the reference well. Gold pins for signal detection and the temperature probe are illustrated.

The performance of the system was evaluated and it was characterized in terms of temperature profile and gas flow rate. P and I values identified after the simulations, were used during temperature tests ($P = 10$, $I = 0.1$). These experiments (see Section 4.2.3 for the description of the protocol) revealed that the model nearly approximates the real system. Specifically, a ramp-like increase of the bath temperature caused the medium temperature to rise and to reach the set point after about 40 min. This value slightly depended on the initial temperature of the water in the reference well (data not shown). Furthermore, after a typical overshoot peak at about 39°C, the temperature measured by PT100 oscillated between 36.5°C and 38°C. In order to reduce these temperature ripples, after the transient phase P was lowered from 10 to 2.5, a value found empirically. Figure 4.4 shows a typical profile of the temperature measured inside the circulating bath (dashed red) and in the reference well (blue).

With regard to the flow control, the gas flow of 70 ml/min maintained medium pH in the physiological range. Accordingly, there was no evidence concerning pH differences between the two setups. Indeed, medium pH values ranged between 7.38 and 7.57 in all the experiments. Furthermore, the 70 ml/min flow induced a sufficient

bubbling to humidify the air in order to avoid hyperosmolarity. Flow increase due to water evaporation in the bubbler was prevented by periodically refilling it. With this flow, the 50 L gas cylinder, used to provide the 10% CO_2 air, lasted more than 10 weeks. Finally, constant pressure values inside the chamber (around 20 mmHg) assured that the chamber was airtight except for the proper air outlet.

Finally, the optical monitoring requirement was verified. Figure 4.5 shows a neuronal network that is grown on microelectrodes of a MEA chip. The image was taken using an inverted microscope (Axiovert 135 TV, Zeiss). The 5x differential interference contrast objective was inserted beneath the MEA housing, through the opening realized in the bottom wall. The picture's quality attests the possibility of monitoring cells inside the chamber during network maturation.

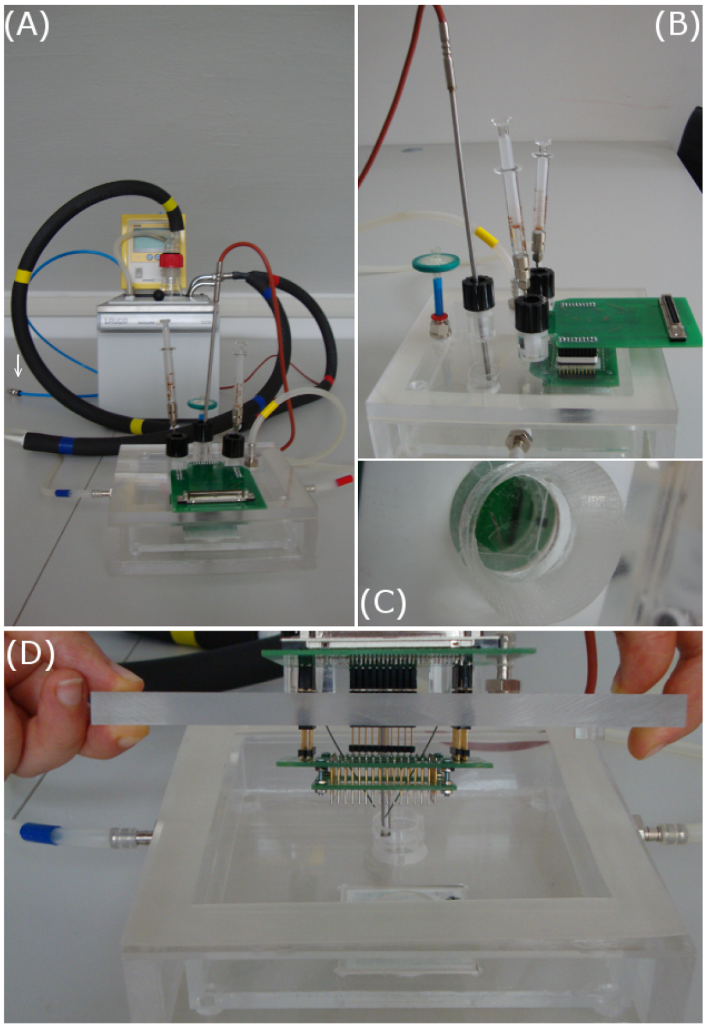

Figure 4.3: (A) System assembly: the custom chamber is connected to the controlled heating bath and to a 50 L / 150 bar gas cylinder (not depicted) by means of an air tube (white arrow). (B) The chamber from the top: on the left the PT100 probe, syringes for medium and drug addition, the air inlet (yellow tube) and the air outlet; on the right the acquisition board. (C) Bottom view of the chamber: opening for the inverted microscope objectives. (D) Inside the chamber: the MEA housing and the reference well.

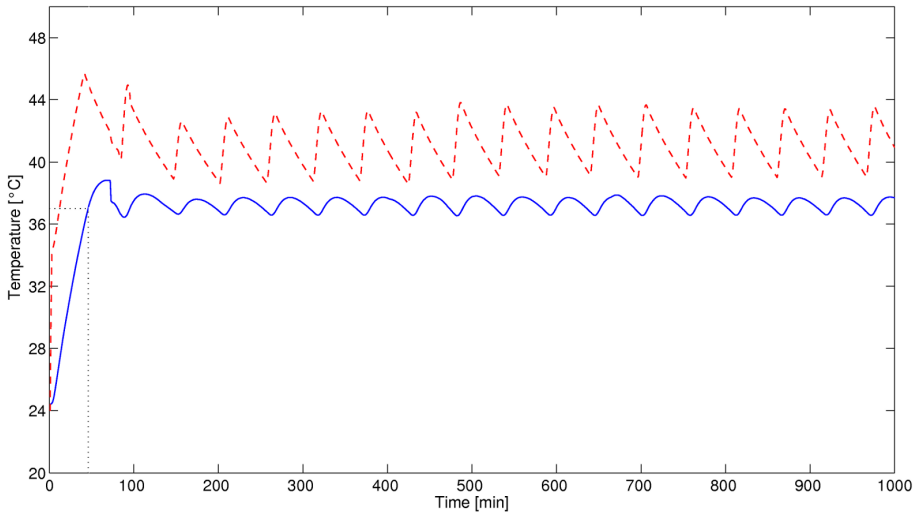

Figure 4.4: Bath (dashed red) and reference well (blue) temperature profiles. The black dashed line identifies the reaching of the set point temperature after about 40 minutes. Then, the temperature of the reference well oscillates between 36.5°C and 38°C and it follows the bath temperature dynamic.

4.3.3 Chamber effect on cell viability

Neither bacterial nor spore contamination of both coverslips and MEAs were observed during the culturing period. Moreover, the moisture content of the air was adequate to avoid considerable evaporation in between successive medium changes. A first qualitative assessment about the morphology of the neuronal networks was performed comparing the immunostaining of two 14 DIV neuronal cultures. Figure 4.6A and 4.6B show the fluorescence of a 14 DIV neuronal culture grown inside a standard incubator and the fluorescence of a 14 DIV neuronal culture grown inside the custom chamber, respectively. The green staining identifies the astrocytes, the red staining marks the neurons and the blue labels nuclei of the cells. The two 20x pictures highlight the same neuronal cell density, network organization and astrocyte morphology and proliferation.

Then, the influence of the custom chamber on the cell vitality was quantitative evaluated by propinium iodide/fluorescein diacetate staining. Figure 4.7A and Figure 4.7B show the staining of a 7 DIV neuronal culture grown inside the standard incubator and a 7 DIV neuronal culture grown inside the custom chamber. No significant differences were found in cell viability (Fig. 4.7C $p = 0.31$, one-way ANOVA, $n = 6$ in each group) under both culture conditions and at different time points, indicating that the custom chamber alters neither the network development nor the neuronal viability over a long period of time.

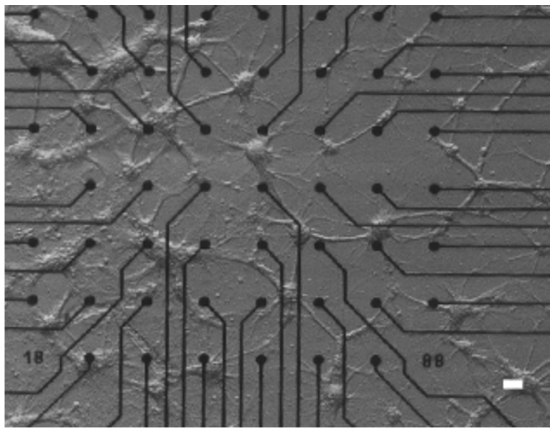

Figure 4.5: 5x differential interference contrast image (DIC) of a neuronal network grown on MEA. Scale bar 100 μm.

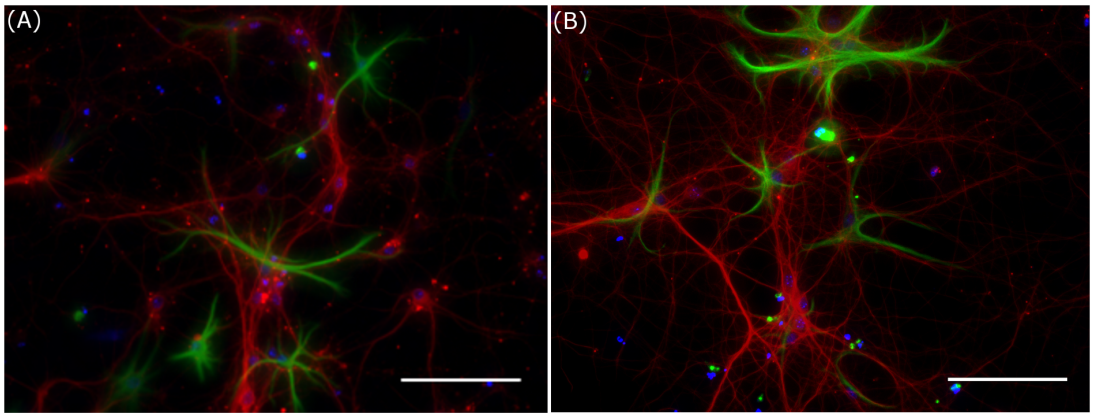

Figure 4.6: Immunofluorescence of two neuronal cultures at 14 DIV grown (A) inside a standard incubator and (B) in the custom chamber. Scale bars 100 μm. Red label: tubulin β-III; green label: GFAP; blue label: Hoechst-33342. Standard 4´-6-diamidino-2-phenylindole (ex: 365/10, em: LP397, dic: 395dclp), green fluorescent protein (ex: 450/40, em: 535/50, dic: 505dclp) and tetramethylrhodamine isothiocyanate (ex: 546/10, em: 575-640, dic: 560dclp) filter set was used to image Hoechst-33342, GFAP and tubulin β-III (Tuj-1 clone), respectively.

4.3.4 Chamber effect on neuronal electrophysiology

Figure 4.8 depicts the two setups used during electrophysiological experiments. The evaluation of SNR showed higher values in the standard setup (about 20dB) than in the custom chamber (18 dB). Specifically, peak to peak noise value was comparable in the two configurations and was equal to 8 μV, while the signal amplitude was reduced in the custom setup (Figure 4.9A and 4.9B). The signal decrease was further observed in the sensitivity values of the custom recordings with respect to the gold standard. Indeed, the sensitivity, which measures the percentage of the action potential identified correctly as spikes, was about 85%. Moreover, a significant difference in spiking frequencies was detected (Wilcoxon test $p < 0.05$, Table 4.2), which was certainly due to the lower SNR value of the custom chamber. In contrast,

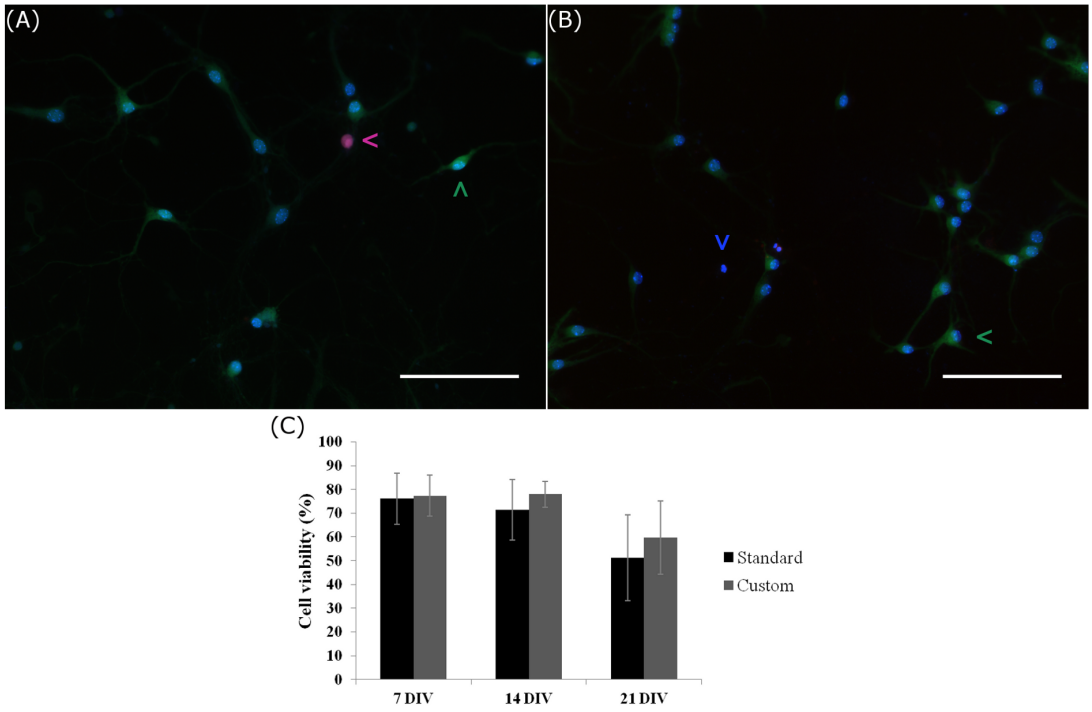

Figure 4.7: Propinium iodide/fluorescein diacetate staining of two neuronal cultures at 7 DIV grown (A) inside a standard incubator and (B) in the custom chamber. Green, blue and violet arrowheads identify viable cells, necrotic/apoptotic cells and necrotic cells, respectively. Scale bars 100 μm. Red label: propinium iodine; green label: fluorescein diacetate; blue label: Hoechst-33342. Standard 4´-6-diamidino-2-phenylindole (ex: 365/10, em: LP397, dic: 395dclp), fluorescein isothiocyanate (ex: 450-490, em: 515-565, dic: 510dclp) and rhodamine (ex: 546/10, em: 575-640, dic: 560dclp) filter set was used to image Hoechst-33342, fluorescein diacetate and propinium iodine, respectively. (C) Statistical analysis of cell viability on cell cultures grown inside a standard incubator (black) or in the custom chamber (grey) at three time points: 7 DIV, 14 DIV and 21 DIV ($p = 0.31$, one-way ANOVA, $n = 6$ in each group).

the neuronal electrical activity recorded by the chamber showed a spiking organization qualitatively similar to standard recordings. Figure 4.9C and 4.9D show the spiking structures (raster plot) of one network, whose activity was acquired by the standard and the custom equipment, respectively. The number of active electrodes and the burst and network burst patterns are clearly comparable. Furthermore, the quantitative data analysis in Matlab confirmed these evaluations. Accordingly, no significant differences in burst and network burst features were identified (Table 4.2).

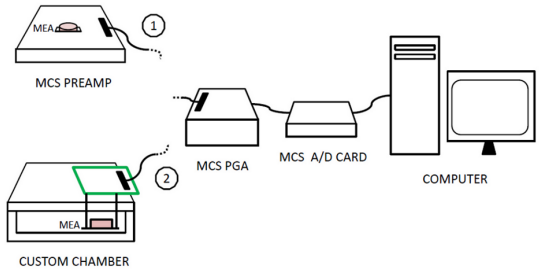

Figure 4.8: Equipments used during electrophysiological experiments. (1) Standard setup: preamplifier stage of the USB-ME64 system (G: 55, bandwidth: 0.02 Hz-8.5 kHz), PGA64 (G: 50, bandwidth: 1 Hz - 5 kHz), A/D card, computer. (2) Custom setup: custom incubating and recording chamber, PGA64 (G: 1000, bandwidth: 1 Hz - 5 kHz), A/D card, computer.

	Mean firing rate (Hz)	Burst length (s)	Burst rate (Hz)	NB electrodes	NB length (s)
Standard system	**1.7±0.6**	0.19±0.1	2.4±1.4	0.6±0.1	0.6±0.2
Custom chamber	**0.7±1.1**	0.16±0.0	1.5±1.6	0.6±0.1	0.4±0.1

Table 4.2: Results of single channel, burst and network burst (NB) analysis. Median ± coefficient of variation (ratio between the interquartile range and the median value). No significant differences were found between the two recording systems, except for the mean firing rate (bold data Wilcoxon test $p < 0.05$).

To verify the improvements in cells viability during data acquisition performed by the custom chamber, three hours recordings of two 18 DIV cultures grown on MEAs were performed. Figure 4.10 shows the kinetics of these data acquisitions in terms of normalized mean firing rate. The time course of the recording performed by the standard setup (Figure 4.10, stars) highlighted a slow decrease of spiking frequency after 30 min. Moreover, after less than two hours, this network was completely silent. On the contrary, the activity of the MEA placed inside the custom chamber (Figure 4.10, dots) was stable for more than three hours.

4.3.5 Single-channel dedicated board

As aforementioned, the main problem observed during electrophysiological measurements inside the custom chamber was the value of the SNR. This was attributed to the lack of a decoupling stage immediately close to the electrodes. Indeed, the stage before the PGA realizes a low-pass filter whose cutoff frequency is given by Equation 4.2:

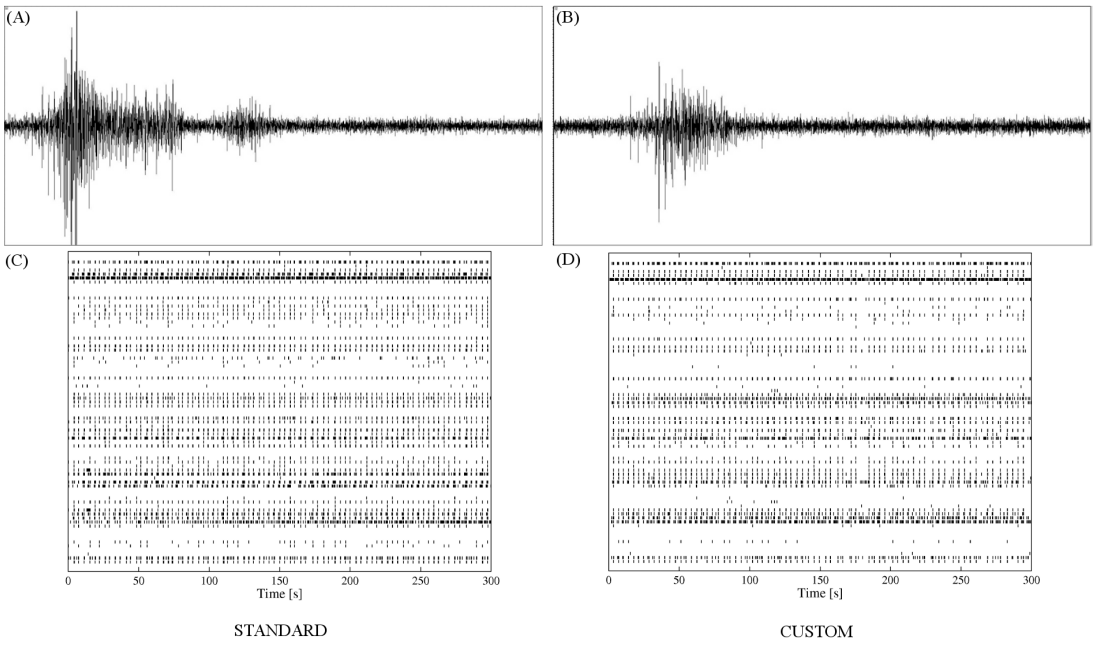

Figure 4.9: Single channel activity (1s) acquired with the standard (A) and the custom (B) equipment (y-axes ranges from -100 μV to +100 μV). Raster plot of 5 minutes activity recorded with the standard (C) and the custom (D) equipment.

$$f_{cutoff} = \frac{1}{2\pi RC} \tag{4.2}$$

where R and C are the equivalent resistance and capacitance presented to the PGA input. Considering the commercial setup, R is the MEA1060 output resistance (300 Ω). On the other hand, in the custom system it is mainly given by the source impedance, which results from electrode impedance and cell coupling / adhesion (1 MΩ). Furthermore, in both equipments C is mainly due to the parasitic shunt capacitance of the MCS cable (128 pF). Therefore, f_{cutoff} is equal to 4 MHz for the commercial setup that means that no signal components are cut, while it is 1.2kHz for the custom chamber, which is within neuronal spike frequency content. Therefore, this causes signal attenuation and prevents from reaching signal acquisitions comparable to the commercial system. Hence, a custom decoupling stage, placed next to signal sources, is necessary.

The circuit design led to the definition of a band-pass filter with corner frequencies placed at 300 Hz and 3 kHz and a frequency response modulus with a gain of 963 and slopes of 60 dB/decade. A gain about 1000 is a typical amplification value which is required to maintain SNR throughout the signal processing cascade [Dabrowski et al., 2004, Mohseni and Najafi, 2004, Wrobel et al., 2007, Borghi et al., 2007, Rieger et al., 2007, Rieger and Taylor, 2009, Charvet et al., 2010]. Figure 4.11 shows the schematic of the single channel which is composed by a preamplifier stage, an high-pass filter and a low pass-filter. Specifically, the preamplifier is made of a

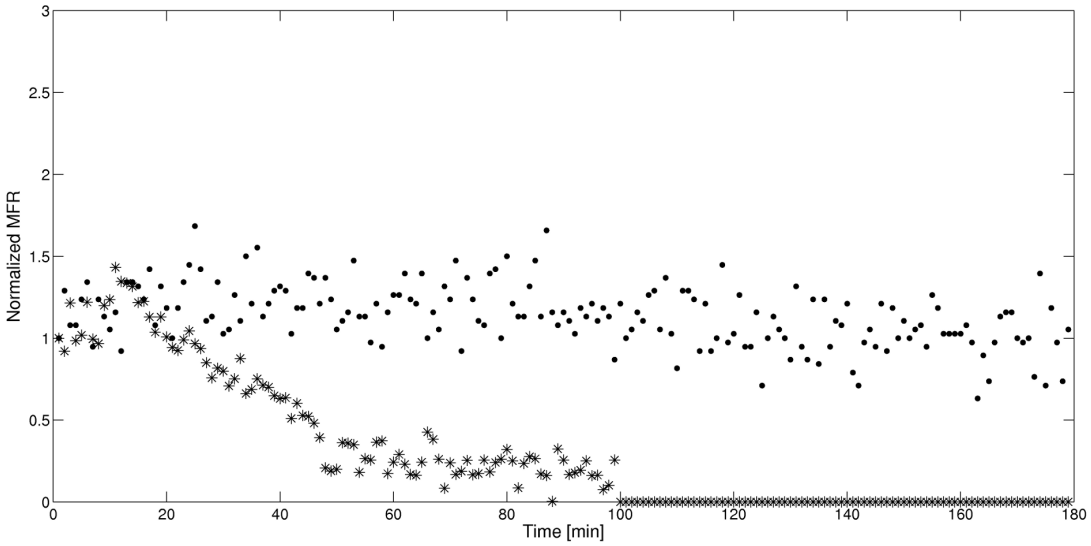

Figure 4.10: Time course of the normalized MFR for two MEAs recorded by the standard (stars) or the custom (dots) equipment for 3 hours. Each marker is the MFR in 1 minute of activity.

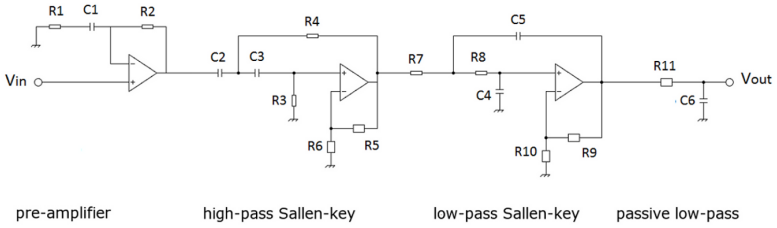

Figure 4.11: Single channel schematic.

non-inverting operational amplifier and passive components. It has a high-pass pole at 300 Hz (C1 and R1) and a zero at 3 Hz (C1, R1 and R2). It gains one before the zero, while after the pole it is set to 107 by R1 and R2. This gain level has been considered a good compromise to avoid saturation due to input electrode offset and to neglect the following stage noise. Furthermore, this value keeps the input referred noise of this stage below the electrode noise (data simulated in Spice). The following stage is a two-pole active high-pass filter which uses a Sallen-key topology. Poles (R3, R4, C2 and C3) and gain (R5 and R6) are equal to 300 Hz and 3, respectively. Passive component values were chosen to form a Butterworth filter which has maximally flat frequency response. Last stages are a two-pole active low-pass filter (Sallen-key topology) and a passive low-pass filter with poles (R7, R8, R9, C4, C5 and C6) and gain (R9 and R10) equal to 3 kHz and 3, respectively. Again, a Butterworth filter was designed. Passive component values were chosen by means of a commercial software (FilterPro™, Texas Instrument). Their values are listed in Table 4.3.

Component	R1	R2	R3	R4	R5	R6	R7	R8	R9	R10	R11	C1	C2	C3	C4	C5	C6
Value	1.13	120	6.49	9.31	20	10	3.01	13.7	20	10	11.3	470	100	47	6.8	10	4.7

Table 4.3: Passive component values of the single-channel circuit for band-pass filtering and amplification. R values are in kΩ. C values are in nF.

For the circuit implementation, it was chosen the OPA132 (Texas Instruments, Dallas, Texas) as operational amplifier (OPamp). It features:

- Low noise (750 nV root-mean-square (RMS) noise from 1 kHz to 10 kHz),
- High input impedance (1013 Ω),
- Low output impedance (lower than 1 Ω),
- Low offset (±500 μV, typical value),
- Low bias current (50 pA, maximum value),
- Dual power supply (from ± 2.5 V to ± 18 V),
- High gain-bandwidth product (8 MHz).

Concerning the power supply, ± 2.5 V has been considered suitable to avoid OPamp saturation due to electrodes and OPamp offset.

Spice simulations confirmed the theoretical considerations about frequency response gain. Figure 4.12 shows that the maximum gain is equal to 940, comparable to the predicted one, and 50 Hz signals are amplified only 5 times. Figure 4.12 also depicts the group delay, which is the derivative of the phase with respect to the angular frequency. The group delay is almost flat in the passband and equal to 180 μs. This means that all sinusoidal components of a signal are equally delayed by the circuit.

Figure 4.12: Bode diagram simulated in Spice. The picture shows the gain (|G|) and the group delay.

Then, it was analyzed the circuit response to a sinusoidal wave with amplitude and frequency equal to 200 μV peak-to-peak and 1 kHz, respectively (features similar to typical neuronal signals *in vitro*). Simulated output voltage was 200 mV peak-to-peak (Figure 4.13A). Figure 4.13B shows circuit response to a real broad-band MEA signal. As designed, low frequency oscillations are cut while neuronal spikes

(100-150 mV peak-to-peak) are amplified and can be identified. Given the small amplitude values of output signal, an analog-to-digital converter with a range of ±200 mV should be used [Dabrowski et al., 2004, Borghi et al., 2007, Rieger et al., 2007, Rieger and Taylor, 2009].

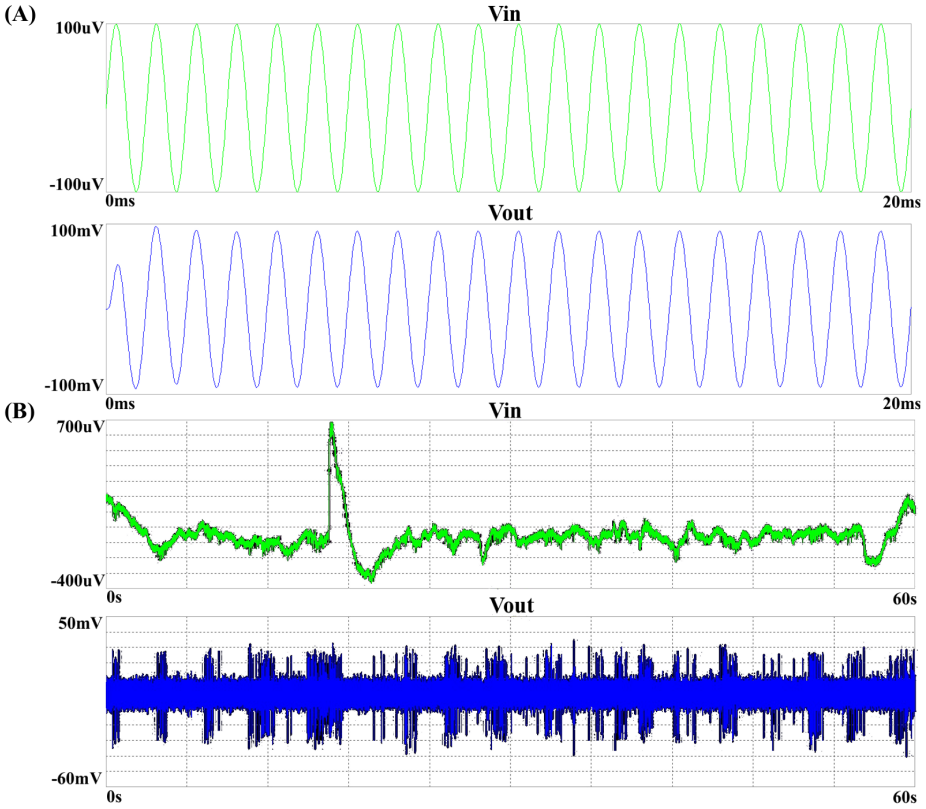

Figure 4.13: Circuit response simulations. (A) Sinusoidal input wave: amplitude 200 μV peak-to-peak, frequency 1 kHz. The output is amplified of about 1000. (B) Real broad-band MEA signal input. The output is a typical filtered extracellular signal.

Results of noise analysis showed that a RMS output noise of almost 460 nV is present between 300 Hz and 3 kHz. This means 2 mV peak-to-peak output noise (under the assumption of Gaussian noise). Input referred circuit noise (obtained by dividing output noise for the passband gain) resulted equal to 3 μV peak-to-peak which is lower than electrode noise, as required.

Afterward, a prototype was realized. Experimental gain was similar to simulated gain profile even if an attenuation of about 9% was observed in the passband (Figure 4.14). This difference was attributed to passive component tolerance and to environmental noise. Then, electronic noise was measured by connecting the input to ground supply. Output noise was nearly 20 mV peak-to-peak, which is a value higher than the simulated one.

Finally, it was evaluated the possibility of integrating a 60-channel front-end circuit with the custom incubating chamber. The necessity of a decoupling stage

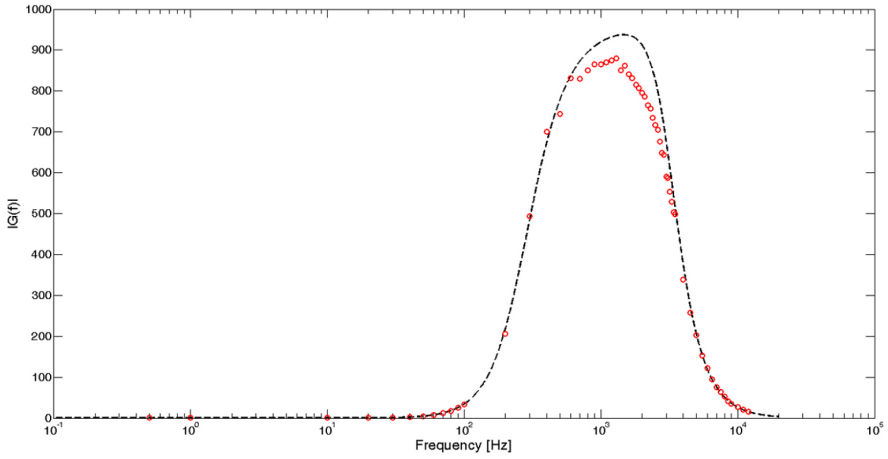

Figure 4.14: Simulated (black) and experimental (red) Bode diagram of the frequency response modulus.

immediately close to the electrodes suggested to divide the front-end circuit in two PCBs. Specifically, the preamplification stage and the following stages could be located inside and outside the custom chamber, respectively (Figure 4.15). Therefore, inner PCB size and thermal heating are constrained by its location, while none of these limitations are necessary for the external PCB.

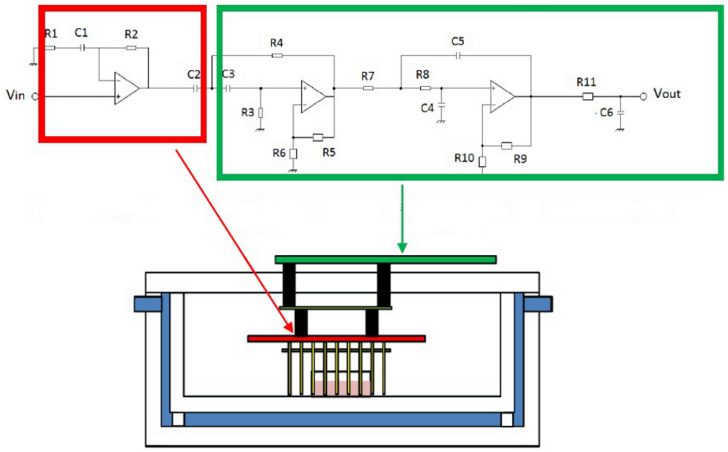

Figure 4.15: 60-channel front-end circuit integrated with the custom incubating chamber. The preamplification stage is located inside the custom chamber, closed to signal sources to improve the SNR, while the following stages are placed outside.

To minimize PCB dimensions, quad OPamps and surface mounting devices (SMDs) should be preferred. A preliminary evaluation was made computing the layout area occupied by the preamplification of four channels (layout drown in Eagle, Cadsoft). SMDs with 0402 package (i.e. 1 mm x 0.51 mm) were chosen. Furthermore, the signal track width was set to 0.254 mm. Figure 4.16 shows the PCB layout. The squared hole (black) in the middle of the board is aligned with MEA housing. Next, 60 holes (green) are the gold pins which contact MEA pads. Ex-

ternally, four 15-pin connectors are designed to drive the 60 preamplified signals to the upper board. Furthermore, a 3-pin connector drives power supply lines and ground. Estimated area is about 2.25 cm^2 for four channels. Therefore, 60 channel area should be 33.75 cm^2. Since maximum available area is nearly 98 cm^2 (PCB size 7 cm x 14 cm), it was conclude that area is not a limiting factor for 60-channel PCB integration within the custom chamber.

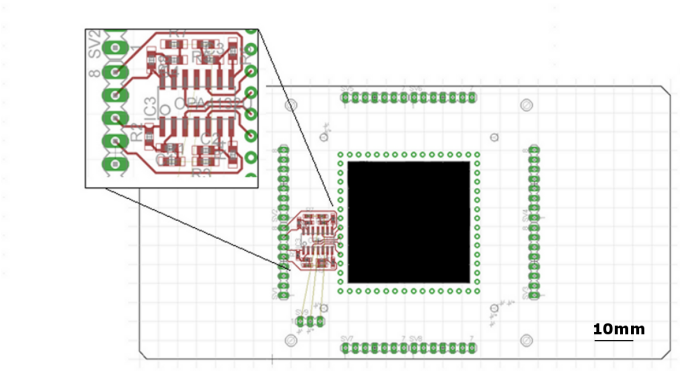

Figure 4.16: PCB layout: squared black hole in the middle of the board is aligned with MEA housing. Green small inner holes: 60 gold pins that contact MEA pads. Green big outer holes: four 15-pin connectors for signals and a 3-pin connector for power supply lines and ground. On the left, detail of the preamplification circuit for 4 channels.

Regarding thermal heating, it is important that the inner PCB does not alter neuronal cell temperature significantly. To estimate the temperature increase due to the preamplification stage, single op-amp power consumption was computed as in Equation 4.3:

$$P_{OPamp} = V_{+} \cdot I_q + V_{-} \cdot (-I_q) = 20mW \tag{4.3}$$

where V_+ and V_- are the positive and negative power supply (± 2.5 V), and I_q is the quiescent current (4 mA for OPA132 device). Power dissipation by resistive components is negligible with respect to P_{OPamp}. Considering 60 channels, power dissipation is 1.2 W. Then, temperature increase ΔT in one second was computed as follows (Equation 4.4):

$$\Delta T = \frac{Q}{C} \tag{4.4}$$

where Q is the heat released by the inner PCB, equivalent to 1.2 J and C is the thermal capacitance of the air contained in the chamber. C is computed as in Equation 4.5:

$$C = c \cdot \rho \cdot v \approx 0.8 \frac{J}{K} \tag{4.5}$$

where c is air specific heat at 37°C ($1060\,^{J}/_{Kg\cdot K}$), ρ is moist-air density at 37°C ($1.165\,^{Kg}/_{m^3}$) and V is air volume inside the chamber ($640\,\mathrm{cm}^3$). Therefore, temperature would rise $1.5\,^{K}/_{s}$ in these conditions.

Besides, a battery power supply should be preferred to fulfill the portability requirement [Obeid et al., 2004]. Here, two 2.5 V batteries could be used in series. Since estimated current that is adsorbed by each channel is 12 mA (3 OPamps for each channel), 60 channels adsorbed 720 mA. Therefore, battery duration is of nearly 27 hours, considering batteries with $20A{\cdot}h$.

4.4 Discussion

Environmental chambers can be classified as closed or open systems depending on their air tightness. Open systems are not suitable for long-term experiments because of the unstable environmental control and potential risk of contamination. Therefore, closed systems should be the preferred method for long experiments [Ho et al., 2005]. In the literature, several closed chambers designed to improve the reliability of long term data are described, which attests to the necessity of similar devices in the biological field [Forsythe and Coates, 1988, Toyotomi and Momose, 1989]. However, these chambers rarely provide a stable control on all the environmental parameters [Blau and Ziegler, 2001] and they are generally used only during the experimental sessions [Gross and Schwalm, 1994, Potter and DeMarse, 2001, Pancrazio et al., 2003] or they are not independent from bulky standard incubators [Mukai et al., 2003].

In this work a custom closed chamber for neuronal growth and electrical activity recording is described. The chamber was realized in PMMA plates and it was assembled with a heating bath and a gas cylinder to provide a controlled environment for cell maturation. Temperature and pH tests were performed to verify the fulfillment of the requirements. Results underlined that the time extent necessary to reach the temperature set point was as good as the one estimated by the thermal model and similar to the literature [Vukasinovic et al., 2009]. Moreover, temperature oscillations did not affect cell survival, as verified by vitality tests. Regarding medium pH, it was stabilized around 7.4 with a constant 10% CO_2 humidified gas flow and it remained stable even at slow flow rate (less than 70 ml/min), which assured a small gas cylinder consumption. The moisture content of the air introduced inside the chamber, was adequate to avoid evaporation and the consequent hyperosmolarity. Therefore, the system showed high stability of controlled parameters, which is a prerequisite for long term cell culture. Finally, the system developed here is accessible from the outside. Indeed, environmental chambers have to guarantee accesses from the outside for medium change and drug addition. These operations

are generally performed after the opening of the chamber under a sterile hood, if a perfusion system is not available [Hales et al., 2010]. The chamber described does not require those processes and thus reduces mechanical stress and changes in cell homeostasis. Concerning the environmental control, some improvements are still needed. Indeed, it would be useful to integrate a CO_2 sensor and to maintain the acid-base homeostasis with pulses of CO_2. This would consequently reduce the air consumption and it would allow the use of smaller cylinders. Furthermore, the integration with a closed perfusion system would maintain a constant medium level, which could completely solve the hyperosmolarity problem.

Further, the influence of the custom chamber on the cell vitality was quantitatively evaluated by immunostainings and dead/alive labeling of neurons grown on standard coverslips. Results highlight that the custom chamber grows neuronal networks with morphology and viability comparable to cell cultures grown in standard incubators. Moreover, it alters neither the network development nor the neuronal viability over the culturing period. Besides, cells in culture were maintained up to 21 DIV since this is generally the period of *in vitro* development where modulation and shaping in the synaptic connectivity occur [Chiappalone et al., 2006]. Anyway, I believe that this system, which provides a controlled and stable environment in terms of temperature, pH and humidity, could guarantee longer experiments.

Furthermore, the chamber allowed to repeatedly record neuronal electrical activity reducing mechanical disturbances and cellular stress. This activity showed physiological features, indicating that the custom chamber does not alter the network electrophysiology. Moreover, a three hours recording, which was performed with the custom chamber, was compared to an acquisition obtained by means of the standard commercial system. This system integrates the temperature control but suffers from disadvantages concerning pH stability and osmotic balance maintenance. Therefore, it induces changes in neuronal activity in about thirty minutes and cell culture decline in less than two hours ([Potter and DeMarse, 2001], Section 2.5). Results of this work confirmed these experimental observations and showed that the system proposed hereby can be a solution for long term recordings.

The main problem observed during electrophysiological measurements was the value of SNR, which influenced the sensitivity of the detection. This was attributed to the lack of a decoupling and preamplification stage immediately close to the electrodes. Indeed, signal attenuation and noise coupling can be significant when external cables are used before any off-chip buffering [Bai and Wise, 2001]. Therefore, it is required a dedicated pre-processing board, housed directly inside the chamber to reduce the effect of parasitic shunt capacitance and channel impedance levels. Hence, a single-channel pre-processing board was designed and developed on breadboard. Both Spice simulations and circuit tests proved that this board fulfills gain

and bandwidth requirements. Indeed, experimental gain was similar to ideal one and passband phase was linear. Furthermore, it showed a good offset tolerance and a significant reduction of power line frequency. In contrast, output noise was nearly 20 mV peak-to-peak which is ten times higher than the simulated one. This was probably due to environmental noise interference and analog-to-digital converter noise. Further investigation has to be performed in order to understand and solve this problem. Finally, it was carried out a feasibility study concerning the integration of a 60 channel preprocessing board within the custom chamber. Area requirement was fulfilled. In contrast, temperature increase due to amplifier power dissipation could be critical if the closed-loop temperature regulation system would not react readily to temperature changes. Furthermore, battery duration was limited to about one day. Therefore, these considerations suggest that operational amplifiers with lower quiescent current (such as OPA4277, Texas Instruments) are needed for further preprocessing board implementation. Besides, the development of an electronic board for data compression, as the one which was previously described [Biffi et al., 2010], would give several advantages concerning data storage (see Chapter 5 for a detailed description).

Another strength of the system is that the electronic board did not show injuries caused by temperature and humidity, after a period longer than one month. Generally, the humid environment found in standard incubators (more than 60%) causes electrical shorts, changes in component properties, and degradation of materials commonly used in electronic devices [Potter and DeMarse, 2001]. For these reasons, few systems described in the literature proposed to control evaporation and to introduce recording equipments inside dry incubators [Potter and DeMarse, 2001, Mukai et al., 2003]. In contrast, thanks to the electronic board sealing obtained with a silicone elastomer, the air content moisture of the chamber proposed was maintained sufficiently high avoiding the use of a cumbersome incubator. As a result, the system is also compact and portable.

Finally, the ability of the system to observe cell cultures grown inside the chamber was demonstrated. The quality of the images guaranteed the possibility of monitoring the network maturation despite the fact that the wall thickness beneath the MEA limited the use of short working distance objectives. Particularly, the 5 mm minimum working distance leads to the choice of phase contrast or DIC objectives with a maximum magnification of 20 x. Although the system cannot work at higher resolution, 20 x objectives allow studying the morphological and structural features of a neuronal network by bright field or fluorescence, coupling optical monitoring to electrophysiological studies.

To conclude, the proposed system is a technological platform able to grow a neuronal network on a MEA chip since the very beginning of its maturation and

to acquire its electrical activity during long term experiments. The device assures environmental parameter stability and eliminates mechanical shock problems. Moreover, it can also be used for both cell culturing and electrical recording. Hence it should be considered an innovative platform for an electrophysiological laboratory, being independent from cumbersome incubators. Finally, since the chamber is not a medium-filled closed system, it is possible to adapt it for multiple MEA housings. In the literature, both the importance of this requirement and the limits imposed by other configurations, have already been discussed [Mukai et al., 2003, Pancrazio et al., 2003]. The platform described here would allow performing parallel long term experiments with neuronal networks grown on MEA chips maintaining both the control and the treated cell cultures in the same environment. This coupled-network configuration assures that variations observed among cell cultures are strictly dependent on the type of treatment and it offers more reliable and reproducible experiments.

Chapter 5

Post-processing on hardware: a feasibility study [1]

MicroElectrode Array (MEA) electrodes record neuronal activity from a region of a cell culture, where generally tens of neurons are present. Therefore, each electrode provides the acquisition of multi-unit activities (MUAs). To extract from a MUA the activity of each firing unit influencing that electrode, a process called spike sorting is needed. This includes action potential (AP) detection, which was briefly described in Section 2.4, and classification. Furthermore, when recording continuously for long periods of time using the chamber developed in this thesis, a huge amount of data has to be handled. Hence, application-specific post-processing electronics is required and on-line and real time analysis, optimization of memory use and data transmission rate improvement become necessary.

This chapter deals with the design and implementation of an adaptive algorithm for amplitude-threshold spike detection and classification of neuronal spikes. First, the state of the art about spike detection and classification methods is investigated. Then, algorithm structure is described. Finally it is proposed the hardware design for spike detection and automatic classification on Field Programmable Gate Arrays (FPGAs) and Digital Signal Processors (DSPs), respectively. The final goal is to execute the data analysis on-line, reducing data storage problems for long term acquisitions in real-time mode.

[1] The work has been published as **Biffi E**, Ghezzi D, Pedrocchi A, Ferrigno G. Development and validation of a spike detection and classification algorithm aimed at implementation on hardware devices. *Comput Intell Neurosci*, 2010, doi:10.1155/2010/659050.

5.1 Spike detection and classification methods: state of the art.

There are two different approaches to acquire and analyze electrophysiological data. Offline sorting requires to store raw traces observed on all electrodes and perform spike detection and sorting later. In contrast, online sorting identifies and sorts spikes during acquisition and stores only sorted spikes [Rutishauser et al., 2006]. A compromise between these approaches is to detect spikes online and store them for offline sorting. Spike detection of neuronal APs can be performed using supervised methods [Chandra and Optican, 1997, Lewicki, 1998] or using unsupervised ones [Watkins et al., 2004, Chan et al., 2008]. Since exact and detailed information on AP morphology is not available before they are detected, supervised detectors (e.g. artificial neural networks) have obvious limits in real applications. In contrast, unsupervised methods do not require *a priori* knowledge about neuronal spike waveforms nor the user presence. Therefore, they are useful for automatic processing purposes. The most widely used unsupervised technique to detect APs is amplitude threshold crossing (Section 2.4). This conventional method compares signal amplitude with a fixed or adaptive threshold, which depends on the Root Mean Square (RMS) value of data in running windows [Guillory and Normann, 1999, Wagenaar et al., 2005]. The use of multielectrode systems makes automatic adjustment of threshold level attractive compared to manual procedures [Chan et al., 2008]. However, both methods suffer from bias induced by high amplitude and high firing-rate neuronal spikes [Watkins et al., 2004]. Since the silencing of biological activity is unfeasible, threshold levels must be estimated from the superposition of signal and noise. Several methods were recently proposed to overcome this difficulty by adopting an unbiased estimate of the standard deviation (SD) of background noise. Accordingly, Wagenaar and collaborators [Wagenaar et al., 2005] proposed a tool which uses different algorithms to estimate noise level. Furthermore, Thakur and colleagues [Thakur et al., 2007] developed an algorithm to automatically detect a spike free segment of signal and estimate SD of background noise by considering only the middle portion of noise amplitude distribution. Besides, embedded systems and chips were developed to detect neuronal spikes and communicate only active portions of data [Perelman and Ginosar, 2006]. Methods such as principal components [Daffertshofer et al., 2004] and Haar transform [Yang and Shamma, 1988] were also used to identify APs. Finally, discrimination methods were introduced. These methods form a feature space defined by spikes and isolate them by creating discrimination boundaries between clusters within that feature space. Discrimination is usually based on different properties of AP waveforms, such as zero crossing and spike width [Mishelevich, 1970] or conduction velocity [Brunner et al., 1990].

As previously said about spike detection methods, classification techniques can be supervised or unsupervised. Methods that are typically used in supervised classification of APs, are template matching and artificial neural networks [Chandra and Optican, 1997, Lewicki, 1998]. On the other hand, Principal Component Analysis (PCA) [Lewicki, 1998] and fuzzy c-means (FCM) clustering [Inan and Kuntalp, 2007] are well-known unsupervised spike sorting algorithms. Classification methods were compared by Wheeler and Heetderks [Wheeler and Heetderks, 1982], that evaluated performances of nine different methods including spike amplitude, conduction latency, PCA and template matching using Euclidean distance. The last two methods were found to perform the best for spike sorting in noisy data. Finally, a new clustering technique, which is gaining in importance, is the hierarchical classifier [Thakur et al., 2007]. In this automatic approach, clusters are successively grouped into greater ones.

Besides, few spike detection and clustering methods were implemented on hardware devices. The two main categories of hardware which were used for these goals were Digital Signal Processors (DSPs) and Field Programmable Gate Arrays (FPGAs). The former are microprocessors optimized to perform recursive instructions. DSPs have many advantages: they are ideal platforms when high flexibility is required. Furthermore, cost effectiveness is another benefit of these devices. In neuronal data analysis they were mainly used for spike waveform capture, sorting and classification [Chandra and Optican, 1997, Guillory and Normann, 1999, Sokal et al., 2000, Schrott et al., 2004].

On the other hand, FPGAs are digital circuits widely used to manufacture complex digital systems due to advantages they offer, such as gate count, speed, high level of parallelism, rapid hardware realization and low development cost [Kumar and Chong, 2008]. Particularly, performances that FPGAs have achieved in last years allow accelerating DSP tasks. A FPGA consists of a regular symmetrical structure of Configurable Logic Blocks (CLBs), interconnected by a programmable network. Furthermore, if is composed of many Input/Output Blocks (IOBs) and Random-Access Memory (RAM) blocks. Specifically, CLBs constitute the main logic resources for implementing synchronous as well as combinatorial circuits. Each CLB contains four slices and each slice contains two small Look-Up Tables (LUTs) and two flip-flops. The LUTs can be used as a 16 bit shift register or as a 16 x 1 distributed memory. Finally, memory can be block or distributed RAM. For application requiring large, on-chip memory, block RAM is preferable. It is organized in columns and each column contains a number of blocks depending on the size of the FPGA [Xilinx Manual, 2008]. Concerning their applicability in neuronal signal analysis, they were used for analogue-to-digital conversion, real-time pre-processing [Zviagintsev et al., 2006, Gandolfo et al., 2010], detection threshold computation

[Schrott et al., 2004] and online spike identification and data compression [Keuer et al., 2004, Hafizovic et al., 2007, Heer et al., 2007, Perelman and Ginosar, 2007].

5.2 Methods

5.2.1 Neuronal cultures

Hippocampal neurons from new-born (P0) mice pups were prepared as previously done [Banker and Goslin, 1998]. Briefly, cells were mechanically dissociated after a treatment with trypsin at 37°C. Then, cells were seeded at 150 cells/mm^2. Standard MEA chips (Ayanda Biosystems SA, Lausanne, Switzerland) with platinum 40 μm round electrodes, 200 μm spaced were used for cell plating. MEAs were previously treated with poly-L-lysine (0.1 mg/ml). Cells were cultured in Neurobasal supplemented with B27 (2%), Penicillin / Streptomycin (P / S, 1%) and L-glutamine (2 mM). 50% medium was changed every week. Spontaneous activity of hippocampal neuronal networks was acquired at 21 days *in vitro* (DIV). These extracellular recordings were carried out with MEA1060 signal amplification and data acquisitions system (Multi Channel Systems MCS GmbH, Reutlingen, Germany). Sampling rate was 25 kHz and each recording lasted 300 s.

5.2.2 Algorithm design

The algorithm, developed in Matlab environment (The Mathworks, Natick, USA), is made up of three focal elements. First of all, an amplitude-threshold spike detector, based on noise level estimation, identifies APs as peaks over threshold. Then APs are bundled into group using PCA. Finally, they are classified with a hierarchical classifier (Figure 5.1).

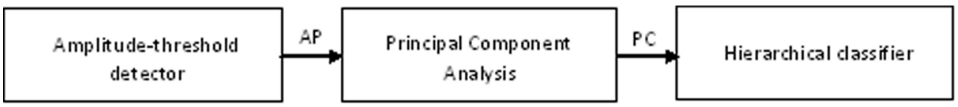

Figure 5.1: Block diagram of the algorithm design.

The whole algorithm was tested first on simulated data and then on neuronal spikes, which were obtained by recording spontaneous activity of hippocampal neuronal networks cultured on MEA substrates. A 60 s simulated signal (Figure 5.2) was artificially made up of both positive and negative triangular waves (each wave was composed by 20 samples). Peak amplitude ranged from 40 to 100 μV. Besides, 2 overlapped and temporally shifted triangular waves, which represent multi-shaped AP in neuronal culture activity, were included in the simulation. The number of

valid spikes, simple and complex waves, was 600. Furthermore, a white Gaussian noise was used to simulate background noise. First, it was band-pass filtered (2^{nd} order Butterworth) between 150 Hz and 2.5 kHz. Then, it was normalized and overlapped to simulated signal. The Signal to Noise Ratio (SNR) was equal to 5 dB, a typical SNR value of neuronal cultures [Bankman et al., 1993].

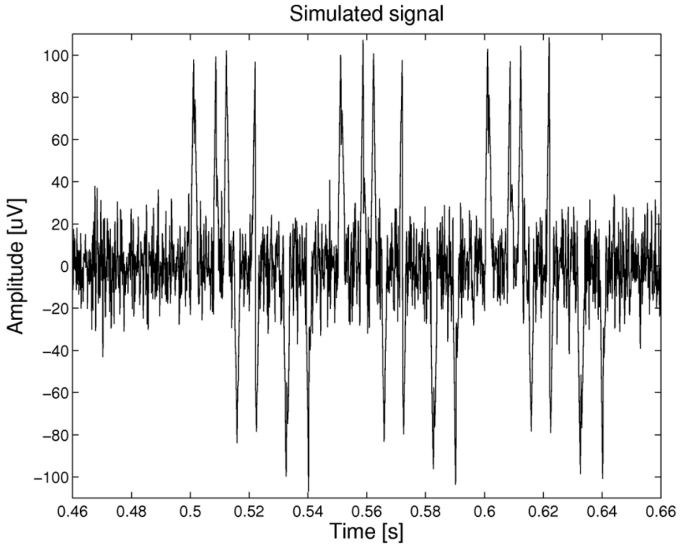

Figure 5.2: Simulated signal (200 ms).

5.2.2.1 Spike detection

The spike detection algorithm is structured as follows. First, the signal is band-pass filtered with a 2^{nd} order Butterworth filter (150 Hz - 2.5 kHz). Then, both positive and negative threshold values are determined as a multiple of noise level estimate. Finally, positive APs over positive threshold and negative APs under negative threshold are detected and validated to prevent double detections of unitary events. A detected peak is tested in $\pm$ 1 ms window. It is checked if that peak is the highest peak of either polarity and if the 50% of its amplitude is higher than other peak of the same polarity [Wagenaar et al., 2005]. If both tests are passed, the detected peak is consider an AP, otherwise it is rejected. Concerning threshold definition, five noise-level estimation algorithms were implemented. Few estimates were suggested by the literature [Wagenaar and Potter, 2004, Wagenaar et al., 2005], others were adapted from it. Then, their performances were compared by means of statistical analysis, to select the best solution.

(a) *BandFlt*. Based on the algorithm described in [Wagenaar and Potter, 2004, Wagenaar et al., 2005], it computes RMS values of three hundred 10 ms windows of data. Then, these values are sorted and the final estimation of noise level is the 25^{th} percentile of this distribution. Positive and negative threshold values are computed

by multiplying noise level estimate by 4. They are equal and fixed.

(b) *Limada* [Wagenaar and Potter, 2004, Wagenaar et al., 2005]. Like *BandFlt*, it splits the data stream into 10 ms windows, and determines the 2^{nd} ($V_{.02}$) and 30^{th} ($V_{.30}$) percentile of the voltage distribution in each window. Then, it performs two tests: it checks if the ratio between $V_{.02}$ and $V_{.30}$ is smaller than 5 (i.e.: no actual spike in the window) and if the absolute value of $V_{.30}$ is significantly non-zero (i.e.: data in the window are not blanked out). If both tests are passed, the window is considered 'clean'. Noise level initial value is defined after the collection of 100 clean windows. Then the current noise level estimate (*NoiseEst*) is updated as (Equation 5.1) :

$$NoiseEst(k) = 0.99 \cdot NoiseEst(k-1) + 0.01 \cdot |V_{.02}| \tag{5.1}$$

where k is the current iteration index. Positive and negative threshold values are computed by multiplying noise level estimate by 4. They are opposite and adaptive.

(c) *AdaFlt* [Wagenaar and Potter, 2004, Wagenaar et al., 2005]. It divides the signal into 10 ms windows and 128 windows of data are read. For each window, maximum and minimum values are measured. Then, results are sorted and the 40^{th} percentile of both collections is computed ($M_{.4}$ and $m_{.4}$). Noise level initial estimates for positive (*NoiseEstP*) and negative (*NoiseEstN*) spikes are based on these data. Thresholds are computed by multiplying noise level estimation by 2. While running, *AdaFlt* keeps collecting minima and maxima in 10 ms windows, although it uses only one every ten windows. Whenever 128 windows have been collected, positive (Equation 5.2) and negative (Equation 5.3) noise level estimates are updated as:

$$NoiseEstP(k) = 0.9 \cdot NoiseEstP(k-1) + 0.1 \cdot M_{.4} \tag{5.2}$$

$$NoiseEstN(k) = 0.9 \cdot NoiseEstN(k-1) + 0.1 \cdot m_{.4} \tag{5.3}$$

(d) *AdaFlt 128* differs from *AdaFlt* because it adapts thresholds after 128 windows, instead of adapting them after 1280. Therefore *AdaFlt 128* is faster and more adaptive than *AdaFlt*, but it suffers more from noise fluctuations.

(e) *AdaBandFlt* is the last algorithm implemented in this work. It is devised as an improvement of *BandFlt* with adaptive properties. It splits the data stream into 10 ms windows, collects 100 windows and calculates RMS values for each window. Then, it determines the 25^{th} percentile of the RMS distribution ($N_{.25}$) and noise level value is initialized. Then, the current noise level estimation is updated as (Equation 5.4):

$$NoiseEst(k) = 0.8 \cdot NoiseEst(k-1) + 0.2 \cdot N_{.25} \tag{5.4}$$

5.2.2.2 Spike classification

After detecting temporal occurrences of APs, validated waveforms must be extracted from data stream applying a 2 ms symmetric window to the signal. Then, their tallest peaks (i.e. time stamps) are aligned, making up a matrix N·c, where N is the number of 'observations' (i.e. neuronal waveforms) and c is the number of samples (i.e. 50 for each 2 ms window). The strong assumption is that neurons usually generate spikes with a characteristic shape on each electrode. Therefore, aim of classification is correlating each source with a characteristic waveform in recorded data. This assumption implies that neurons maintain the AP shape and that the whole system does not move or change.

The classification algorithm proposed here is based on PCA and hierarchical classification. First, PCA finds an ordered set of orthogonal basis vectors that capture the largest directions of data variation [Lewicki, 1998]. Then, APs are grouped by projecting data onto the principal components. Finally, hierarchical classification is used. Hierarchical classifier is a method of cluster analysis that splits N observations into a series of M clusters. M can range from 1 (all observations grouped into one cluster) to N (each observation is a cluster). The strength of this technique is that it gives the possibility of increasing (or decreasing) the number of clusters depending on the required level of aggregation [Abeles and Goldstein, 1977]. Particularly, hierarchical classification algorithm starts with N clusters, each containing just one object. Then, likeness between each couple of observation is evaluated by computing the Euclidean distance between all combinations of cluster centroids. Afterward, data are combined in couples of neighbors and a binary tree diagram is built. Then, these binary clusters are grouped forming bigger clusters until a hierarchical tree diagram is obtained. During grouping, data dispersion (D_i) and center of mass (Cm_i) are computed for each cluster. The hierarchical level, significant for the grouping, was defined when the center of mass distances (Cm_{i-j}) between one cluster ($cluster_i$) and the others ($cluster_j$) was greater than D_i, as in Equation 5.5:

$$D_i < Cm_i - Cm_j \; i, \; j = 1, ..., \; number \; of \; clusters \tag{5.5}$$

After clustering, the number of spikes in each cluster is determined. Generally, clusters should be composed by more than one element. However, it was decided not to constrain the number of elements in each cluster since it's possible that the best data grouping would be characterized by the presence of one cluster with only one element. Therefore, it was preferred to exclude this cluster at the end of classification if needed, avoiding possible inaccurate re-arrangements.

5.2.3 Performance evaluation

Performances of spike detection algorithms were evaluated with statistical screening tests and, subsequently, with the Big O Notation.

5.2.3.1 Algorithm Screening Tests

Performances of the algorithms were statistically evaluated using both simulated neuronal signal (described in Section 5.2.2) and 5 s neuronal activity. Real spikes were previously identified in MEA recordings by experts' visual inspection. Then, a screening test was performed. Briefly, it determined True and False Positives (TPs and FPs) that were, respectively, APs and noise peaks detected. Furthermore, it identified True and False Negatives (TNs and FNs) that were, respectively, noise peaks and APs not identified. Using these 4 parameters the Sensibility (Se), which is the probability that a noise peak could be detected by the algorithm, and the Specificity (Sp), the probability that an AP could not be detected by the algorithm, were computed. Moreover, it was evaluated the Positive Predicted Value (PPV), the probability that a test-positive peak was an AP, and the Negative Predicted Value (NPV), the probability that a test-negative peak was noise. The parameters (Equations 5.6-5.9) are mathematically described as

$$Se = \frac{TP}{TP + FN} \tag{5.6}$$

$$Sp = \frac{TN}{TN + FP} \tag{5.7}$$

$$PPV = \frac{TP}{TP + FP} \tag{5.8}$$

$$NPV = \frac{TN}{TN + FN} \tag{5.9}$$

This evaluation allowed identifying two algorithms with good performances. To choose between them the Big O Notation was used.

5.2.3.2 The Big O Notation

The Big O Notation allows to quantitatively evaluate the performance or complexity of an algorithm as a function of number of its input data. It describes the worst-case scenario, and can be used to illustrate the execution time required or the space used (e.g. in memory or on disk) by an algorithm. This allows designers to select an algorithm among many in a way that is independent of computer architecture or clock rate. The Big O Notation is defined as O(f(N)), where N is the number of input data.

The two best algorithms previously identified were assessed with this method. Particularly, the product between the Big O Notation of each instruction was considered to evaluate nested instructions. Finally, to assess sequentially commands only the worst and the most restraining notation was considered.

5.2.3.3 Classification performances

Performances of classification algorithm were evaluated on simulated signal by knowing the different kinds of waveform artificially designed. Then, they were assessed on real signal. This required visual inspection of neuronal activity (5s signal). Then, results of visual inspection were compared to algorithm outcome.

5.2.4 Hardware architecture

The hardware architecture was designed ad shown in Figure 5.3. The input is filtered, amplified, digitalized and transferred into an FPGA, where spikes are detected. Time stamps and waveforms are memorized in a static RAM (SRAM). Then, they enter a DSP for the spike validation, waveform alignment and classification.

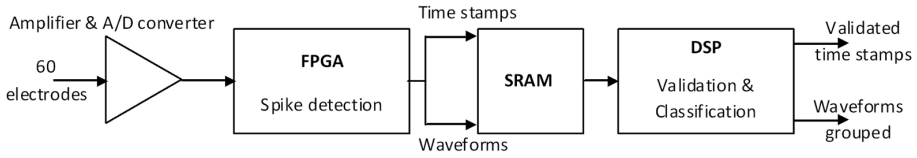

Figure 5.3: Hardware design.

Feasibility of spike detection implementation on FPGA was verified by evaluating the required hardware space in terms of CLB number, memory occupation and timing performances. Furthermore, it was decided to develop PCA on DSP, as suggested by the literature [Han et al., 2004]. Indeed, it was verified that the FPGA core was too slow for this computation [Morizet et al., 2007]. Finally, it was planned to develop also the hierarchical classifier on DSP, as already proposed [Kim et al., 2003].

5.3 Results

5.3.1 Performances of spike detection: Algorithm Screening Tests

5.3.1.1 Algorithm Screening Tests on simulated signal

Algorithm Screening Tests were performed on spikes detected but not validated in simulated neuronal signal. FP and FN values were computed for each algorithm. Results are shown in Figure 5.4A and 5.4B, respectively. *BandFlt* underestimates noise level and identifies more FPs than others. In contrast, it identifies noise level values more stable than standard deviation and only 1 FN, which confirms previous results [Wagenaar and Potter, 2004, Wagenaar et al., 2005]. *AdaFlt* finds the smallest number of FPs but several FNs, because of the excessively slow threshold adaptation. In contrast, *AdaFlt 128* is faster and more adaptive than *AdaFlt*. Accordingly, it identifies a small number of FNs caused by noise fluctuations. Concerning *Limada*, it is quite reliable in threshold identification. Indeed, it finds a small number both of FPs and FNs. Moreover, it is an adaptive method, which is necessary for real time analysis. The main disadvantage is that it needs approximately 5 s to initialize threshold value that causes to lose many spikes. Finally, *AdaBandFlt* method is like *BandFlt* in terms of FNs (i.e. 1 FN) but it finds less FPs and it is an adaptive method. Therefore, it is possible to identify two groups of algorithms: a group characterized by finding most of FPs and really few FNs and a group characterized by finding very few FPs and some FNs.

Then, Se (Figure 5.4C) and Sp (Figure 5.4D) values were computed. Moreover, PPV was evaluated and depicted in Figure 5.5, whereas NPV was not reported because of its low meaningfulness. *BandFlt* and *AdaFlt* were immediately rejected because of their low value of Sp and Se, respectively. *Limada* was selected because it has high Se and Sp; moreover it has the highest PPV. Likewise, *AdaBandFlt* was chosen because its Se is the highest one, even if its SP and PPV are comparable to *AdaFlt 128*. As a matter of fact, the Se parameter was favored and it was preferred to reject some spikes later (after classification) instead of loose true spikes at the beginning of the analysis. This choice was motivated by the future hardware implementation, where spike detection is not reversible.

5.3.1.2 Algorithm Screening Tests on real signal

Algorithm Screening Tests were performed on spikes detected (but not validated) in a 5 s fragment of a 300 s neuronal activity recorded by MEA. FP and FN values were computed for each algorithm. Results are shown in Figure 5.6A and 5.6B, respectively. Then, Sp (Figure 5.6C) and Se (Fig. 5.6D) were evaluated. Perfor-

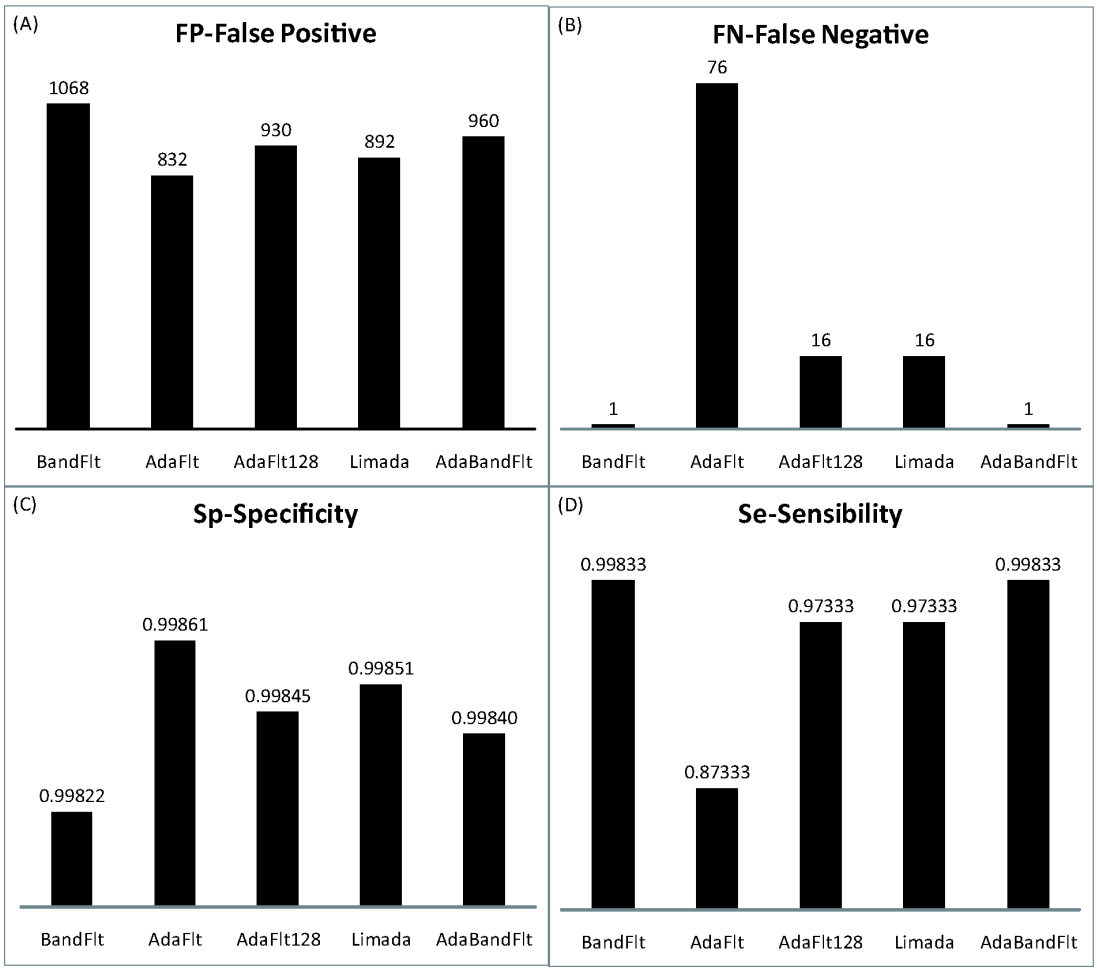

Figure 5.4: Screening test results for noise level estimation methods on simulated signals. (A) FP-False Positive, (B) FN-False Negative, (C) Sp-Specificity and (D) Se-Sensibility.

mance evaluation of spike detection algorithms on real recorded electrical activity agreed with the analysis on simulated signal. *BandFlt* and *AdaBandFlt* find more FPs than other algorithms. On the other hand *AdaFlt*, *AdaFlt 128* and *Limada* lose more APs. Furthermore, differences in Se value become more evident examining neuronal activity. Indeed, performance assessment on experimental data highlights that *AdaFlt*, *AdaFlt 128* and *Limada* has an extremely low sensibility on them. Moreover, differently from what was observed on simulated data, *BandFlt* specificity is equivalent to *AdaBandFl*t on experimental data. However, since the only difference between these two algorithms is in adaptability, it was selected *AdaBandFlt*, being adaptation a crucial requisite for long term acquisitions.

5.3.2 Performances of spike detection: the Big O Notation

Performances of the two best algorithms (i.e. *Limada* and *AdaBandFlt*) were evaluated using the Big O Notation. Specifically, it was considered only the threshold

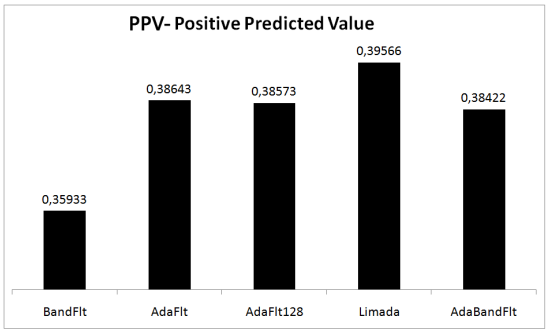

Figure 5.5: PPV-Positive predicted values: evaluation among algorithms.

initialization, which was recognized as the most time consuming step of both algorithms. They are reported in pseudocode in Figure 5.7, to have a compact and high-level description. The O(f(N)) notation (where N is the number of inputs) is noted in bold near each statement.

AdaBandFlt and *Limada* complexity is described by Equation 5.10 and Equation 5.11, respectively:

$$O(100^2 \cdot F) \tag{5.10}$$

$$O(100 \cdot F \cdot N^2) \tag{5.11}$$

considering the worst-case performance scenario. Therefore, if N is bigger than 10 samples, *Limada* has worse performances than *AdaBandFlt*, regardless of hardware. Since 10 samples are few for a reliable threshold identification, *AdaBandFlt* was selected as the noise level estimation method which fulfills all requirements.

5.3.3 Hardware architecture feasibility

To verify the feasibility of *AdaBandFlt* implementation on FPGA, CLBs number, memory occupation and timing were evaluated. Figure 5.8 shows a block architecture to compute threshold values for 1 channel. The input is a 12 bit data stream, coming from an analog to digital converter (ADC). To compute the threshold, the system has to evaluate the RMS value of 250 samples (i.e. 10 ms windows, assuming a sample frequency equal to 25 kHz). Then, the system has to collect 100 RMS values and sort them. The threshold is the 25^{th} percentile of this ordered distribution. Note that the algorithm was simplified with the following assumptions:

(a) squared RMS values (i.e. MS) were used and compared to squared samples, which avoided computing the root (Equation 5.12):

$$25^{th}percentile(MS) = (25^{th}percentile(RMS))^2 \tag{5.12}$$

(b) the problem of division using FPGA was skipped out by rounding 250 samples

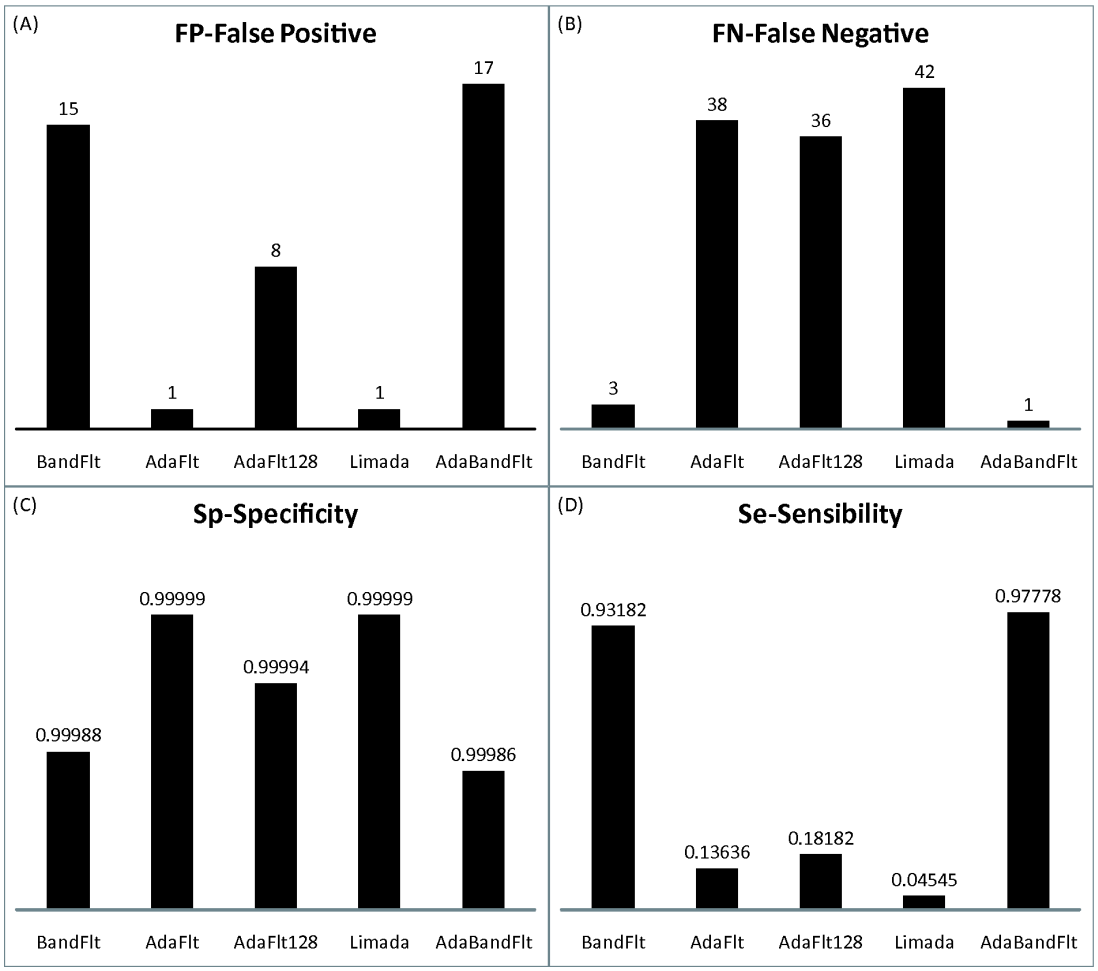

Figure 5.6: Screening test results for all the noise level estimation methods on neuronal spikes. (A) FP-False Positive, (B) FN-False Negative, (C) Sp-Specificity and (D) Se-Sensibility.

to 256 (i.e. 2^8). This allowed to divide by 256 just shifting the decimal point of 8 positions.

Therefore, input enters the embedded multiplier 18 x 18 and its output is a 24 bit word (one more bit was used to keep track of sign). Then, it is recursively added to other samples. To perform the sum, the adder utilizes an accumulator, intrinsically controlled by a finite state machine, shared with all channels. The division result is, in the worst case, a 32 bit word, 24 bits before the point and 8 bits after the point. To a first approximation, MS value can be defined by the first 24 bits. In terms of hardware occupation, to compute a MS value it is needed:

- 1 differential IOB
- 1 embedded multiplexer
- 32 LUTs for the adder [XILINX-Inc., 2009] and 32 flip-flops for the accumulator, i.e. 4 CLBs
- 1 32 bit shift register, i.e. 2 CLBs
- 1 CLB for the finite state machine.

```
AdaBandFlt
number_of_samples=0;
number_of_windows=0;
F; // definition of sample frequency //
while number_of_windows < 100 do                                   O(100)
        while number_of_samples < F*0.01 // define a 10ms window//  O(F*0.01)
                take a sample
                number_of_samples ← number_of_samples + 1;
        end
        compute the RMS and put it in a vector named "error"       (1)
        number_of_windows ← number_of_windows + 1;
end
BubbleSort(error) // sort the vector of 100 RMS //                 O(100²)
define the threshold initial value (25th percentile)               O(1)

Limada
number_of_samples=0;
number_of_windows=0;
threshold_init=0;
F; // definition of sample frequency //
ok=false;
while ok == false do //ok is false until 100 clean windows are collected //   O(N)
        while number_of_samples < F*0.01 // define a 10ms window //            O(F*0.01)
                take a sample
                number_of_samples ← number_of_samples + 1;
        end
        BubbleSort(samples) //sort the voltage values of a window //          O(100²)
        compute the 2nd (V.02) and the 30th (V.30) percentiles                O(1)
        if number_of_windows < 100                                            O(N)
                test= V.02/ V.30;                                             O(1)
                if test < 5 & |V.30| is significantly non zero                O(1)
                        threshold_init ← 0.99* threshold_init + 0.01*|V.30|
                        number_of_windows ← number_of_windows + 1;
                end
        else ok==true; // 100 clean windows are collected //
        end
end
```

Figure 5.7: Pseudocode for *AdaBandFlt* and *Limada*.

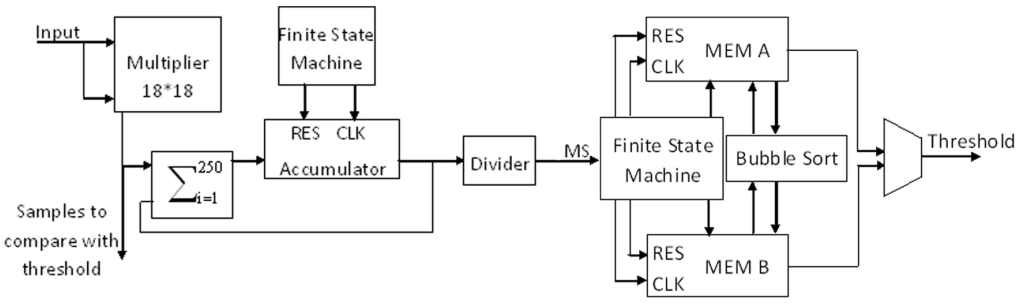

Figure 5.8: Architectural blocks to compute a threshold value.

After computing MS value, it is memorized. Specifically, first 100 MS values are memorized in MEM A and second 100 MS values are memorized in MEM B, while

values contained in MEM A are sorted by BubbleSort logic. The following step is dual: MEM A is filled while values in MEM B are sorted. This is controlled by a finite state machine, shared with all channels. Furthermore, the finite state machine manages the computation of the 25^{th} percentile index, counted as follows (Equation 5.13):

$$I_k = (0.5 + n \cdot {}^{k}/_{100}) \tag{5.13}$$

where n is sorted vector length and k the k-th percentile.

Therefore, in this instance I_k is about 25 ($n = 100$ and $k = 25$). Since computing the 25^{th} percentile means choosing the 25^{th} sample in sorted vectors, the first value of threshold comes out from MEM A, the second from MEM B and so on. In terms of hardware occupation, to compute a threshold value it is needed:

- 1 CLB for the finite state machine
- 2.3 kbits of RAM for each memory block (i.e. 4.6 kbits)
- 50 CLBs for BubbleSort (i.e. $N/2$ pipelined stages, where N is the length of sorted input vectors) [Benkrid and Crookes, 2003]
- 24 2:1 multiplexers.

After computing the 24 bit threshold value, the system places it into a 24 bit RAM location, named Thres_{k-1} in Figure 5.9. Likewise, it places a following threshold value in Thres_k. Then, threshold values are updated as in Equation 5.4. Briefly, Thres_{k-1} is multiplied by 4 (i.e. shifted left of 2 positions), added to Thres_k and multiplied by 0.2. Finally, Thres_k becomes Thres_{k-1} and a new threshold is memorized in Thres_k location. These operations are controlled by a finite state machine, shared with all channels. In terms of hardware occupation, to update the threshold value it is needed:

- 48 bits of RAM
- 1 CLB for the finite state machine
- 1 32 bit shift register, i.e. 2 CLBs
- 3 CLBs for the adder
- 5 CLBs for the multiplier.

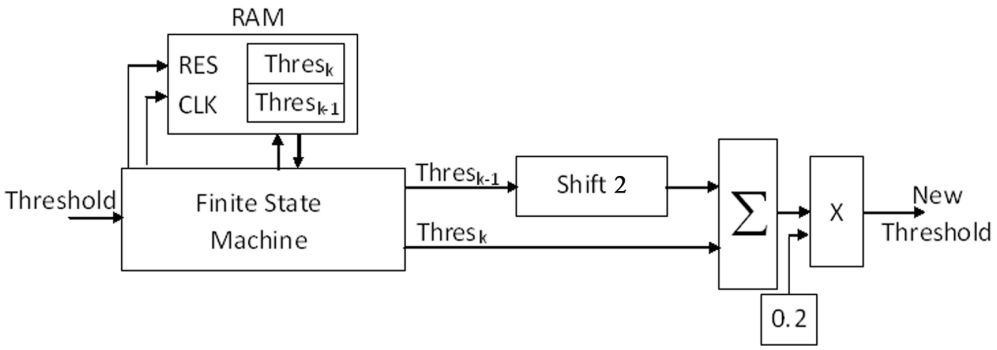

Figure 5.9: Hardware blocks to update the threshold.

Pipelined with threshold counting, the system detects spikes. First, it compares the i-th squared sample with threshold to find over-threshold values. Then, it verifies if the detected value is a maximum (or a minimum), as shown in Equation 5.14. Furthermore, it was decided to realize these comparisons subtracting each couple and looking at the sign. Thus Equation 5.14 can be re-written as follows (Equation 5.15)

$$|x_i^2| > |Thres| \;\&\; |x_i^2| > |x_{i-1}^2| \;\&\; |x_i^2| > |x_{i+1}^2| \tag{5.14}$$

$$PS(|x_i^2| - |Thres|) \;\&\; PS(|x_i^2| - |x_{i-1}^2|) \;\&\; PS(|x_i^2| - |x_{i+1}^2|) \tag{5.15}$$

where PS checks if values inside brackets are positive signed.

This could be realized using 1 LUT for each couple of compared bits. Moreover, additional XOR and AND gates are required to compare complete words [Kumar and Chong, 2008]. Approximately, 3 CLBs are needed for each comparison (24 bit words), that means 9 CLBs for a detection.

With the design outlined above, it was estimated FPGA occupation. Taking into account 64 MEA channels, *AdaBandFlt*, mapped on FPGA, requires

- 64 differential IOB
- 64 dedicated multipliers
- 4803 CLBs
- 291 kbits of RAM
- 1536 dedicated 2:1 multiplexers.

Therefore, two suitable solutions were identified for *AdaBandFlt* implementation. The first one requires the use of a single FPGA. It was identified the device XC3S5000 of Xilinx Spartan-3 family, whose architecture fulfills the requirements:

- 300 differential IOB
- 104 dedicated multipliers

- 8320 CLBs
- 1872 kbits of block RAM
- 65 k 2:1 dedicated multiplexers.

This gives a FPGA utilization around 58%, which seems a comfortable margin [Xilinx Manual, 2009]. Furthermore, RAM occupation was analyzed in detail. A suitable organization of memory for these data is 512 x 32 bits. Block RAM of XC3S5000 device is ordered in 104 blocks of 18 kbits. Therefore, it was considered to use one block for each couple of RAM A and RAM B used to compute threshold values (one block for each channel). Specifically, RAM A can be addressed from 1 to 100 and RAM B from 101 to 200. This allows to sort RAM A and to fill RAM B almost contemporaneously. Besides, even if XC3S5000 is the biggest device within Spartan-3 family, it is not too expensive (less than $120).

The second solution envisages the use of a smaller FPGA, XC3S4000 (Xilinx Spartan-3 family). Specifically it is required to use one device every 32 channels. Indeed, each FPGA contains:

- 300 differential IOB
- 96 dedicated multipliers
- 6912 CLBs
- 432kbits of distributed RAM, organized in 96 18kbit blocks
- 54k 2:1 dedicated multiplexers.

This gives a FPGA utilization around 35%. Differently from the first solution, this design allows a modular approach, useful for future improvements. Furthermore, this device is rather cheap: in 2004, the volume pricing was under $100 for 250 XC3S4000 devices [Xilinx Manual, 2003].

Finally, BubbleSort was identified as the bottleneck of this architecture and, thus, it was evaluated in terms of temporal requirements by verifying if its timing was consistent with other operations. To sort a n-length vector, bubble sort makes n-1 steps through the data. In each step, adjacent elements are compared and swapped if necessary. Notice that after the first pass through the data, the largest element in the sequence has bubbled up into the last array position. In general, after k passes through the data, the last k elements of the array are correct and are not considered any longer. A preliminary estimate hypothesized 3 clock cycles for each comparison, $n/2$ clock cycles for each couple of values in the vector and $n-1$ clock cycles for the whole sorting [Preiss, 2009]. Therefore, the device needs about 15000 clock cycles to sort a 100 elements vector. This means that it takes about 1.5 ms for each sort operation, even considering a slow FPGA (e.g inner frequency equal to 10 MHz). Since device sorts a vector after collecting 100 windows of 250 samples each, there is a 500 ms delay between two sorting steps, even considering the maximum sampling frequency (i.e. 50 kHz) of the data acquisition system. Hence, that gives a secure

margin. Besides, $n-1$ passes through the data are required to guarantee that the list is sorted in the end but it is possible for the list to become sorted much earlier. When no exchanges at all are made in a given pass, then the array is sorted and no additional steps are required. A minor algorithmic modification would be to count exchanges made in a pass, and to terminate the sort when no exchanges are performed.

5.3.4 Performances of spike classification

5.3.4.1 Spike classification on simulated signal

Spike detection algorithm was applied to simulated neuronal signal and detected APs became the input of the classification algorithm. First, they were projected along the first two principal components (Figure 5.10A) to get APs into separated groups. Indeed, it was already demonstrated that 1^{st} and 2^{nd} component eigenvalues can represent useful characteristics of classification [MacNabb, 2003]. Then, hierarchical classifier provided an accurate classification (Figure 5.10B). The algorithm identified 6 clusters plus one single element cluster (i.e. formed by only one element), which was rejected after the analysis. Figure 5.10C shows all classes: five of them match exactly waveforms that were artificially made up in the simulated neuronal signal. Furthermore, the yellow cluster is formed by two data groups (i.e. data projections around zero in Figure 5.10A and 5.10B) which represent clusters of false positive detected spikes. Indeed, their peak-to-peak amplitudes are less than 30 μV. Therefore, the classification was satisfactory and allowed rejecting FPs, which were classified all together. This is an important feature considering that a less specific spike detection algorithm had been chosen not to lose spikes. The final goal was the signal reconstruction using classified waveforms. Figure 5.10D depicts reconstructed simulated signal. It is possible to single out all waveform morphologies previously made up in the simulated neuronal signal.

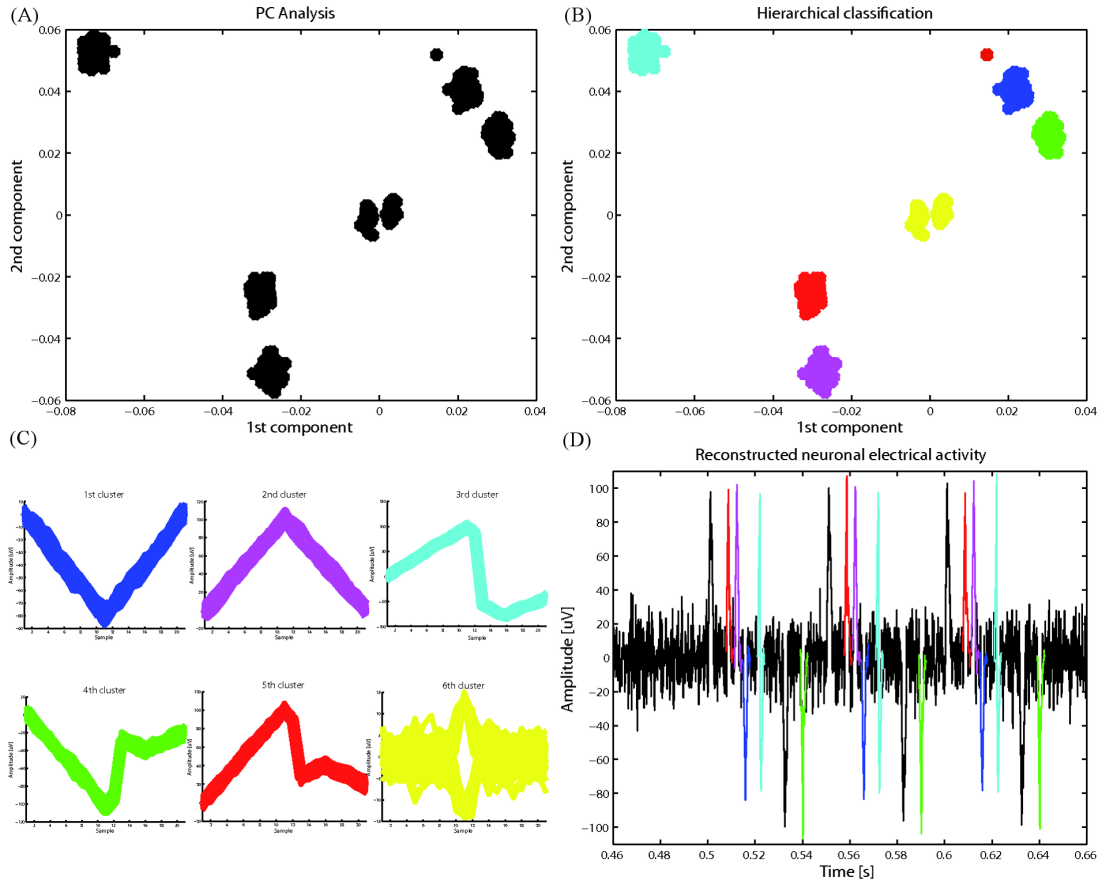

Figure 5.10: (A) Simulated data projected along the first two principal components. (B) Simulated data grouped and classified in the principal component space. (C) Six clusters identified by hierarchical classification. (D) Reconstructed simulated signal (200 ms).

5.3.4.2 Spike classification on real signal

Spike detection algorithm was applied on 300 s real data. Then, hierarchical classification was performed. Classifier performances were evaluated by visual inspection on a portion of signal (5 s). Figure 5.11 depicts an example of 5 s neuronal electrical activity . Furthermore, Figure 5.12A and 5.12B show waveform projections on the 1st and the 2nd component eigenvalues and data hierarchical classification, respectively.

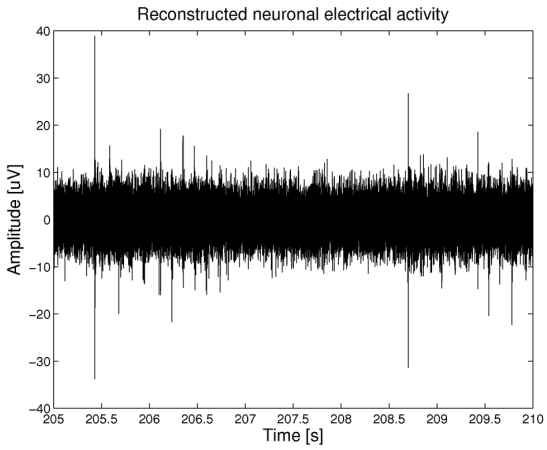

Figure 5.11: Neuronal electrical activity (5 s) recorded by MEA60 acquisition system.

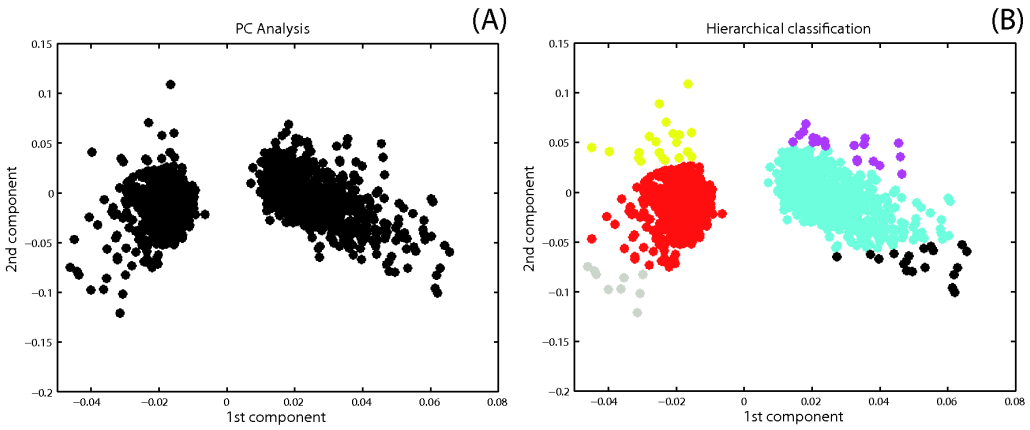

Figure 5.12: (A) Electrical activity projected along the first two principal components. (B) Hierarchical classifier output. Real data grouped and classified in the principal component space.

Figure 5.13 shows clusters that were identified. Amplitudes and morphological characteristics of each cluster are different. Note that the algorithm distinguishes false positive spikes also within real signal (Figure 5.13C and 5.13D, clusters centered around zero in the principal component space). Finally, the neuronal electrical activity was reconstructed. Figure 5.14 depicts a 5 s segment of activity. It is possible to clearly distinguish red and light-blue spikes, that represent positive and negative noise clusters, respectively. Furthermore, biphasic with no extreme polarization APs (yellow group), few biphasic and positive raised pink APs and some black peaks (essentially monophasic 40µV waveforms) can be observed.

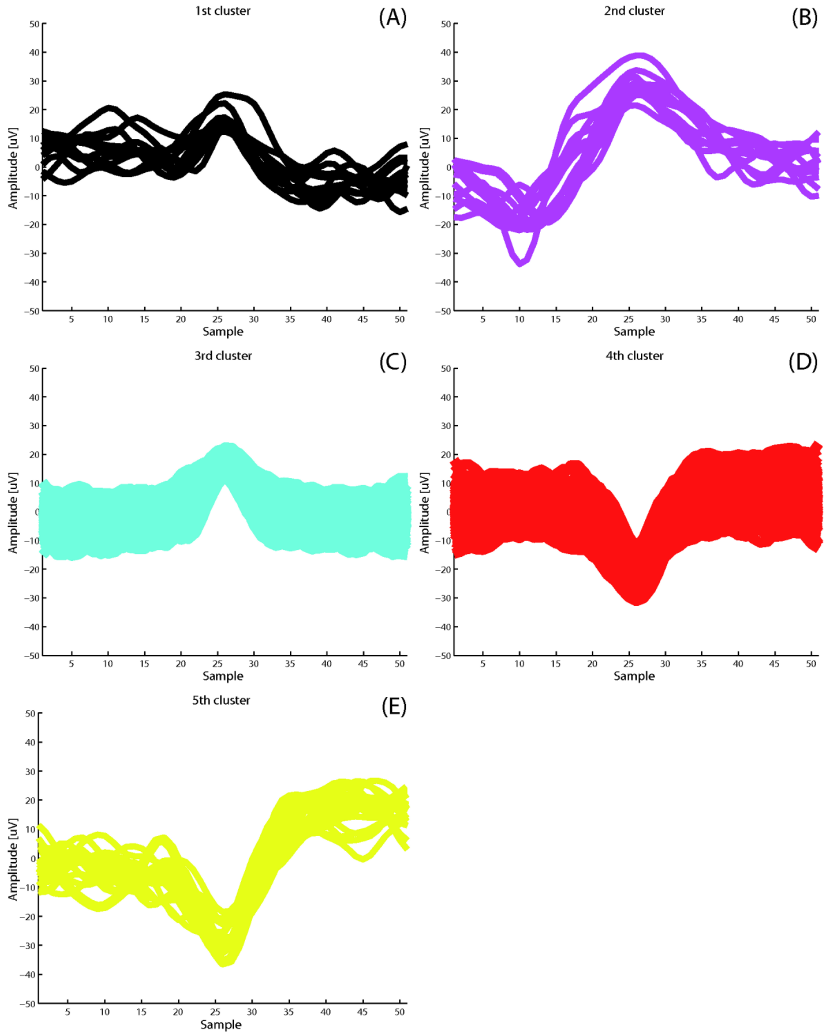

Figure 5.13: Clusters identified within 5 s of real neuronal signal.

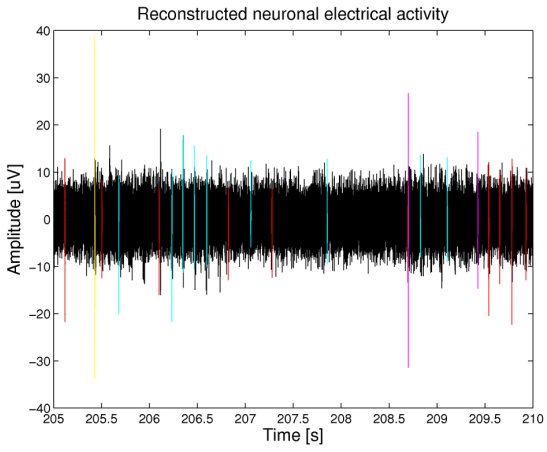

Figure 5.14: Reconstructed neuronal activity (5 s).

5.4 Discussion

In the context of extracellular electrophysiology, an efficient and reliable identification of spikes has to be reached. Furthermore, it is important to distinguish between application-specific and generalized methods [Maccione et al., 2009]. In this chapter an application-specific algorithm have been proposed. Specifically, it aims at future hardware integration (on FPGA and DSP) for real-time long term acquisitions. The threshold-amplitude spike detection method computes threshold as a multiple of basal noise level. Five noise estimation methods were developed in Matlab (The Mathworks, Natick, USA) and their performances were statistically evaluated, both on simulated neuronal signal and on real electrical activity, recorded by MEA1060 (Multi Channel Systems MCS, Gmbh).

The adaptability and sensitivity (minimum number of false negative) had priority when choosing the optimum spike detection method. The former is required due to the noise level drift on a time-scale of hours. The latter is needed because of the non-reversibility of spike detection procedure. Statistical analysis identified two algorithms that satisfied these requirements, *AdaBandFlt* and *Limada*. Then, their performances were evaluated by using the Big O Notation. This determined the minor complexity of *AdaBandFlt*. Furthermore, since long term recording analysis is the final goal, spike detection must be adaptive, unsupervised and fast. Hence, this task could clearly benefit from the acceleration achievable with FPGAs. Therefore, hardware requirements of the spike detection algorithm developed here were assessed in terms of CLBs number, memory and timing request. Two feasible solutions were identified: the first one envisages the use of XC3S5000 (Xilinx Spartan-3) that satisfies hardware requirements for all channels. The second solution allows modular assembling using two smaller FPGAs (XC3S4000, Xilinx Spartan-3), each for 32 channels. Concerning the spike classification algorithm, an automatic and reliable shape clustering was favored. After spike detection, the algorithm extracts waveforms and sorts them around time stamps. Then, it bundles waveforms into groups with PCA and classifies APs with a hierarchical classifier. The classification algorithm was tested on simulated signal, comparing its output to the artificially designed waveforms. Furthermore, it was evaluated on real data, comparing results with visual inspection of waveform morphologies. The analysis on both simulated and real data stated the quality of the clustering procedure. Finally, it was decided to develop PCA and hierarchical classifier on DSP, as already done in literature [Kim et al., 2003, Han et al., 2004, Morizet et al., 2007].

To conclude, the spike detection and classification algorithm developed here shows the highest performances in order to achieve long period recordings of neuronal electrical activity. Particularly, it avoids data leakages and allows hardware

implementation. Furthermore, the final aim is to develop an integrated hardware which is composed of FPGAs and DSPs. Thanks to high speed hardware devices, post-processing can be executed on-line, just keeping time stamps and waveforms and, thus, reducing data storage problems. So far, the feasibility of spike detection design on FPGA was verified and its hardware implementation is ongoing.

Chapter 6

A new descriptor of neuronal connectivity[1]

It is now ascertain that many pharmacological compounds act through multiple targets by affecting indirectly multiple pathways. This implies that the modulation of a receptor or a channel function has complex consequences on functionality of target cells. Particularly, this occurs on integrated neuronal systems, where cellular properties are influenced by the physiology of the biological context. All these considerations support the current idea that effects of a potential drug for Central Nervous System (CNS) pathologies is fully valuable only in physiological models. For these reasons, modern drug discovery has started focusing attention on *in vitro* models as complex neuronal networks, moving from the classical study of single channel expressed in a heterologous system to more physiological models. Indeed, reconstituted networks *in vitro* maintain a large scale of complexity remaining pharmacologically histiotypic and providing reliable, quantitative data on drug interactions with neuronal tissues [Morefield et al., 2000]. Again, the approach to study these complex systems and their activity is represented by neuronal networks cultured on Micro Electrode Arrays (MEAs). In this framework, spike detection procedure (Chapter 5) and standard data analysis (Section 2.4 and 3.2.4) are necessary steps. Another important point is the definition of simple parameters able to take into account the behavior of a neuronal network as a whole. Section 2.4 presented classical parameters which were described in the literature. These are able to well characterize spontaneous electrophysiological activity. In contrast, when the focus lies on neuropharmacology, a validation on a single comprehensive and high sensitive parameter still lacks.

This chapter deals with the development and implementation of an intra Network

[1]The work has been published as **Biffi E**, Menegon A, Regalia G, Maida S, Ferrigno G, Pedrocchi A. A new cross-correlation algorithm for the analysis of "*in vitro*" neuronal network activity aimed at pharmacological studies. *J Neurosci Methods*, 2011, 199(2): 321-327.

Burst (NB) correlation analysis which aims at providing a method for the evaluation of neuronal network functionality. The goal is to extract a quantitative unitary index of global level of network activity by a correlation analysis computed during network burst phenomena. In order to evaluate the sensitivity of the method, cortical cultures were processed in presence of bicuculline (BIC) in maximal and sub-maximal concentrations. Then, algorithm potential use in pharmacological studies was investigated by means of γ-aminobutyric acid (GABA) additions. Results demonstrated the high sensitivity of this analysis and the efficacy of this method in pharmacological dose-response studies. A strength of this methodology is the possibility of analyzing drug effects on the comprehensive correlative properties of integrated neuronal networks. Finally, at the end of the chapter, it is discussed the opportunity of using this algorithm for the study of drugs able to alter network correlation properties (e.g. antiepileptic drugs, anxiolytics). The project was carried out with the Advanced Light and Electron Microscopy Bio-Imaging Center (San Raffaele Scientific Institute, Milan).

6.1 Cross correlation in *in vitro* neuropharmacology: state of the art.

Effects of potential drugs can be studied looking at the functional changes induced in a neuronal network in terms of spiking and bursting activity [Gramowski et al., 2005]. Furthermore, drug addition can modulate network structural information, investigated by means of statistical methods as Granger causality [Cadotte et al., 2008], non linear correlation [Esposti and Signorini, 2008] and information theory-based methods [Garofalo et al., 2009]. One of the basic approach requires an estimate of the cross-correlation (CC) function between pairs of spike trains. Specifically, it measures the probability $C_{XY}(t)$ of observing a spike in a train Y at time t (called the time lag), knowing that there was a cuncurrent spike in a train X [Knox, 1981]. The inability to record intracellular signals from many neurons *in vitro* makes the CC analysis a useful tool for assessing internal parameters of a neuronal system when using extracellular electrical activity recordings [Knox, 1974]. Moreover, it is a simple method for studying synaptic interactions within nervous system by identifying neuronal causal relationships [Knox, 1981, Salinas and Sejnowski, 2001]. Finally, it could be seen as a tool to understand inner qualities of neuronal cultures and their functional connectivity [Knox, 1974, Baruchi et al., 2006, Rubinsky et al., 2007, Baruchi et al., 2008, Garofalo et al., 2009]. CC, computed on the whole spike train sequence, is widely used in the literature to detect neuronal interactions [Knox, 1981], to study network functionality modifications [Sokal et al., 2000, Li et al.,

2007a], to quantify reproducibility of correlated spike timing [Tateno and Jimbo, 1999] and to evaluate correlation changes during network maturation [Chiappalone et al., 2006, 2007]. Furthermore, correlative and pharmacological approaches can be coupled. These offered the unique opportunity to address basic questions about network synchrony and its relationship with the processing of information and sensory coding. Accordingly, with these techniques network maturation mechanisms were explored [Chiappalone et al., 2006, Li et al., 2007a], spontaneous and evoked neuronal activity features were deepened [Eytan et al., 2004] and neuronal information processing was studied [Segev et al., 2004, Bonifazi et al., 2005].

Since it is possible to strongly change the synchronization level of the neuronal population in terms of burst pattern by using different kind of pharmacological manipulation [Chiappalone et al., 2007], network burst phenomena can be identified as an important target of drug modulation. Particularly, the intrinsic balance of excitatory and inhibitory connections can be pharmacologically modulated. Furthermore, a recent study by Baruchi and Ben-Jacob [Baruchi and Ben-Jacob, 2007] shows the possibility to understand learning and memory by means of local chemical stimulation, looking for induced persistent alterations in the correlative patterns of neuronal firing.

In the literature, however, the different approaches closed on CC were proposed over specific testing platforms. Moreover, it is not frequent to find a study in which the effect of a small dose of a drug is explored through the analysis of the CC, but usually they are limited to the investigations of the drug effect at maximal concentration. In order to be used in pharmacological studies for CNS pathologies, CC analysis should benefit from the definition of a simple parameter able to take into account the behavior of the integrated neuronal network as a whole and to distinguish between the effects of different drug concentrations.

6.2 Methods

6.2.1 Neuronal preparation

Primary neuronal cultures were obtained from CD1 mice at E17.5. Brains were dissected in cold HBSS (Hank's balanced salt solution; Gibco) supplemented with Glucose 0.6% and 5 mM Hepes pH 7.4 (Sigma). The cerebral cortices of embryos were removed and mechanically dissociated in single cells by using fire-polished Pasteur pipettes. Then, cells were re-suspended in culture medium containing 50% D-MEM (Dulbecco's modified eagles medium; Gibco); 50% Ham's F12 (Gibco); 5 mM Hepes pH 7.4; 0.6% Glucose; 1% Glutamax (Invitrogen); 30 nM Na-Selenite (Sigma); 20 nM Progesterone (Sigma); 60 nM Putrescine (Sigma); 100 μg/ml Trans-

ferine (Sigma) and 5 μM Insulin (Sigma). Dissociated cells were plated at 700 cells/mm^2 on autoclaved MEA chips (electrode spacing 200 μm, electrode diameter 30 μm; Multi Channel Systems, MCS GmbH, Reutlingen, Germany), treated overnight with poly-L-lysine (2 mg/ml) and laminin (10 μg/ml; Sigma) and made more hydrophilic by a 4 hours treatment with plating medium (NeuroBasal medium + 10% Fetal Bovine Serum + 1% Penicillin and Streptomycin). Cells were maintained in a humidified incubator (5% CO2, 95% air, 37 $^\circ$ C) and half of the medium was changed weekly.

6.2.2 Electrophysiological recordings

Extracellular recordings were carried out with a MEA1060 signal amplification and data acquisition system (Multi Channel Systems, MCS GmbH, Reutlingen, Germany) at 37°C, defining the sampling rate at 25 kHz. Single recordings started right after the stabilization of the electrical signals, verified by visual inspection, minimizing the interference of mechanical disturbances. On average, the time to reach stability was 10 minutes. Recordings lasted 5 minutes and were replicated twice. These repetitions were exploited to assess stability (Mann-Whitney test $p>0.05$); hence, the analysis were performed on the first dataset. After raw data recording, spikes were detected using MC Rack Software (Multi Channel System, MCS GmbH); the spike detection threshold for each channel was set to seven times the standard deviation of average noise amplitude computed during 500 ms at the beginning of each measurement. The dead time value was set equal to 3 ms.

6.2.3 Pharmacological protocols

The electrical activity of 10 cortical cultures was recorded at 13 days *in vitro* (DIV). Sequential 5 minutes recordings of electrical activity were performed for each chip. Chemical compounds were added to the medium in the correct amount to reach the desired concentration. Indeed, it was decided to avoid the medium change to reduce the cellular stress. Each recording started after 2 minutes from the addition of the drug in order to allow its diffusion and to reach the plateau phase of the maximal effect of the dose (data not shown). The first experiment was carried out with different concentrations of bicuculline (a GABA receptor antagonist): absence of BIC, BIC 1 μM (sub-maximal concentration; EC50: 0.03-3 μM [Feigenspan and Weiler, 2004, Gramowski et al., 2005, Willumsen, 2006] and BIC 20 μM, a concentration able to induce the maximal pharmacological effect (data not shown) [Gramowski et al., 2005]. As reported in the literature, $GABA_A$ receptor blockade by BIC induces a transition from a native pattern into a rhythmic activity, coordinated within channels, with an increase of firing and burst rates on all electrodes [Khatami et al.,

2004, Gramowski et al., 2005]. The second pharmacological protocol was aimed at measuring GABA concentration-response curves. GABA, the physiological GABA receptor agonist, was added to cultures in 7 increasing concentrations (in μM): 0.01, 0.1, 0.3, 1, 3, 10 and 100. Electrical activity of 3 cortical cultures was recorded for 5 minutes starting after 2 minutes from GABA addition in order to allow the diffusion of the drug.

6.2.4 Algorithm description

6.2.4.1 NB identification

The first step of the intra NB correlation method presented here is the automatic detection of NB events as shown in [van Pelt et al., 2005, Chiappalone et al., 2005]. The method takes advantage of the property that both the number of active sites and their firing rate increase during NBs. Specifically, the signal is divided in 25 ms bins and the product of number of active sites and of total spikes is computed for each bin, highlighting significant peaks related to NB events. A threshold method is applied to identify the initial and the final points of the NB; bins belong to a NB if the computed product in that NB is bigger than 9 (i.e. the threshold value suggested in the literature) and if other bins over threshold are present within 2 s (maximum intra NB interval is 2 s [Pasquale et al., 2010]). Finally, only NBs that involve more than 80% of total active electrodes are chosen, as previously done by Segev and co-workers [Segev et al., 2004] and the remaining recorded data are discarded.

6.2.4.2 CC definition

The second step of the method, formed by a convolution stage and a CC evaluation stage, is performed for each selected NB. Specifically, spike trains belonging to each NB are convoluted with a Gaussian function with $\sigma = 0.2$. This value was chosen by authors considering the firing rate as done by [Segev et al., 2004]. Indeed, taking into account that sample and hold frequency is equal to 1/3 ms^{-1}, depending on MCRack windowing during the spike detection process (see Section 6.2.2), $\sigma = 0.2$ means that the Gaussian full width at half maximum is equal to 1.4 ms and that the maximal width of the function is about 30 ms. Since 10-25 Hz is a standard range of spiking rate [Stevens and Zador, 1998, Chiappalone et al., 2008], the time distance between two spikes is about 70 ms. Consequently, low frequency spikes are not combined by convolution, while spikes belonging to higher frequency periods, as bursts activity (60 Hz [Chiappalone et al., 2006]), are partially merged. Tests on data with different σ values confirmed that below 0.15, the convolution follows the shape of the whole raster plot even when firing rate is very high. On the other

hand, values of σ bigger than 0.4 smooth the raster plot preventing to discriminate neighboring spikes. Therefore, σ equal to 0.2 is a trade-off concerning temporal resolution. After Gaussian convolution, the algorithm computes the continuous CC on each NB and asks the user to select the delay value for the analysis. In this work the algorithm was validated by extracting values in $\tau = 0$ ($C_0(i,j)$), usually employed as a measure of synchronization [Baruchi et al., 2006, Chen et al., 2006, Rubinsky et al., 2007] between activities of the i-th and the j-th channels within the same NB. To assess the global network activity, the parameter Total Corr was selected. Total Corr for the x-th NB, i.e. NB_x, was defined as (Equation 6.1):

$$Total\,Corr_{NB_x} = \frac{1}{ac_{NB_x}} \cdot \sum_{i} \sum_{j \neq \mathrm{i}} C_0(i,j) \tag{6.1}$$

where ac_{NB_x} is the number of active channels in the NB_x and i ,j indicates each couple of channels in the NB_x. $Total\,Corr_{NB_x}$ represents the normalized integral of the correlation matrix of active channels for each NB. For each culture, the median of $Total\,Corr_{NB_x}$ on all the NBs (MTC) was kept as the outcome measure of the network activity. The algorithm was implemented in Matlab (The Mathworks, Natick).

6.2.5 Shuffled data

To have a basal measure of correlation, CC matrix was computed on shuffled data, determined for each experimental condition. These data were generated simulating random NBs that shared, with the corresponding experimental data, the number of spikes for each electrode and for each NB, but with shuffled interspike interval distribution [Perkel et al., 1967]. Specifically, signals with a variable number of spikes (from 1 to 1000) were simulated, 1000 repetitions apiece (mean length and frequency comparable to NBs length and frequency, by visual inspection), and MTC was computed, obtaining a reference look up table (LUT), whose elements referred to couples of channels with a specific number of spikes.

6.2.6 Statistical analysis

Statistical analysis was divided into three phases. First, MTC values computed on neuronal recordings were compared to MTC values computed on shuffled data using a Mann-Whitney test to validate the results obtained [Pasquale et al., 2008]. Indeed, if the MTC value computed on the original data is significantly different with respect to the MTC value computed on the shuffled data, then real data and shuffled data are uncorrelated, being the MTC value of original data significant with respect to randomness [Perkel et al., 1967]. Second, each experimental dataset was

evaluated in term of differential MTC with respect to its corresponding shuffled data (extracted from the LUT). This was done by subtracting the MTC values computed for the equivalent shuffled data (with the same number of spikes in each channel and in each NB), from the MTC values determined on neuronal recordings. This means that the MTC values computed for each NB were purified from the random and non authentic information. Then, a non-parametric statistical analysis (Wilcoxon matched pair test) between values of MTC in the untreated and bicuculline-treated conditions was performed. Third, the total number of spikes [Anschel et al., 2004] and MTC values, extracted from recordings after GABA additions, were used to realize mean concentration-response curves. Curves were normalized to the maximum response, obtained with saturating concentration of GABA. Non-linear regression was used to fit data in a variable slope sigmoidal model with a 95% confidence interval (Prism, GraphPad Software Inc.) and the range of concentrations causing 50% of the maximal response (EC_{50}) was observed. The goodness-of-fit was assessed using the Coefficient of Determination R^2. Data are given as median and its variation stated as percentiles (25^{th} and 75^{th}). Concentration-response curves are shown as mean ± SEM. Statistical analysis was performed by Statistica (StatSoft Inc). The significance level was established at $p < 0.05$.

6.2.7 Comparative cross-correlation analysis

To assess the reliability of MTC, its results were compared to the mean firing rate (MFR) after BIC additions. MFR was selected because it is widely used in the literature to assess network features [Khatami et al., 2004, Martinoia et al., 2005, Chiappalone et al., 2006, 2008, Berdondini et al., 2009b, Garofalo et al., 2009]. Indeed, this parameter is considered one of the most consistent and repeatable characteristic for neuronal cultures. Therefore, the correlation between MFR and MTC values was computed and a non-parametric analysis on MFR during BIC additions was performed. Moreover, correlation-based methods to test the dataset used were identified among an extensive literature survey of algorithms concerning functional correlation and connectivity. Thus, the sensitivity of the algorithm proposed was compared to the algorithm described by Li and co-workers [Li et al., 2007a], in the following indicated with Li, and the method illustrated in [Tateno and Jimbo, 1999, Eytan et al., 2004, Chiappalone et al., 2006, 2007], indicated with TJ. These two algorithms were implemented in Matlab (The Mathworks, Natick, USA) and were applied to the same dataset.

6.2.7.1 Li method

Li and colleagues introduced cross-correlation function to explore the contribution of inhibitory and excitatory connections during development, comparing bicuculline-induced firing patterns with spontaneous activity. In this work, authors studied the network functional changes induced by a maximal dose of BIC (10 μM) [Gramowski et al., 2005] added to culture medium. Li and co-workers computed the non-smoothed cross-correlogram (correlation window: 200 ms; bin width: 5 ms) from 300 s of spike train recorded from single electrode, to another one from the same MEA chip. To compare results before and after BIC treatment, they extracted the maximum value of the correlation function for a couple of electrodes, eliciting local information about network correlation. In that work, the rules to choose which couple of electrodes compare are not described; thus, it was decided to choose the couple of electrodes with the highest correlation difference between 0 μM and 20 μM conditions for each culture. Moreover, to assess Li algorithm from a network point of view and to summarize this information in a single parameter, it was evaluated the maximum of the cross-correlograms between each electrode and all the others and it was extracted Total Corr Li, equivalent to MTC, to characterize these matrices. Total Corr Li was then defined, for each culture, as in Equation 6.2

$$Total\,Corr\,Li = \sum_{i} \sum_{j \neq i} M(i,j) \tag{6.2}$$

being *M(i,j)* the maximum value of C(i,j) and i , j each couple of channels under advisement.

6.2.7.2 TJ method

The second method that was selected, TJ, was proposed by Tateno and Jimbo [Tateno and Jimbo, 1999] to quantify the reproducibility of correlated spike timing. Then, it was used by Chiappalone and colleagues [Chiappalone et al., 2006] to evaluate correlation changes during network maturation as well as to investigate the characteristics of cortical networks under electrical and pharmacological stimulation [Chiappalone et al., 2007]. In TJ method the CC function was built according to the method of activity pairs [Eytan et al., 2004], using a correlation window of $\pm$ 150 ms and bins equal to 10 ms and normalizing by the number of spikes in i-th train and by the dimension of the bin. Then, to represents the level of synchronization between each couple of active channels, authors used a parameter called Coincidence Index (CI_{ij}), described as "the ratio of the integral of a cross-correlation function in a specified area around zero to the integral of the total area" [Jimbo et al., 1999, Tateno and Jimbo, 1999]. CI_{ij} is defined as follows (Equation 6.3):

$$C_{ij} = \frac{\sum_{\tau=-5ms}^{5ms} C_{ij}(\tau)}{\sum_{\tau=-T}^{T} C_{ij}(\tau)} \tag{6.3}$$

for each couple of channels i ,j. Authors did not extract a unique and inclusive parameter for the whole culture; indeed, the distribution of CI_{ij} values was plotted and observed qualitatively to evaluate correlation alterations. In contrast, in this chapter, CI_{ij} values, extracted for each couple of active channels, were summarized with a single outcome measure, computing Total Corr TJ, equivalent to MTC, defined as in Equation 6.4:

$$Total\,Corr\,TJ = \sum_{i} \sum_{j \neq i} CI_{ij} \tag{6.4}$$

for each culture.

6.3 Results

6.3.1 Cross-correlation analysis

First of all, the Mann-Whitney test recognized significant differences between MTC values computed on neuronal recordings and MTC values computed on a shuffled version of them ($p < 0.01$ for each experimental condition). Second, correlation values increased owing to BIC addition. Qualitative changes in network functional connectivity were evaluated by means of correlation matrices and connectivity networks projected on the MEA space as done in [Segev et al., 2004, Baruchi et al., 2006, 2008]. Figure 6.1 shows an example concerning correlative alterations which followed the addition of BIC 1 μM and 20 μM to one untreated culture (UC). It is possible to appreciate an increase in correlation strength and in the number of electrodes with correlated activities.

These changes in correlations can be observed quantitatively in Figure 6.2. MTC highlighted significant differences (Wilcoxon matched pair test $p < 0.01$) between untreated cultures and cultures treated with BIC 20 μM , as in the literature [Li et al., 2007a]. Moreover, it was able to significantly distinguish the 1 μM setting (Wilcoxon matched pair test $p < 0.01$), both from the nominal and the maximum imbalance condition. Concerning MFR, it was evaluated its correlation with MTC determining $R^2 = 0.92$ between UC conditions, $R^2 = 0.95$ between BIC 1 μM experiments and $R^2 = 0.97$ between BIC 20 μM groups. Furthermore, it was identified an increasing drift in this parameter but the Wilcoxon matched pair test recognized significant differences only between UC and BIC 20 μM (Figure 6.3A). Results obtained by Li method showed significance differences ($p < 0.01$) between UC, BIC 1 μM and BIC

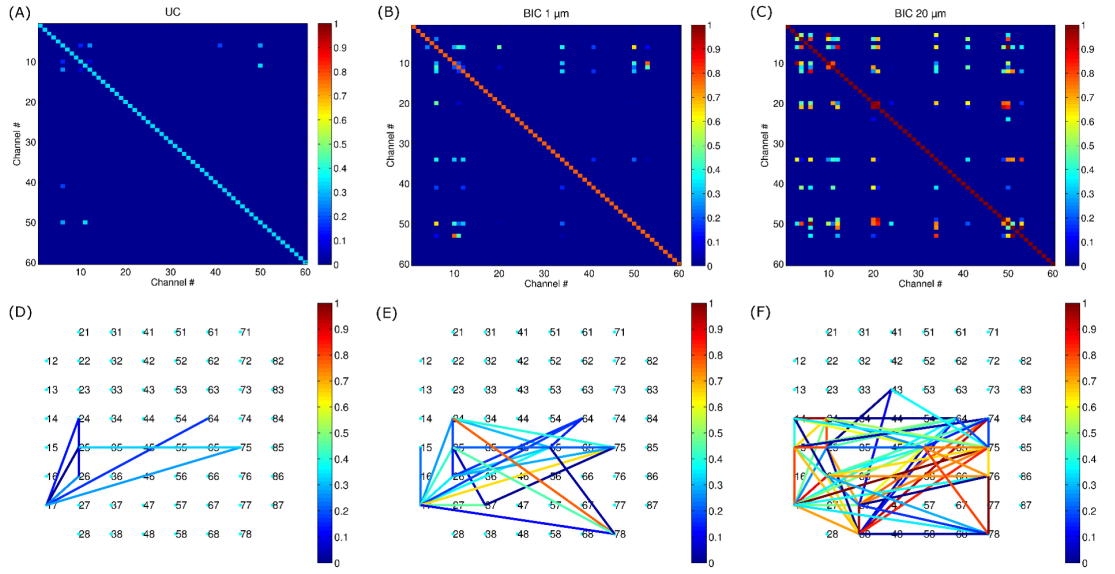

Figure 6.1: Example of correlation matrices (A-C) and connectivity networks (D-F) of a NB, obtained by mapping multichannel recordings on MEA space, while varying the concentration of BIC in the culturing medium. The color code represents the values of CC, normalized on the correlation value obtained after adding BIC 20 μM. A and D concern untreated culture; B and E are related to the culture after BIC 1 μM treatment; C and F regard the culture after BIC 20 μM treatment.

20 μM conditions (Figure 6.3B), comparing the maximum value of the correlation function for a couple of electrodes (see Section 6.2.7.1). On the contrary, comparable values of Total Corr Li were observed evaluating Li algorithm from a network point of view (Figure 6.3C). Concerning Total Corr TJ (Figure 6.3D), statistical differences ($p < 0.01$) were identified between BIC 20 μM and both untreated and submaximal experiments, while the median value of UC and BIC 1 μM were not distinguishable.

6.3.2 Concentration-response curves

Figure 6.4A shows GABA concentration-response curve obtained from 3 cultures, considering the total number of spikes. The EC_{50} value ranged from 0.4 μM to 3 μM and the goodness-of-fit, assessed using the Coefficient of Determination R^2, was 0.7659, showing that GABA addition alters the spontaneous activity of neuronal networks in a dose dependent manner. Figure 6.4B shows GABA concentration-response of the MTC data, with an estimated EC_{50} ranging from 2 μM to 8 μM and a R^2=0.7408. All the estimated EC_{50} values agreed with the literature [Boldyreva, 2005].

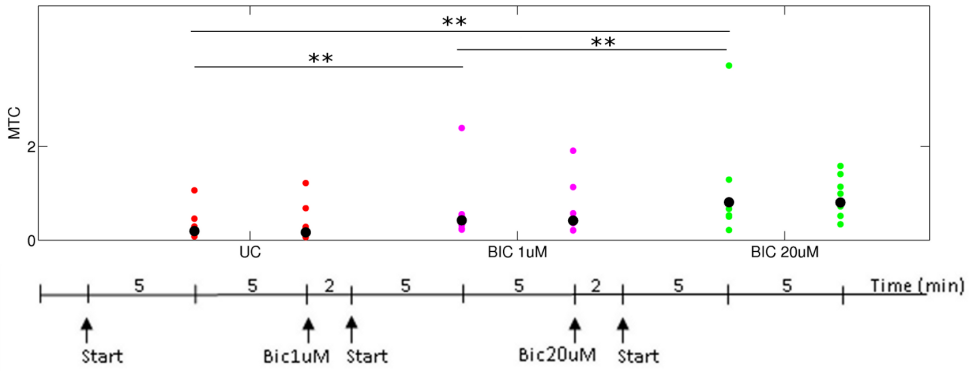

Figure 6.2: MTC values for the three experimental conditions (median on 10 cultures): untreated cultures (UC; red), cultures treated with BIC 1 μM (pink) and BIC 20 μM (green) computed on the first 5 min of recordings and on the following 5 min. Median values are plotted as black dots. Statistical analysis on these distributions did not recognize significant differences between MTC values in the two different intervals (Mann-Whitney test $p > 0.05$). On the contrary, the Wilcoxon matched pair test recognized significant differences between UC and BIC 1 μM, UC and 20 μM and between BIC 1 μM and BIC 20 μM (** $p < 0.01$). Below the x-axis steps of the protocol are shown. Start means the beginning of 5 min recordings (repeated twice); instants of drug addition are also pointed out.

6.4 Discussion

In this work it is proposed an intra network burst correlation algorithm aimed at providing a comprehensive functional evaluation of neuronal network communication properties. The method was evaluated processing cortical cultures in presence of GABA and bicuculline. These two drugs are able to modulate the balance between the excitatory and inhibitory circuits, which alters the integrative properties of neuronal network communication. Moreover, additional assessments were performed comparing algorithm outcome measure (MTC) to the mean firing rate, a widely used parameter for the evaluation of neuronal network activity [Khatami et al., 2004, Martinoia et al., 2005, Chiappalone et al., 2006, 2008, Berdondini et al., 2009b, Garofalo et al., 2009]. Then, it was compared to Total Corr Li, a parameter extracted from the method introduced by Li and colleagues [Li et al., 2007a] and to Total Corr TJ, derived from the work of Tateno and Jimbo [Tateno and Jimbo, 1999, Chiappalone et al., 2006, 2007]. These results showed that the proposed intra NB CC analysis is capable of detecting changes in the correlation properties of a neuronal circuit, allowing studies in which alterations of the functional connectivity are induced (e.g. pharmacological manipulations, genetic alterations, etc.). Furthermore, the outcome data of the defined parameter MTC have been demonstrated to have high statistical significance compared to shuffled data, which validates these results and confirms the algorithm reliability [Perkel et al., 1967, Pasquale et al.,

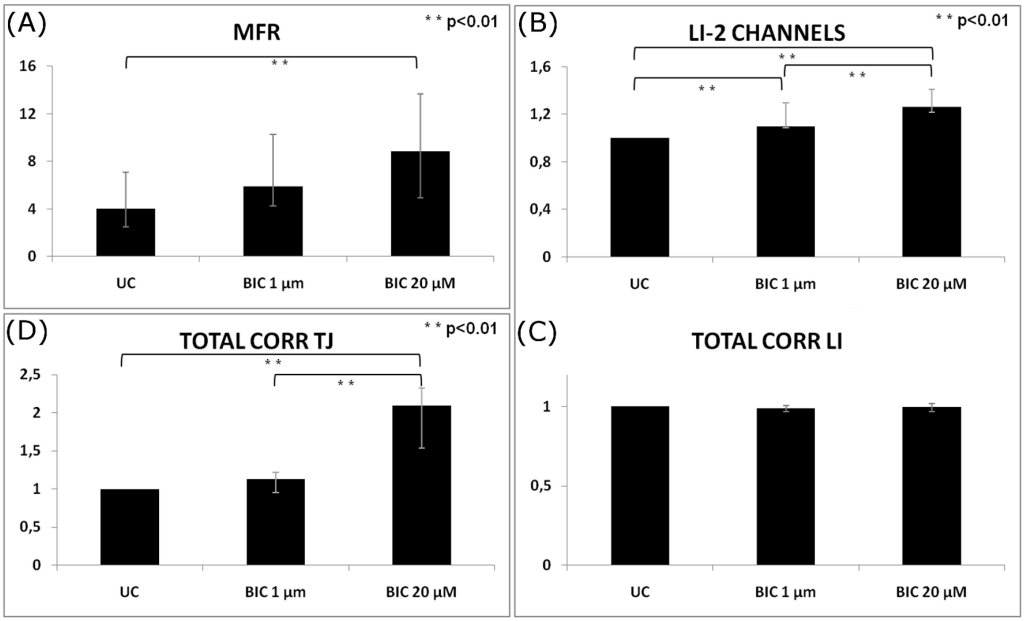

Figure 6.3: (A) Increasing trend of MFR after drug treatments. (B) Li method: maximum of correlation between two channels; high significance on local data. (C) Li method: Total Corr Li showed no significant differences. (D) TJ algorithm: Total Corr TJ was able to distinguish the maximal drug concentration (20 μM) while BIC 1 μM was not identified (y-axis labels are reported as title of each graph).

2008]. Afterward, MTC demonstrated high sensitivity. Indeed, it was able to discriminate effect induced by pharmacological application of drugs known to alter neuronal network functional connectivity even at sub-maximal concentration.

The MFR is a common metrics used in the literature to evaluate the spontaneous activity of the networks [Khatami et al., 2004, Berdondini et al., 2009b, Garofalo et al., 2009], to compare different pharmacological experimental conditions [Martinoia et al., 2005], to study network maturation [Chiappalone et al., 2006] or to select the culture to be studied with the desired level of activity [Chiappalone et al., 2008]. It was showed that variations in MTC are strictly connected to MFR variations. This is due to pharmacological treatments used, which were able to alter both the firing properties and the functional connectivity of networks. Under these conditions, however, only the MTC algorithm was able to distinguish the effects of submaximal concentration of drug, while MFR detected significant differences only between untreated and maximal-treated conditions.

Further, the assessment of the proposed algorithm highlighted that MTC is a sensitive parameter for an instant and reliable evaluation of neuronal network correlative properties, with respect to Total Corr Li and Total Corr TJ. Particularly, Total Corr TJ is inadequate for the detection of small pharmacological compound concentrations, being unable to discriminate effects induced on network activity by submaximal drug additions. On the other hand, the use of Total Corr Li is limited

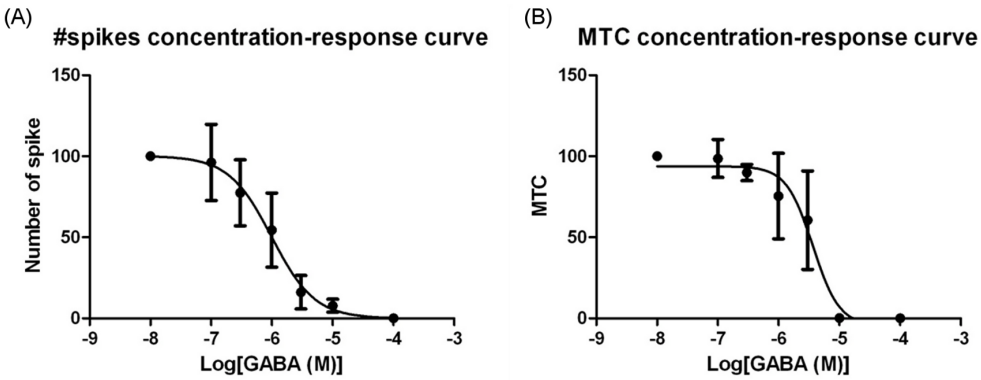

Figure 6.4: Non linear regression in a variable slope sigmoidal model with a 95% confidence interval of (A) the total number of spike (R^2=0.7659; EC_{50} ranged from 0.4 μM to 3 μM) and (B) MTC values (R^2=0.7408; EC_{50} ranged from 2 μM to 8 μM), obtained adding GABA in 7 increasing concentrations (in μM): 0.01, 0.1, 0.3, 1, 3, 10 and 100. All data were normalized on the untreated cultures.

to a local evaluation because it showed high sensibility studying the behavior of two single electrodes while it was unable to follow whole neuronal network variations induced by drug modulation. The outcome of the proposed algorithm provides information not only concerning the electrical activity of single electrodes but also the interactions between them during NB events by means of a unique and high impact parameter. This approach is able to analyze the functional correlative properties of neuronal networks condensing the information in a simple, reliable and highly sensible parameter. Definitely, the choice of this method is led by the aim of a fast and automatic (pharmacological) screening of neuronal connectivity. The choice of other methods and parameters could be necessary for different goals.

The proposed algorithm computes the entire cross-correlation function and requests the value of τ that the user is interested in. This procedure could be repeated for several values of τ. Anyway, the present study was limited to $\tau = 0$ as a proof of concept of the algorithm reliability and sensitivity, taking advantages from the bicuculline functional modulating effect on neuronal networks. Despite only the cross-correlation at $\tau = 0$ was taken into account for simplicity and to be relevant with the literature, the study of correlation at different τ gives the possibility to highlight the presence of delayed correlation peaks, allowing to evaluate variations in network correlation properties. These variations can occur when the communication characteristics of constituent neurons changes, modifying the process of information fluxes. These changes can be due to variations in cell number, connections as well as alterations in functional properties like those induced by treatments (e.g. antiepileptic drugs, anxiolytics). Moreover, τ can reflect the time needed for a region of a network to excite a functionally related second region. Being this delay related to the number of synapses on the path and to the physical distance between

network regions, this allows the functional mapping of a network. Finally, the computational costs are reduced, even performing the entire cross-correlation function, since it is computed on the length of each NB (from hundreds of milliseconds to few seconds) instead of on the whole recording session, which typically lasts some minutes.

MTC use in pharmacological studies

Drug discovery for CNS disorders is increasing its attention to candidate compounds that target receptors and channels with a modulatory function on neuronal activities. This implies two major considerations: 1) the effect of a molecule should be studied in a neuronal context in order to take into account all the complex and integrated plastic phenomena that govern neuronal function; 2) the modulatory effect of candidate compounds should be efficiently detected. The MEA based technology is a good response to the first consideration while an efficient and simple detection method to study functional alterations of neuronal network properties is still missing. The algorithm propose here represents an answer to the second issue, being an innovative and efficient method for the study of molecules able to modulate neuronal network functions. In this work, GABA concentration-response experiments were performed and neuronal network activity was analyzed by means of the intra NB correlation algorithm. Data demonstrate the possibility of using MTC in classical pharmacological experiments, with the advantage of studying the effect of drugs on the comprehensive correlative properties of integrated neuronal networks. A further interesting application of the proposed algorithm should be envisaged in genetic manipulations studies, e.g. the investigation of the molecular mechanisms at the base of dysfunctions observed in models of genetic pathologies of the CNS. In addition MTC could be useful to follow the organization of network connectivity *in vitro*.

Chapter 7

Local network stimulation using microfluidics. A feasibility study [1]

When the goal is to figure out electrophysiological effects of unknown molecules on neurons *in vitro*, biochemical stimulation protocols are a crucial element. As discussed in Section 2.6.2, currently standard techniques make use of pipettes and require a partial or complete change of culture medium. Disadvantages of these protocols are the unknown kinetic of the interaction between molecules and cells, and the rapid changes in the cellular environment, respectively. Moreover, these stimulation protocols often lack of defined spatio-temporal control [Kothapalli et al., 2011] and are demanding in terms of reagent consumption and costs [Sung et al., 2010]. These drawbacks indicate that current systems used to study drug effects on *in vitro* neuronal cultures need to be refined. Furthermore, another technical hitch of standard neuropharmacological measures is the comparability of data obtained with different substrates. Indeed, network functionality partially depends on culture to culture variability. Therefore, cultures that are seeded at the same time and subjected to the same feeding schedules and protocols reduce this variability and improve comparability in terms of response to compounds tested [Johnstone et al., 2010]. Recently, the potential importance of microfluidic techniques in improving pharmacological studies has been widely recognized. Particularly, microfluidics can precisely define biochemical cell microenvironment [Taylor and Jeon, 2010], it allows a localized pharmacological intervention [Shi et al., 2010] and the delivery of micro-scale volumes of drugs to the desired neurons [Wang et al., 2009]. Hence, microfluidic-based cell cultures, provided with adequate perfusion systems, offer a great potential for drug screening [Sung et al., 2010].

[1] The validation of the micro-chamber for neuronal growth and recording has been published as **Biffi E**, Menegon A, Piraino F, Pedrocchi A, Fiore GB, Rasponi M. Validation of long-term primary neuronal cultures and network activity through the integration of reversibly bonded microbioreactors and MEA substrates. *Biotechnol Bioeng*, 2012, 109(1): 166 - 175.

This chapter deals with the validation of an integrated microfluidic chamber for long-term primary neuronal cell cultures and for spatially-controlled drug stimulation. For this purpose, a device was developed by coupling a reversibly bonded poly(dimethylsiloxane) (PDMS) microfluidic chamber with a commercial flat MEA (Multi Channel Systems, MCS GmbH). Specifically, two configurations are described here. First, a single channel configuration was used to assess the neuronal viability inside this device. Then, a dual channel layout was used to stimulate twin networks, cultured in the same microenvironment, in a spatially controlled manner. As a proof of concept, tetrodotoxin (TTX), a neurotoxin known to block action potentials, was selected as test molecule. The project was carried out in collaboration with the Laboratory of Micro- and Bio-Fluid Dynamics (Biomechanics Research Group, Bioengineering Dept, Politecnico di Milano, Milan) and with the Advanced Light and Electron Microscopy Bio-Imaging Center (San Raffaele Scientific Institute, Milan).

7.1 Microfluidics in neurobiology: state of the art.

Microfluidics is a technology which features the manipulation of small amounts of fluids in channels with dimensions of tens to hundreds of micrometers. Its widespreading was due to development of soft lithography, a technique characterized by fabrication procedures similar in concept to photolithography. Soft lithography was introduced by Whitesides in the 1990s [Qin et al., 1996, Duffy et al., 1998, McDonald et al., 2000] and took advantage of a silicon-based elastomeric material named PDMS. PDMS is a relatively cheap material, easy to mold and with good optical properties; moreover, it is non-toxic to cells and it is gas permeable, offering a suitable solution for cell and tissue culture experiments [Young and Beebe, 2010]. The processed PDMS can be coupled, reversibly or irreversibly, with glass or PDMS substrates. Recently, reversible sealing has become effectively used in microdevice-based research including the fabrication of micro and nanodevices, flow analysis at the microscale, biomolecules analysis and cell studies [Anwar et al., 2011]. Reversible bonding offers some interesting advantages as the possibility of reusing and disassembling the substrate, and as the chance of employing uncommon materials. Recently, inexpensive reversible techniques of fluidic devices, based on magnetic forces and able to withstand a higher range of working pressures (from 50 to 145 kPa), were introduced [Rafat et al., 2009, Rasponi et al., 2011]. Particularly, the method developed by Rasponi and collaborators extended the use of the magnetic reversible bonding approach to microfluidic-sized devices.

Microfluidic devices have already been used in a wide range of biological applications thanks to their low consumption of samples and reagents, the ability to precisely control parameters within the cellular microenvironment and the capa-

bility to perform highly concurrent and reproducible analyses. In the last years, microfluidics was involved in many research areas including stem cell differentiation, drug discovery and development, cardiovascular research and cancer biology [Gupta et al., 2010, Wu et al., 2010, Young and Simmons, 2010, Wlodkowic and Cooper, 2010].

Microfluidic devices have also been widely used in the field of neuroscience [Gross et al., 2007, Pearce and Williams, 2007, Taylor et al., 2010] thanks to their scale, compatible with neuron size. Starting from the Campenot chambers [Campenot, 1977] used to compartmentalize axons and cell bodies, microfabricated versions of these devices were developed to perform *in vitro* studies of neuronal populations, both in 2D [Park et al., 2009a,b, Hosmane et al., 2010, Kunze et al., 2011b, Gao et al., 2011, Majumdar et al., 2011] and in 3D structures [Rowe et al., 2007, Kunze et al., 2011a, Gao et al., 2011]. Furthermore, they were used to develop culture methods for neuritic isolation and study [Taylor et al., 2003, Shi et al., 2010, Kothapalli et al., 2011], to manipulate synaptic regions *in vitro* [Taylor et al., 2010, Taylor and Jeon, 2010] and to create patterns of neuronal cells [Romanova et al., 2004, Nam et al., 2004, Rhee et al., 2005, Claverol-Tinture et al., 2007]. Particularly, the direct integration of microfluidic devices on Micro Electrodes Arrays (MEAs) allow the coupling of neuronal electrical activity recording, simultaneously from many channels, together with the inherent high control of the cell microenvironment, typical of microfluidic devices. This integration has been used to record from isolated bundles of axons [Dworak and Wheeler, 2009], to show the influence of temperature on the firing rates of dorsal root ganglion neurons [Pearce et al., 2005] and to investigate neuronal degeneration induced by axon stimulation [Ravula et al., 2007]. Furthermore, PDMS microfluidic devices coupled with MEAs were developed to study the electrical activity of physically grouped neuronal populations [Morin et al., 2005, 2006, Kanagasabapathi et al., 2009, 2011].

Another interesting application of microfluidics is the spatially resolved delivery of substances which is promising for pharmacological assays and cell-based biosensors [Mourzina et al., 2006]. Indeed, microfluidics can be used for local cell stimulation, for the creation of dynamic concentration gradients or for high content pharmacological screening [Morin et al., 2006]. Recently, tools based on microfluidic structures that enable the delivery of chemicals locally to specific regions of the cellular culture were proposed. Specifically, a parallel pumping scheme and multiple laminar flows were used for localized chemical stimulation of cardiomyocytes [Kaji et al., 2003] and myoblasts [Zhu et al., 2004]. These systems were also combined with patch-clamp technique and used to study neuronal cultures [Mourzina et al., 2006, Pihl et al., 2005]. Besides, Kraus and collaborators integrated these microfluidic devices with MEA technology [Kraus et al., 2006]. However they only tested them on HL-1

cardiomyocyte cultures.

Therefore, although microfluidic systems have shown potential in neuropharmacology, until now few efforts have been dedicated to microfluidic-based neuropharmacology [Wang et al., 2009]. Hence, so far, there are no microfluidic devices able to selectively and locally stimulate subgroups of neurons grown and maintained in identical environmental conditions for pharmacological and toxicological tests.

7.2 Methods

7.2.1 Device Fabrication

A two-mold fabrication process was developed to obtain magnetic devices as previously described [Rasponi et al., 2011]. The whole process is presented in Figure 7.1. Briefly, the process includes the manufacturing of a top layer, to be filled with iron micropowder and PDMS, and a bottom layer, containing microfluidic channels. The top layer cavities for the inclusion of magnetic suspension were realized by machining out a poly(methyl metacrylate) (PMMA) substrate and then curing PDMS into it. Then, this PDMS structure was manually filled with the iron powder/PDMS suspension (in a ratio 4:1, w/w) and cured in oven at 80°C for 120 minutes. The bottom layer, containing the microfluidic channels, was obtained in PDMS by replica molding from a silicon/SU8 4" wafer master obtained through standard soft lithography techniques [Xia et al., 1997]. Then, PDMS was spin coated on the mold, degassed and cured in oven at 80°C for 60 minutes. Subsequently, the top layer was manually aligned under a stereomicroscope to the partially cured bottom layer with the openings, filled with iron powder, downside. By means of a biopsy puncher (tip diameter 8 mm) input and output wells were created (approximate volume of 400 μl each). The fluidic device was finally assembled closing the channels against a 60-electrode flat MEA biochip (electrode spacing 200 μm, electrode diameter 30 μm; Multi Channel Systems, MCS GmbH) and by placing a neodymium magnet (40x20x10 mm, magnetization N42) on the opposite side. Direct optical inspection of microfluidic channels was possible through the top layer, upon temporary magnet removal.

Figure 7.2 shows the single channel layout, which consists of an input channel, a culture region, 2 mm wide and 7 mm long (trued up with MEA electrodes) and 2 outlet channels. These channels have a width of 500 μm, while the height of all the features in the layer was 100 μm.

Then, a second advanced configuration was prepared. This configuration differs from the previous one due to the presence of a 100 μm wall which was developed in the middle of the main channel. The wall partially divides the main channel in two

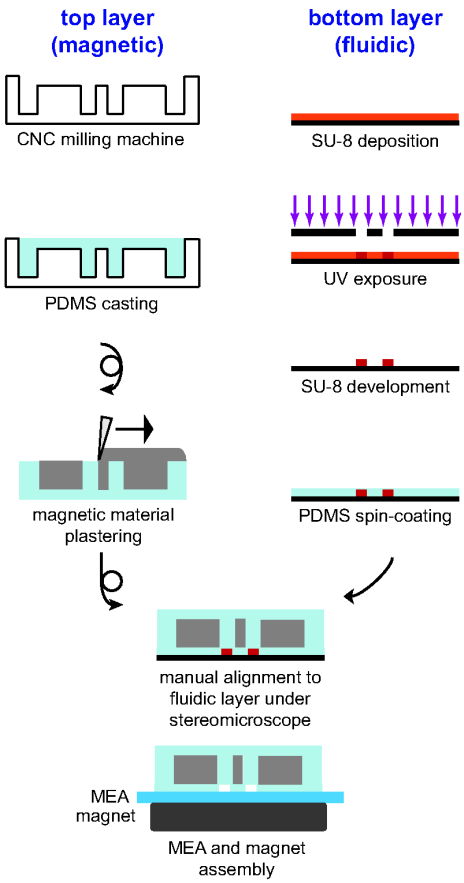

Figure 7.1: Fabrication of the magnetic device. To obtain the magnetic layer (left column) a PMMA mold was realized with a CNC milling machine. PDMS was cast and a ferromagnetic suspension (iron powder/PDMS) was manually plastered into specific cavities. The fluidic layer (right column) was obtained by spin-coating PDMS on a silicon mold, previously realized with standard soft-lithography techniques. Finally the two layers were manually aligned under a microscope taking advantage of the optical transparency of the top layer in the channel regions.

sub-channels of 1050 μm in width and 100 μm in height, respectively. This wall also separates 60 MEA electrodes in two subgroups of 30 electrodes as shown in Figure 7.3. In the following sections, the two compartments are named upper and lower compartment, in agreement with the layout depicted in Figure 7.3.

7.2.2 Surface preparation

All the device components were cleaned with ethanol (EtOH) in class II biosafety cabinet hood. After EtOH evaporation, the device was assembled directly in a Petri dish (bottom part of the dish between the MEA chip and the magnet) to preserve sterility. Before cell seeding, the fluidic path (MEA substrate and PDMS channels) was preconditioned with 100% EtOH for 10 minutes and successively rinsed three times with bidistilled and autoclaved water (dH2O). After the injection of a solu-

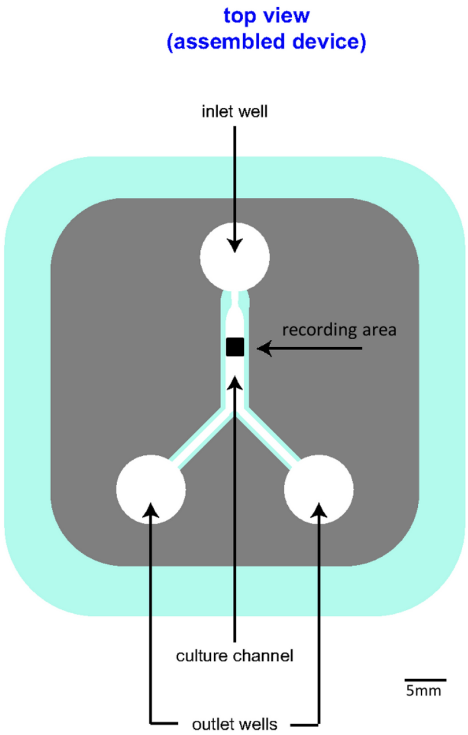

Figure 7.2: Top view of the final assembled devices: single channel configuration.

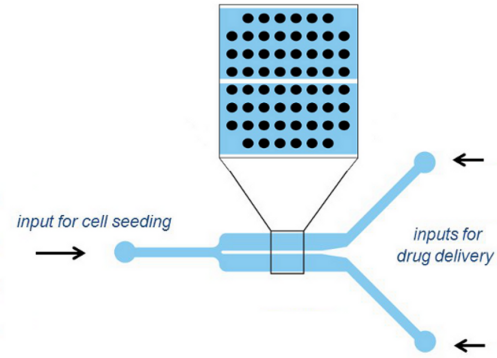

Figure 7.3: Dual channel configuration.

tion of plating medium (Neurobasal medium (NBM; Invitrogen), 10% Fetal Bovine Serum (FBS; Lonza), 1% Penicillin and Streptomycin, (Gibco) to increase the surface hydrophilicity, the device was incubated 2 hours. Subsequent a three times rinse with dH2O, it was treated with 2 mg/ml poly-L-lysine (Sigma) in 100 mM Borate Buffer pH 8.5 and placed overnight in a humidified incubator at 37°C (5% CO_2). After treatment, the device was thoroughly rinsed with dH2O and placed for 6 hours in the incubator, completely filled with dH2O. Finally, after further washing, it was incubated overnight with plating medium.

7.2.3 Cell isolation and culture preparation

Primary neuronal cultures were prepared from CD1 mouse embryos at E17. Hippocampi were extracted, treated with Trypsin (0.25%; Sigma) for 10 minutes at 37°C and mechanically dissociated using glass pipettes. Cells were concentrated to $2x10^6$ cells/ml and 30 μl of cell suspension were loaded in the magnetic device as described by Harris and colleagues [Harris et al., 2007], so as to achieve a final plating density of about 10^3 cells/mm^2. Particularly, cells were introduced within the device by means of the single inlet in both configurations. To allow cell adhesion, the device was incubated for 4 hours, and successively 800 μl of culture medium, composed of NBM, B-27 1x (Invitrogen), 1% Penicillin and Streptomycin and Glutamax 1 mM (Invitrogen), were added. The medium was changed the first day after plating and every 12 hours until the end of the experiments.

7.2.4 Experimental protocols

Concerning the single channel configuration, 5 minute extracellular recordings were performed with a MEA1060 signal amplification and data acquisitions system (Multi Channel Systems, MCS GmbH) from 8 to 18 days *in vitro* (DIV). Recordings of neuronal electrical activity were carried out every two days at different time frames after the removal of the magnet: straight after, 5 minutes, 45 and 50 minutes later. The sterility was preserved by means of a PDMS slab used as a cover during the recordings. Moreover, the device was placed in the incubator between the first two and the last two recordings. At the end of each recording cycle, the magnet was positioned again under the MEA biochip and the device was placed in the incubator.

Concerning the dual channel configuration, subsequent recordings were carried out at 14 DIV. First, a static activity recording was performed. Then, the device was connected to a syringe pump (Harvard Apparatus, USA) by means of a small PDMS cap, which was plugged inside the inlet well, and recordings were performed during medium/drug delivery. Specifically, at first medium was perfused inside both channels at 10 μl/min. Next, cells plated inside the upper channel were stimulated with 0.5 μM tetrodotoxin (TTX), while cells in the lower compartment were continuously subjected to medium flow. Pharmacological stimulation was carried on for 3 minutes at 10 μl/min. Then a flow rate of 300 μl/min was used to wash cell cultures for 5 minutes. Afterward, the same protocol was applied in a mirrored configuration: the lower channel was treated with TTX for 3 minutes, while the upper one was used as control. Electrophysiological recordings were performed continuously during drug stimulation. Flow rate values were selected as a trade-off between a fast cell stimulation and a limited cellular shear stress. Tests with a dye were previously carried out to verify that 10 μl/min allowed to reach quickly the drug maximal

concentration. During these experiments, images focused on the central part of one channel were acquired at 20Hz by a CCD camera (Unibrain, Greece). Then, intensity values were extracted from each image and a concentration curve was built. Concerning the wash out flow rate, 300 μl/min was identified as the necessary value to efficiently wash TTX from neurons (data not shown).

In both configurations, signal amplification gain and sampling frequency were fixed to 1100 and 25 kHz, respectively. Then, spikes were detected from raw data with MCRack Software (Multi Channel System, MCS GmbH), using for each channel a fixed threshold equal to seven times the standard deviation of average noise amplitude in the first acquired 500 ms.

7.2.5 Signal analysis and statistics

7.2.5.1 Single channel configuration

On the first configuration, a systematic study of hippocampal culture development was performed by investigating spontaneous neuronal electrical activity over 60 electrodes for up to 18 DIV. The off-line analysis was implemented in Matlab (The Mathworks, Natick, USA) by means of standard algorithms for burst and network burst identification (see Section 2.4 and 3.2.4 for more details). The parameters evaluated after burst analysis were

- the number of channels displaying bursts,
- the burst duration,
- the intra-burst frequency in Hz,
- the bursting rate, defined as the total number of bursts in 5 minutes,
- the number of channels displaying network bursts,
- the intra-network burst frequency in Hz,
- the network bursting rate (network bursts/min).

These parameters were analyzed for each recording and the median value of the 4 repeated data sets was computed for each day of supervising (from 8 to 18 DIV). A statistical analysis (Wilcoxon matched pair test) was performed to identify functional differences among days of maturation. Finally, the 4 repetitions were exploited to assess stability of the electrical signal during the experiments after the removal of the magnet. The differences between the 4 recordings were investigated with a Mann-Whitney test. Data are given as median and its variation stated as percentiles (25^{th} and 75^{th}). Statistical analyses were performed with the commercial tool Statistica (StatSoft Inc). The significance level was established at $p < 0.05$.

7.2.5.2 Dual channel configuration

First, morphology and density of each sub-culture were evaluated qualitatively by means of optical microscopy. Then, a cross correlation analysis [Biffi et al. 2011, Chapter 6] was performed inside each compartment and between compartments to assess independence between the two neuronal networks. Specifically, the inter-compartments values were calculated as (i) cross-correlation among electrodes across the wall and (ii) cross-correlation among electrodes placed close to its end. Furthermore, cross-correlation values were purified from the random and non authentic information by evaluating cross-correlation on shuffled data (Section 6.2.5) and subtracting it. Then, few network parameters were evaluated for each compartment and electrophysiological activities were compared (see Section 2.4). Specifically

- the number of channels displaying spikes,
- the mean firing rate (Hz),
- the number of channels displaying bursts,
- the burst duration

were computed. Finally, mean firing rate (MFR) values were evaluated in each compartment (bin width 60 s) during delivery of TTX and fresh medium. Data are given as median and its variation, stated as percentiles (25^{th} and 75^{th}).

7.3 Results

Figure 7.4 depicts a device placed in a Petri dish to preserve sterility.

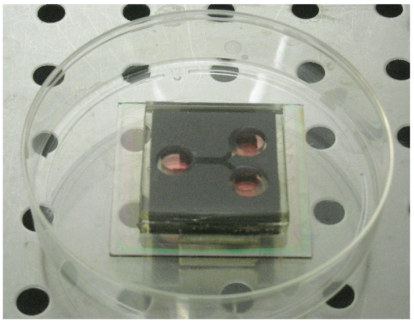

Figure 7.4: The picture shows the PDMS fluidic device leant on the MEA surface, aligning the culturing channel with the array of 60 microelectrodes. The microchamber is placed in a Petri dish to preserve sterility and a neodymium magnet is positioned on the opposite side to guarantee the hydraulic tightness.

7.3.1 Single channel configuration

Hippocampal neurons were cultured up to three weeks in healthy conditions. Cells started emitting neurites few hours after plating and a neuronal network was formed

within a few days. Pictures, which were taken by a transmitted light phase contrast microscope (Axiovert 135TV, ZEISS, objective 5x) after magnet removal, are shown in Figure 7.5. Specifically, a 4 DIV developing neuronal network on MEA surface can be observed in Figure 7.5A. Figure 7.5B illustrates a detailed image of neurons surrounding one electrode.

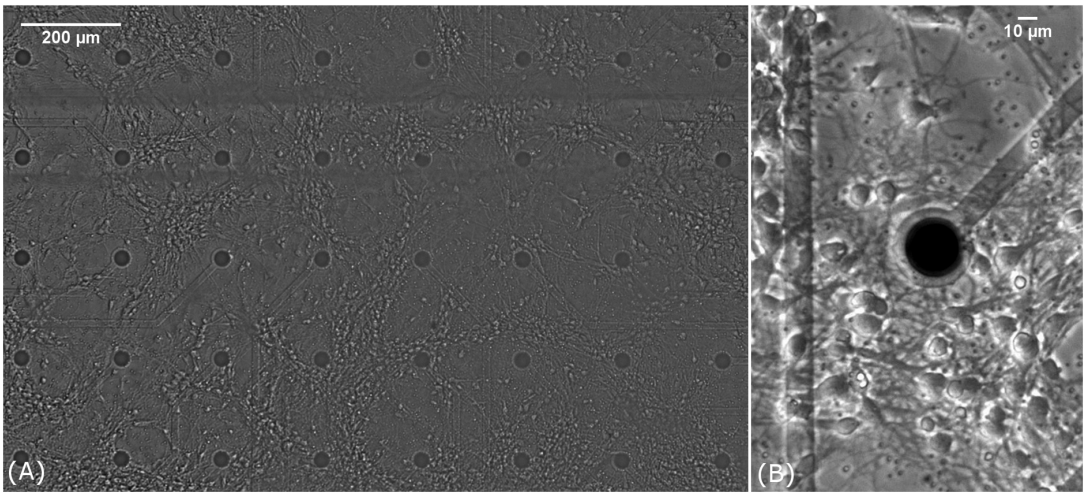

Figure 7.5: A) Phase contrast image of the hippocampal neuronal network cultured in the microfluidic device at 4 DIV. The black solid circles are the microelectrodes, 30 μm in diameter and spaced 200 μm on to the other. (B) One electrode and surrounding cells.

Spontaneous electrical activity was recorded from 8 to 18 DIV. Figure 7.6 shows a typical 60 second time frame of recording from the 60 electrodes at 14 DIV. The signal amplitude (from 100 μV to 200 μV peak-to-peak) and the number of spiking channels were comparable with signals acquired using commercial MEA chambers, by visual inspection.

The first column of Figure 7.7 shows the total number of active channels (Figure 7.7A), the MFR (Figure 7.7B) and the percentage of bursting channels (Figure 7.7C), defined as the ratio between the number of channels displaying bursts and the number of active electrodes, as a function of the culture time. A pronounced increasing trend is shared between all histograms, although the number of active channels decreases after having reached its highest value at 14 DIV (about 30 spiking channels). The MFR is lower than 1 Hz at 8 DIV and then it increases up to 16 Hz. The percentage of bursting channels is equal to zero at 8 and 10 DIV, while cultures start showing burst activity at 12 DIV. However, at 18 DIV the 50% of channels highlights bursting activity. The second column of Figure 7.7 shows the burst duration (Figure 7.7D), the intra-burst frequency (Figure 7.7E) and the bursting rate (Figure 7.7F). After the organization of electrical activity in bursts, neurons showed a substantially steady electrical pattern, characterized by 600 ms bursts, an intra-burst frequency of about 40 Hz and a median number of bursts per

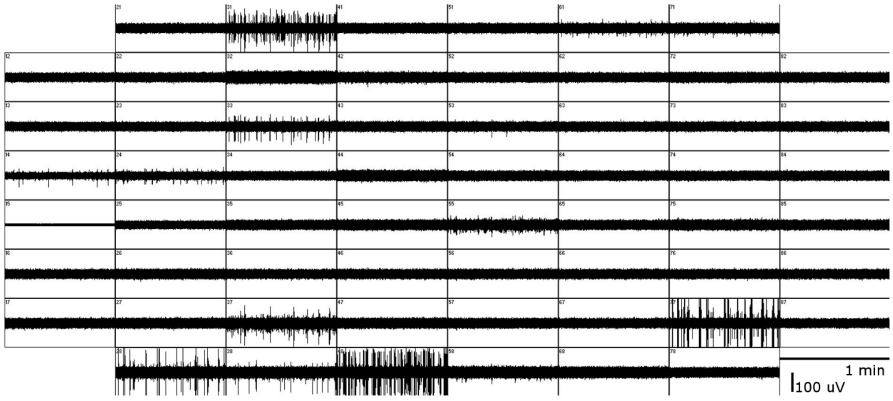

Figure 7.6: Neuronal electrical activity was recorded by means of the 60-electrode array; here,a time span of 60 seconds is shown. Electrode 15 was set as reference and the noise recorded at each electrode was lower than 30 μV peak-to-peak. The spike amplitude was typically 100-200 μV peak-to-peak. The graphical user interface here depicted is by Multi Channel System (McRack Software, MCS GmbH).

minute equal to 15. The number of channels displaying network bursts, the intra-network burst frequency and the network bursting rate did not show significant changes after their onset at 14 DIV (data not shown). The Wilcoxon matched pair test highlighted significant differences ($p < 0.05$) among the 10 DIV scenery and the 12, 14, 16, 18 DIV settings for each parameter, while no significant differences where emphasized between 8 and 10 days of maturation. Finally, with regard to possible differences of the recordings among the 4 time frames, no considerable trend between subsequent recordings was detected, with the exception of the percentage of bursting channels (Figure 7.8). Particularly, recordings performed 5 and 50 minutes after the removal of the magnet showed significantly different values of percentage of bursting channels ($p < 0.05$), compared to the recordings performed 45 minutes after the removal of the magnet.

7.3.2 Dual channel configuration

Hippocampal neurons grew inside both compartments. The two environments were fluidically connected under static conditions, thanks to the partial separation offered by the thin central wall. Optical inspection highlighted homogeneous cell density and similar network morphology (Figure 7.9 and 7.10).

Furthermore, cross correlation analysis showed that correlation values inside each compartment were similar (i.e. 0.25 and 0.22 in the upper and lower compartment, respectively). Besides, these values were ten times higher than correlation between compartments (i.e. 0.02 at the interface along the wall and 0.03 close to its end) which proved that the two networks were not functionally connected. These features can be qualitatively observed in Figure 7.11, which depicts 5 minutes spike trains

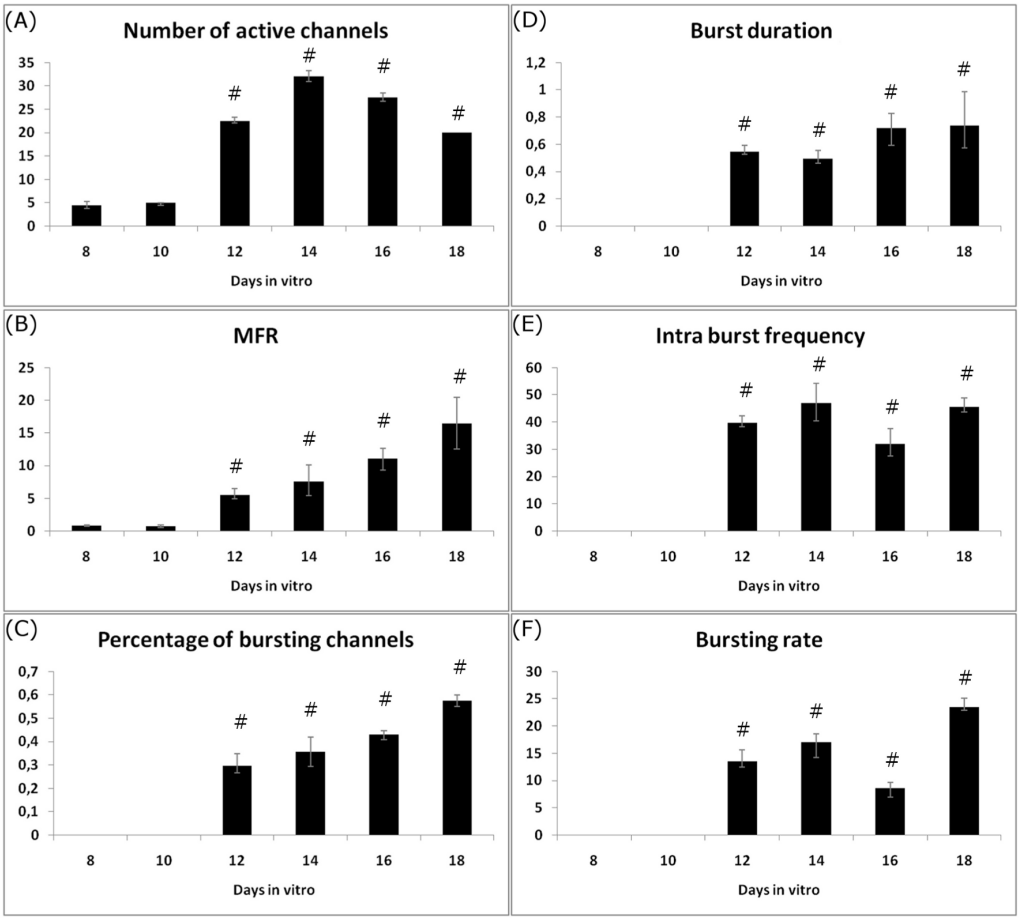

Figure 7.7: Development and maturation of neuronal networks were assessed by monitoring six parameters (y-axis units are reported as title of each graph): (A) number of active channels, (B) mean firing rate in Hz, (C) ratio between the number of channels showing bursts and the number of active channels, (D) burst duration in seconds, (E) intra-burst frequency in Hz, (F) number of bursts occurring in 5 minutes. The pound key identifies significant differences ($p<0.05$) compared with the 10 DIV data.

for all the active electrodes. Specifically, red bars refer to spikes which occurred in the upper compartment, while black bars are spikes in the lower one. Synchronous phenomena are clearly uncorrelated between the two sub-networks.

Activity features were also evaluated quantitatively in the two compartments (Table 7.1): network parameters did not evidence noticeable differences between the two sides.

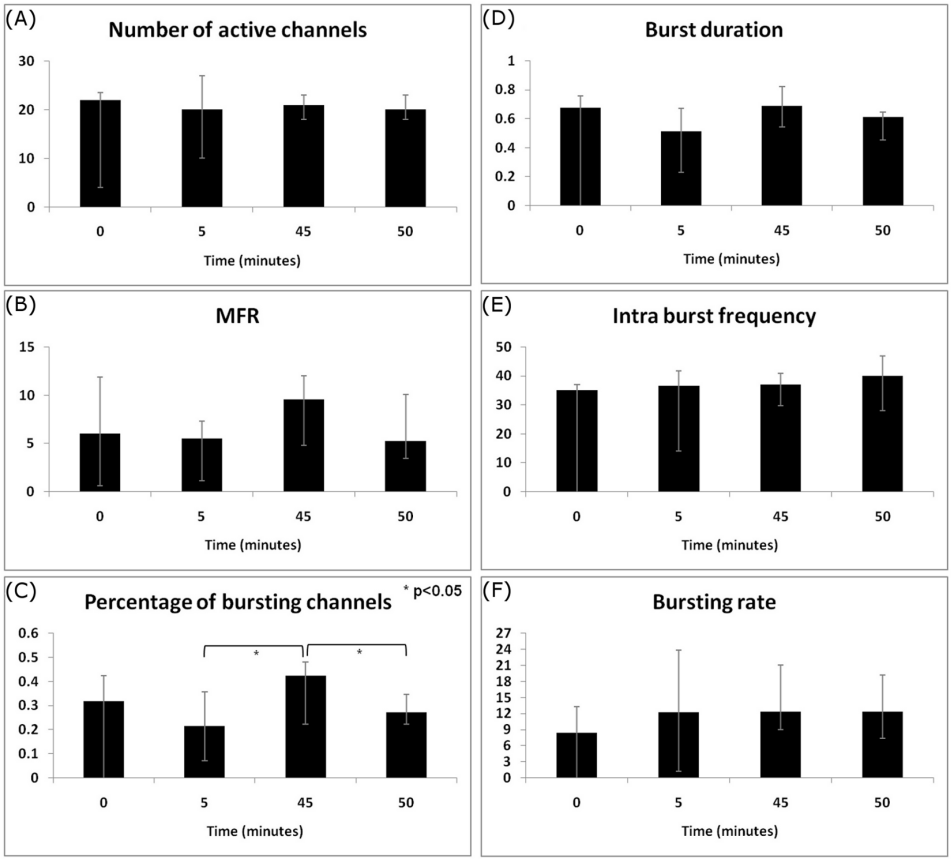

Figure 7.8: Network parameters were evaluated 4 times at each observation occurrence (i.e.: straight after, 5 min, 45 min, 50 min after the removal of the magnet). Monitored parameters were (y-axis units are reported as title of each graph): (A) number of active channels, (B) mean firing rate in Hz, (C) ratio between the number of channels showing bursts and the number of active channels, (D) burst duration in seconds, (E) intra-burst frequency in Hz, (F) number of bursts occurring in 5 minutes. The star identifies significant differences ($p < 0.05$) between values enclosed by braces.

	Spiking channels	Mean firing rate (Hz)	Bursting channels (%)	Burst length (s)
Lower compartment	8	6.42	0.25	0.26
Upper compartment	13	5.51	0.23	0.28

Table 7.1: Example of parameter values which describe neuronal activity in the lower and upper compartments.

Finally, the device was tested for spatially resolved drug delivery. Intensity values were extracted from each image acquired during the dye delivery at a flow rate of 10 μl/min, i.e. 5 μl/min in each channel. Figure 7.12 depicts the dye kinetic. At this flow rate, the dye reached its maximal concentration (upper constant value of the curve) after about six seconds, which is a negligible duration in 3 minute exper-

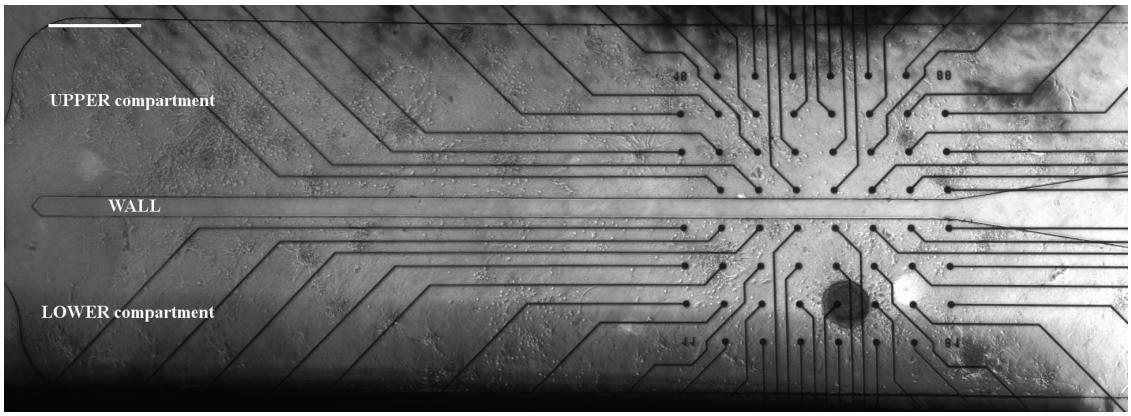

Figure 7.9: Composition of 5x differential interference contrast images (DIC) of a neuronal network grown within the microfluidic device (dual channel configuration). In the middle, it is possible to observe the 100 μm wall which creates two compartments. Scale bar 500 μm.

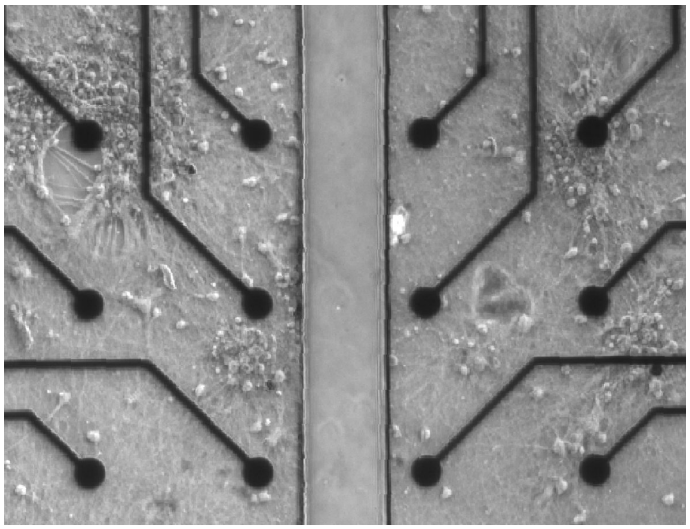

Figure 7.10: Details of Figure 7.9.

iments. Accordingly, TTX delivery was carried on at a flow rate of 10 μl/min. The mean firing rate decreased as expected during its addition in the treated side while the untreated compartment maintained a constant mean firing rate. Moreover, TTX reversible bond to neurons gave the possibility of washing the treated part and thus performing the same protocol in a mirrored configuration. Figure 7.13 shows normalized MFR values of five significant time points during a stimulation experiment. First, neuronal activity in both compartments is acquired during fresh medium addition. Then, TTX is added in the upper compartment, inducing the MFR_{up} to drastically decrease. In contrast, MFR_{low} remains constant. Subsequently, both compartments are washed with fresh medium and the activity of the upper network recovers. This underlined that the selected flow rate (300 μl/min) was sufficient for a complete washing but not high enough to compromise cellular adhesion. Then,

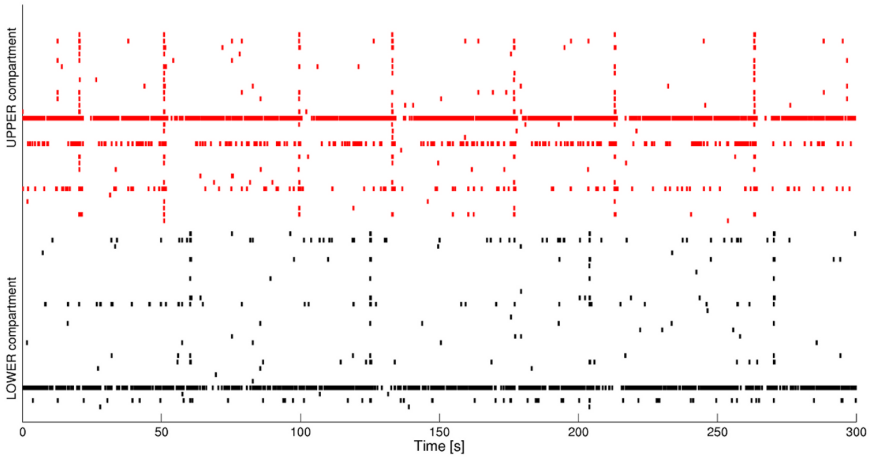

Figure 7.11: Example of neuronal electrical activity within a dual channel device. Each bar line is a spike which is detected by electrodes of the upper (red) or the lower (black) compartment.

TTX is added in the lower compartment, letting the MFR_{low} decreasing down to zero, and again recovering after fresh medium addition.

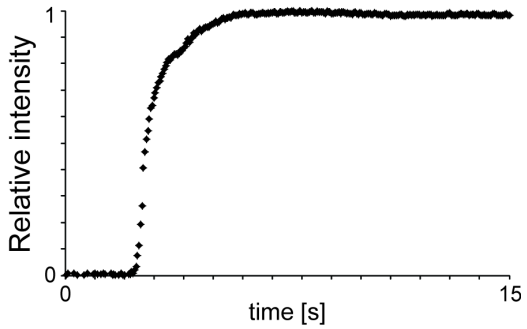

Figure 7.12: Dye experimental concentration profile resulted from quantitative evaluation of the dye intensity in each image acquired with a camera during the dye delivery (flow rate 10 μl/min). After few seconds the dye reaches its maximal concentration.

7.4 Discussion

In this chapter, it is proposed a method to culture and chemically stimulate neuronal networks using a magnetic microfluidic device reversibly coupled to an array of microelectrodes for extracellular electrophysiology. The presented device was developed using a two-mold fabrication process that allowed to obtain two bonded PDMS layers, one partially filled with iron powder and the other one containing microfluidic channels [Rasponi et al., 2011]. PDMS device was leant on a flat MEA surface, aligning under a stereomicroscope the culturing channel with the array of 60 microelectrodes, and a neodymium magnet was placed on the opposite side of the MEA

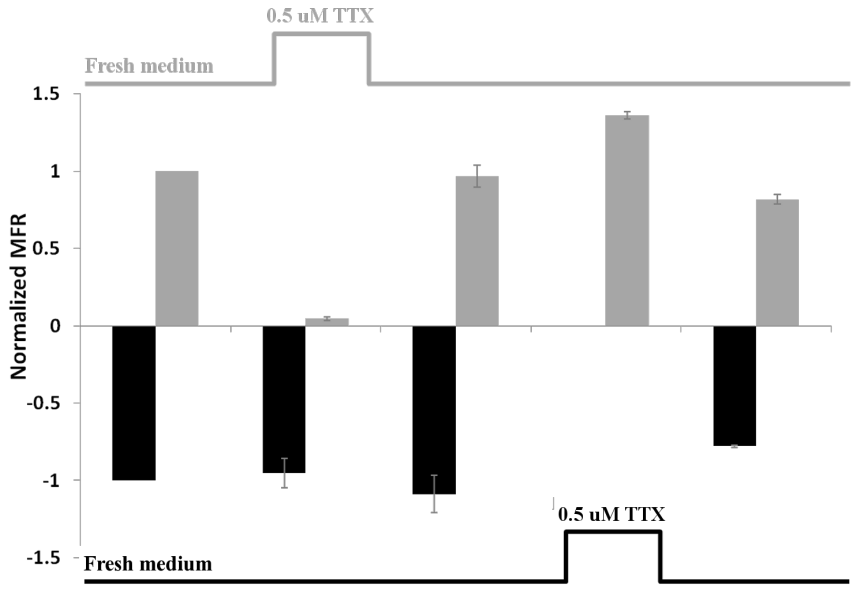

Figure 7.13: Stimulation experiments of the upper (gray) and lower (black) compartments. Values are mediated on 1 minute bins and normalized on the first untreated value. Variability is stated as 25^{th} and 75^{th} percentiles. The two lines represent the delivery protocol for each compartment.

chip, guaranteeing a reversible bonding. In general, reversible bonding is based on van der Waals forces, partial plasma treatment or vacuum seal by aspiration [Anwar et al., 2011] but the maximum pressures sustained with these methods are not sufficient for an efficient sealing. An hydraulic reliable tightness has a key role in long-term electrophysiological experiments, when procedures can induce mechanical stresses and consequently leakages that, even confined, would harm neuronal activity recordings. The magnetic bonding used here is more stable and ensures hydraulic tightness of the micro-channels even under high pressure conditions [Rasponi et al., 2011]. The possibility to work with high flow rates in a reliable way allows introducing pharmacological compounds by means of syringe pumps without hydraulic leakages, and in turn reduces device failure chances. Certainly, a good compromise with pressures sustained by neuronal cells must be found during drug additions. Furthermore, the reversibility of the bonding makes possible the re-use of expensive substrates like the MEA biochip employed for electrophysiological studies.

The design of the described microfluidic device guaranteed simple procedures for cell seeding, offering at the same time a good solution for the long-term growth of dissociated neurons. Indeed, neuronal networks were able to differentiate within few days and to form complex functional networks in the following weeks. Furthermore, maturation of morphological characteristics (e.g. cells' shape, amount of neurites and axons) were comparable with that of networks cultured in macro-environment (Petri dishes or MEA biochips with plastic ring), by expert visual inspection. More-

over, the ability of culturing neurons up to three weeks confirmed that the magnet did not have negative effects on neuronal development.

The characteristics of neuronal electrical activity changed over time during neuronal network differentiation and maturation. Previous works reported the existence of a relationship between the age of the culture and its functionality, expressed as spiking activity [Ichikawa et al., 1993, Ben-Ari, 2001, Chiappalone et al., 2006]. At 7 DIV, cultures show low synaptic density and minor neuronal cell connectivity, with a significant increase at 14 DIV [Ichikawa et al., 1993], which reflects the maturation of electrophysiological properties. Indeed, at 7 DIV the electrical activity is characterized by single spikes and almost no bursts, whereas at 14 DIV the network exhibits an increase in firing rate, a rich and stable burst pattern and high synchronized periods of high frequency activity, encompassing simultaneously a large number of channels [Chiappalone et al., 2006]. Results presented in this chapter are in agreement with the state of the art, proving that these devices can be considered and used likewise macroscale devices for neuronal growth and electrophysiology, with the additional advantage that experiments can be performed in a microenvironment, suitable for manipulation of small fluid volumes. Furthermore, this drastically reduces the experimental costs related to compounds and reagents.

The statistical analysis of the 4 recordings performed at different time frames did not highlight significant changes among them with the exception of the percentage of bursting channels after 45 minutes from the removal of the magnet. These recordings occurred after the repositioning of the biochip from the incubator to the recording setup. Previous works [Streit et al., 2001, Chiappalone et al., 2006] stressed the importance of waiting 5 to 20 minutes to record a stable signal, since neuronal cultures are particularly sensitive to mechanical disturbances. This effect could explain differences determined in the percentage of bursting channels. Moreover, it can also justify the variability, higher than the others, found in the first recordings for all parameters. These mechanical stresses would be avoided by using a system that grows neurons and records their activity, as the one presented in Chapter 4. Except for the slight differences observed in the 45 minute recordings, these data allowed dismissing the idea of a possible influence of the magnetic field on neuronal activity, since data recorded at different time frames were comparable. The effect of a static magnetic field on neurons has been previously studied in the literature with both molecular [Hirai et al., 2002, Hirai and Yoneda, 2004] and electrophysiological approaches[Sonnier et al., 2000, McLean et al., 1995, Cavopol et al., 1995]. Evidence of a modulatory effect of the magnetic field on electrical activity was reported. Currently, alteration of the activation kinetics of voltage dependent calcium channels is considered the most likely mechanism that causes this effect [Prina-Mello et al., 2006]. In this work, hippocampal networks were

maintained for 18 days in a continuous static magnetic field with intensity roughly equal to 50 mT. This field intensity is 1-fold lower than the threshold (500 mT) for cellular stress response and for the alteration of the calcium channels kinetics [Prina-Mello et al., 2005, 2006]. In addition, the proposed microfluidic device enables hydraulic tightness even with a discontinuous magnetic field exposure, thus limiting the use of magnet only to the most critical operations [Rasponi et al., 2011].

These features were exploited in the dual channel configuration which was obtained by placing a thin PDMS wall in the middle of the main channel. This thin wall partially divided the device in two compartments, whose microenvironments were in communication under static conditions, while they were fluidically separated during delivery. Moreover, the wall perfectly matched the inter electrode distance which allowed not to lose active recording electrodes. Furthermore, this configuration arranged neuronal cells into two networks which were qualitatively similar in morphology, which was quantitatively verified by comparing descriptors of the electrophysiological activity computed inside both compartments. It was also quantified the functional connectivity between the two sub-networks (inter-compartmental functional connectivity). Then, it was compared with the intra-compartmental functional connectivity, which was established in the network within a single compartment. It revealed that functional connectivity was influenced by the compartmentalization since inter-compartmental functional connectivity was lower than the intra-compartmental one. Therefore, these devices can be used to culture twin networks similar in cell density and functionality and not functionally connected. Although these two networks conceptually correspond to two individual MEAs, cells are here seeded together and grown in the same biochemical microenvironment, thus reducing the experimental variability [Johnstone et al., 2010].

Further, the relevance of the twin network configuration in drug delivery experiments was proven. First, the experimental concentration profile of the dye was assessed and attested the possibility of using low flow rate and concurrently reaching maximal concentration values after a limited and controlled time extent. Then, it was demonstrated the possibility of stimulating each neuronal network individually. Moreover, it was observed neither electrode saturation nor cell undesirable response during molecule delivery.

To conclude, the proposed microfluidic approach represents an innovative methodology to perform biological, pharmacological and electrophysiological experiments. Indeed, thanks to the features offered by microfluidics, the device configurations developed here make the delivery of substances to cells easier and cheaper than traditional methods. Furthermore, they overcome the limitations due to standard drug stimulation techniques such as unknown drug-cell interaction kinetic, inaccurate drug concentration, uncontrolled time duration necessary for a maximal stimula-

tion, electrode saturation and cellular response caused by rapid macro-environmental changes. Finally, the twin network configuration reduces biological variability. This has important outcomes on pharmacological and drug screening and thus represents a new experimental approach for *in vitro* cellular physiology in health and in disease.

Chapter 8

Conclusions and future developments

My PhD thesis first underlines the high impact of standard multisite electrophysiological studies on neurons towards brain disease research. Indeed, in this work, Micro Electrode Arrays (MEAs) were used to study electrophysiological properties of neuronal networks which modelled physiological or pathological conditions. Specifically, it was mimicked the typical inflammatory milieu of active neuro-inflammation by treating *in vitro* neuronal cultures with pro-inflammatory cytokines (Chapter 3). Then, changes in neuronal electrical activity between control and impaired states were detected by means of MEAs. Thanks to these experiments, it was found out that chronic inflammatory stimulation of neuronal networks leads to profound alteration of γ-aminobutyric acid (GABA) transmission. Furthermore, MEA recording protocols and standard algorithms for electrophysiological analysis were arranged. Finally, experiments highlighted that it was valuable to follow continuously network activity and to deepen cytokine-neuron interaction kinetic. Furthermore, the addition of cytokines and other modulatory molecules underlined difficulties in network stimulation by means of pipettes which often provoked electrode saturation or neuronal cell uncontrolled response.

Hence, during these years my work aimed at progressing standard technologies for neuronal multisite recording and drug stimulation. Specifically, the final outcome of this thesis is the development and assessment of systems which allow MEA continuous long-term investigations and controlled local cell stimulations.

The incubating and recording chamber developed hereby (Chapter 4) solves the problem of MEA long term acquisitions by growing cells and recording their activity since the beginning of their maturation. This reduces thermal, osmotic and mechanic shocks, which neurons are usually subjected to, and thus improves data reproducibility [Gross and Schwalm, 1994]. It was demonstrated that this chamber can grow neuronal networks with morphology and viability comparable to cell cultures grown in standard incubators. Furthermore, it allowed to repeatedly record neuronal electrical activity reducing mechanical disturbances and cellular stress and

thus increasing experimental duration. Another strength of the system is the possibility of housing multiple MEAs inside the chamber, which guarantees parallel tests in the same controlled environment. Furthermore, the completion of the 60-channel preprocessing board will make the chamber portable and indipendent not only from incubators but also from standard recording equipments. Therefore, the system will guarantee multisite long-term continuous recordings of neuronal activity. These will be definitively feasible by developing dedicated and specific hardware for signal post-processing, whose design was presented in Chapter 5. Indeed, the integration of a Field Programmable Gate Array (FPGA) and a Digital Signal Processors (DSP) will allow online data analysis and thus data occupation reduction. Furthermore, the ability of extracting comprehensive parameters of correlated network activity will enhance the compactness and the automation of the device. Several parameters were proposed in the literature and used in this thesis with the aim of describing spontaneous electrophysiological activity. In addition, a single comprehensive and high sensitive descriptor, focused specifically on neuropharmacology, was developed and validated within this PhD work (Chapter 6). All these technologies have high impact in the neuroscience field. Indeed, many studies are now based on long-term network plasticity and development, which are important phenomena in learning and memory processes [van Pelt et al., 2004a, Baruchi and Ben-Jacob, 2007]. Moreover, investigations which require continuous monitoring of neuronal activity, such as test of drugs with unknown kynetics, would take advantage of them [Johnstone et al., 2010]. Finally, they would allow to follow electrophysiological changes of networks obtained from pathological animal models and to deepen our understanding on neurodegeneration.

Concerning cell stimulation, the microfluidic device, described in Chapter 7, solves the drawbacks of standard stimulation techniques. Particularly, the microchamber enables to work with twin networks which are two identical networks grown in the same microenvironment but not functionally connected. Furthermore, it allows to stimulate selectively only one of them and avoids electrode saturation and undesiderable cell response, which are usually caused by standard stimulation. Once more, this approach reduces the variability which characterizes experiments with different MEAs [Johnstone et al., 2010] and provides, on the same device, both the treated and the control trial. This feature is valuable in neuropharmacological research since a big question in network functionality measured by MEAs is culture-to-culture variability [Wagenaar et al., 2006a,b]. Moreover, the device would improve comparability of compounds tested within the same plate [Johnstone et al., 2010]. Finally, it would allow to grow and stimulate on a single device both physiological and pathological animal models, comparing their electrophysiology in a more reliable manner.

To conclude, it is appealing the perspective of an integration of these devices into a single one. Indeed, they may be coupled in a compact system after simple changes. Specifically, it would be necessary only to configure the culturing and recording chamber for syringe pump lines insertion and to replace the standard MEA with the PDMS microfluidic chamber. Furthermore, positive outcomes of this integration would be enhanced by culturing concurrently an animal model of disease and a its control network. As Figure 8.1 depicts, the system would permit long-term electrophysiological and optical examination of *in vitro* brain models during selective and controlled stimulation of cell activity, while maintaining environmental conditions. This integrated system could have a high impact on the screening of neuroactive molecules promoting a better understanding of brain pathologies and neurodegenerative diseases. To conclude, this thesis work provides the elements that establish an integrated electrophysiological and pharmacological workstation for brain studies and offers great advantages in central nervous system research.

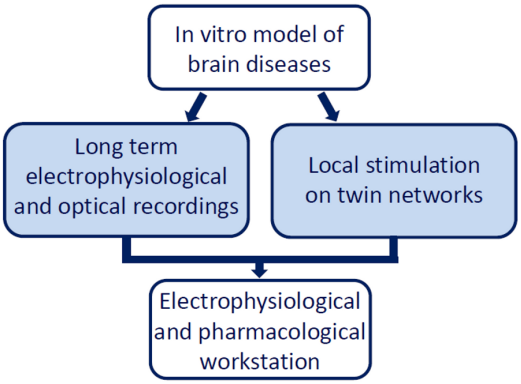

Figure 8.1: Hypothesis of the final integration of the developed devices.

Bibliography

M Abeles and MH Goldstein. Multispike train analysis. *Proc IEEE*, 65:762–773, 1977.

L Aloe, F Properzi, L Probert, K Akassoglou, G Kassiotis, A Micera, and M Fiore. Learning abilities, ngf and bdnf brain levels in two lines of tnf-alpha transgenic mice, one characterized by neurological disorders, the other phenotypically normal. *Brain Res*, 840:125–137, 1999.

DJ Anschel, E Ortega, and RS Fisher. Diazepam prophylaxis for bicuculline-induced seizures: a rat dose-response model. *Neurosci Lett*, 356:66–68, 2004.

K Anwar, T Han, and SM Kim. Reversible sealing techniques for microdevice applications. *Sensors and Actuators B: Chemical*, 153:301–311, 2011.

H Arimochi and K Morita. High salt culture conditions suppress proliferation of rat c6 glioma cell by arresting cell-cycle progression at s-phase. *J Mol Neurosci*, 27: 293–301, 2005.

Q Bai and KD Wise. Single-unit neural recording with active microelectrode arrays. *IEEE Trans Biomed Eng*, 48:911–920, 2001.

BJ Baker, EK Kosmidis, D Vucinic, CX Falk, LB Cohen, M Djurisic, and D Zecevic. Imaging brain activity with voltage- and calcium-sensitive dyes. *Cell Mol Neurobiol*, 25:245–282, 2005.

G Banker and K Goslin. *Culturing nerve cells*. 2nd ed. MIT Press, 1998.

IN Bankman, KO Johnson, and W Schneider. Optimal detection, classification, and superposition resolution in neural waveform recordings. *IEEE Trans Biomed Eng*, 40:836–841, 1993.

J Barclay and M Rees. Mouse models of spike-wave epilepsy. *Epilepsia*, 40 Suppl 3: 17–22, 1999.

R Bartesaghi, S Guidi, and E Ciani. Is it possible to improve neurodevelopmental abnormalities in down syndrome? *Rev Neurosci*, 22:419–455, 2011.

I Baruchi and E Ben-Jacob. Towards neuro-memory-chip: imprinting multiple memories in cultured neural networks. *Phys Rev E Stat Nonlin Soft Matter Phys*, 75: 050901, 2007.

I Baruchi, D Grossman, V Volman, M Shein, J Hunter, VL Towle, and E Ben-Jacob. Functional holography analysis: simplifying the complexity of dynamical networks. *Chaos*, 16:015112, 2006.

I Baruchi, V Volman, N Raichman, M Shein, and E Ben-Jacobch. The emergence and properties of mutual synchronization in in vitro coupled cortical networks. *Eur J Neurosci*, 28:1825–1835, 2008.

BD Bavister. A minichamber device for maintaining a constant carbon dioxide in air atmosphere during prolonged culture of cells on the stage of an inverted microscope. *In Vitro Cell Dev Biol*, 24:759–763, 1988.

EC Beattie, D Stellwagen, W Morishita, JC Bresnahan, BK Ha, MV Zastrow, MS Beattie, and RC Malenka. Control of synaptic strength by glial tnfalpha. *Science*, 295:2282–2285, 2002.

Y Ben-Ari. Developing networks play a similar melody. *Trends Neurosci*, 24:353–360, 2001.

K Benkrid and D Crookes. New bit-level algorithm for general purpose median filtering. *J Electron Imaging*, 12:263–269, 2003.

BD Bennett and JP Bolam. Synaptic input and output of parvalbumin-immunoreactive neurons in the neostriatum of the rat. *Neuroscience*, 62:707–719, 1994.

L Berdondini, PD. van der Wal, O Guenat, NF de Rooij, M Koudelka-Hep, P Seitz, R Kaufmann, P Metzler, N Blanc, and S Rohr. High-density electrode array for imaging in vitro electrophysiological activity. *Biosens Bioelectron*, 21:167–174, 2005.

L Berdondini, M Chiappalone, PD van der Wal, K Imfeld, NF de Rooij, M Koudelka-Hep, M Tedesco, S Martinoia, J van Pelt, G Le Masson, and A Garenne. A microelectrode array (mea) integrated with clustering structures for investigating in vitro neurodynamics in confined interconnected sub-populations of neurons. *Sensors and Actuators B: Chemical*, 114:530–541, 2006.

L Berdondini, K Imfeld, A Maccione, MT, S Neukom, M Koudelka-Hep, and S Martinoia. Active pixel sensor array for high spatio-temporal resolution electrophysi-

ological recordings from single cell to large scale neuronal networks. *Lab Chip*, 9: 2644–2651, 2009a.

L Berdondini, P Massobrio, M Chiappalone, M Tedesco, K Imfeld, A Maccione, M Gandolfo, M Koudelka-Hep, and S Martinoia. Extracellular recordings from locally dense microelectrode arrays coupled to dissociated cortical cultures. *J Neurosci Methods*, 177:386–396, 2009b.

R Bhat, R Axtell, A Mitra, M Miranda, C Lock, RW Tsien, and L Steinman. Inhibitory role for gaba in autoimmune inflammation. *Proc Natl Acad Sci U S A*, 107:2580–2585, 2010.

E Biffi, D Ghezzi, A Pedrocchi, and G Ferrigno. Development and validation of a spike detection and classification algorithm aimed at implementation on hardware devices. *Comput Intell Neurosci*, page 659050, 2010.

E Biffi, A Menegon, G Regalia, S Maida, G Ferrigno, and A Pedrocchi. A new cross-correlation algorithm for the analysis of "in vitro" neuronal network activity aimed at pharmacological studies. *J Neurosci Methods*, 199:321–327, 2011.

C Bjartmar, JR Wujek, and BD Trapp. Axonal loss in the pathology of ms: consequences for understanding the progressive phase of the disease. *J Neurol Sci*, 206: 165–171, 2003.

A Blau, T Neumann, C Ziegler, and F Benfenati. Replica-moulded polydimethylsiloxane culture vessel lids attenuate osmotic drift in long-term cell cultures. *J Biosci*, 34:59–69, 2009.

AW Blau and CM Ziegler. Prototype of a novel autonomous perfusion chamber for long-term culturing and in situ investigation of various cell types. *J Biochem Biophys Methods*, 50:15–27, 2001.

MD Boehler, BC Wheeler, and GJ Brewer. Added astroglia promote greater synapse density and higher activity in neuronal networks. *Neuron Glia Biol*, 3:127–140, 2007.

AA Boldyreva. Lanthanum potentiates gaba-activated currents in rat pyramidal neurons of ca1 hippocampal field. *Bull Exp Biol Med*, 140:403–405, 2005.

LL Bologna, V Pasquale, M Garofalo, M Gandolfo, PL Baljon, A Maccione, S Martinoia, and M Chiappalone. Investigating neuronal activity by spycode multi-channel data analyzer. *Neural Netw*, 23:685–697, 2010.

P Bonifazi, ME Ruaro, and V Torre. Statistical properties of information processing in neuronal networks. *Eur J Neurosci*, 22:2953–2964, 2005.

T Borghi, A Bonfanti, G Zambra, R Gusmeroli, AL Lacaita, AS Spinelli, and G Baranauskas. An integrated low-noise multichannel system for neural signals amplification. In *Proc. 33rd European Solid State Circuits Conf. ESSCIRC 2007*, pages 456–459, 2007.

GJ Brewer. Isolation and culture of adult rat hippocampal neurons. *J Neurosci Methods*, 71:143–155, 1997.

DA Brown and PE Sawchenko. Time course and distribution of inflammatory and neurodegenerative events suggest structural bases for the pathogenesis of experimental autoimmune encephalomyelitis. *J Comp Neurol*, 502:236–260, 2007.

EN Brown, RE Kass, and PP Mitra. Multiple neural spike train data analysis: state-of-the-art and future challenges. *Nat Neurosci*, 7:456–461, 2004.

M Brunner, G Karg, and UT Koch. An improved system for single unit isolation from multiunit nerve recordings by velocity analysis. *J Neurosci Methods*, 33:1–9, 1990.

O Butovsky, Y Ziv, A Schwartz, G Landa, AE Talpalar, S Pluchino, G Martino, and M Schwartz. Microglia activated by il-4 or ifn-gamma differentially induce neurogenesis and oligodendrogenesis from adult stem/progenitor cells. *Mol Cell Neurosci*, 31:149–160, 2006.

G Buzsáki, Z Horváth, R Urioste, J Hetke, and K Wise. High-frequency network oscillation in the hippocampus. *Science*, 256:1025–1027, 1992.

AJ Cadotte, TB DeMarse, P He, and M Ding. Causal measures of structure and plasticity in simulated and living neural networks. *PLoS One*, 3:e3355, 2008.

RB Campenot. Local control of neurite development by nerve growth factor. *Proc Natl Acad Sci U S A*, 74:4516–4519, 1977.

MD Caramia, MG Palmieri, MT Desiato, L Boffa, P Galizia, PM Rossini, D Centonze, and G Bernardi. Brain excitability changes in the relapsing and remitting phases of multiple sclerosis: a study with transcranial magnetic stimulation. *Clin Neurophysiol*, 115:956–965, 2004.

AV Cavopol, AW Wamil, RR Holcomb, and MJ McLean. Measurement and analysis of static magnetic fields that block action potentials in cultured neurons. *Bioelectromagnetics*, 16:197–206, 1995.

A Ceccarelli, MA Rocca, M Neema, V Martinelli, A Arora, S Tauhid, A Ghezzi, G Comi, R Bakshi, and M Filippi. Deep gray matter t2 hypointensity is present in

patients with clinically isolated syndromes suggestive of multiple sclerosis. *Mult Scler*, 16:39–44, 2010.

D Centonze, L Muzio, S Rossi, F Cavasinni, V De Chiara, A Bergami, A Musella, M D'Amelio, V Cavallucci, A Martorana, A Bergamaschi, MT Cencioni, A Diamantini, E Butti, G Comi, G Bernardi, F Cecconi, L Battistini, R Furlan, and G Martino. Inflammation triggers synaptic alteration and degeneration in experimental autoimmune encephalomyelitis. *J Neurosci*, 29:3442–3452, 2009.

HL Chan, MA Lin, T Wu, ST Lee, YT Tsai, and PK Chao. Detection of neuronal spikes using an adaptive threshold based on the max-min spread sorting method. *J Neurosci Methods*, 172:112–121, 2008.

R Chandra and LM Optican. Detection, classification, and superposition resolution of action potentials in multiunit single-channel recordings by an on-line real-time neural network. *IEEE Trans Biomed Eng*, 44:403–412, 1997.

G Charvet, L Rousseau, O Billoint, S Gharbi, JP Rostaing, S Joucla, M Trevisiol, A Bourgerette, P Chauvet, C Moulin, F Goy, B Mercier, M Colin, S Spirkovitch, H Fanet, P Meyrand, R Guillemaud, and B Yvert. Biomea: a versatile high-density 3d microelectrode array system using integrated electronics. *Biosens Bioelectron*, 25:1889–1896, 2010.

C Chen, L Chen, Y Lin, S Zeng, and Q Luo. The origin of spontaneous synchronized burst in cultured neuronal networks based on multi-electrode arrays. *Biosystems*, 85:137–143, 2006.

H Chen and JH Zhang. Cerebral amyloid angiopathy-related microhemorrhages in alzheimer's disease: a review of investigative animal models. *Acta Neurochir Suppl*, 111:15–17, 2011.

Y Chen, C Guo, L Lim, S Cheong, Q Zhang, K Tang, and J Reboud. Compact microelectrode array system: tool for in situ monitoring of drug effects on neurotransmitter release from neural cells. *Anal Chem*, 80:1133–1140, 2008.

M Chiappalone, A Vato, M Tedesco, M Marcoli, F Davide, and S Martinoia. Networks of neurons coupled to microelectrode arrays: a neuronal sensory system for pharmacological applications. *Biosens Bioelectron*, 18:627–634, 2003.

M Chiappalone, A Novellino, I Vajda, A Vato, S Martinoia, and J van Pelt. Burst detection algorithms for the analysis of spatio-temporal patterns in cortical networks of neurons. *Neurocomputing*, 65:653–662, 2005.

M Chiappalone, M Bove, A Vato, M Tedesco, and S Martinoia. Dissociated cortical networks show spontaneously correlated activity patterns during in vitro development. *Brain Res*, 1093:41–53, 2006.

M Chiappalone, A Vato, L Berdondini, M Koudelka-Hep, and S Martinoia. Network dynamics and synchronous activity in cultured cortical neurons. *Int J Neural Syst*, 17:87–103, 2007.

M Chiappalone, P Massobrio, and S Martinoia. Network plasticity in cortical assemblies. *Eur J Neurosci*, 28:221–237, 2008.

CB Chien and J Pine. Voltage-sensitive dye recording of action potentials and synaptic potentials from sympathetic microcultures. *Biophys J*, 60:697–711, 1991.

ES Chornoboy, LP Schramm, and AF Karr. Maximum likelihood identification of neural point process systems. *Biol Cybern*, 59:265–275, 1988.

GS Christiansen, B Danes, L Allen, and PJ Leinfelder. A culture chamber for the continuous biochemical and morphological study of living cells in tissue culture. *Exp Cell Res*, 5:10–15, 1953.

E Claverol-Tinture, J Cabestany, and X Rosell. Multisite recording of extracellular potentials produced by microchannel-confined neurons in-vitro. 54:331–335, 2007.

RJ Clements, J McDonough, and EJ Freeman. Distribution of parvalbumin and calretinin immunoreactive interneurons in motor cortex from multiple sclerosis post-mortem tissue. *Exp Brain Res*, 187:459–465, 2008.

W Dabrowski, P Grybos, and AM Litke. A low noise multichannel integrated circuit for recording neuronal signals using microelectrode arrays. *Biosens Bioelectron*, 19:749–761, 2004.

A Daffertshofer, CJ Lamoth, OG Meijer, and PJ Beek. Pca in studying coordination and variability: a tutorial. *Clin Biomech (Bristol, Avon)*, 19:415–428, 2004.

Ted M Dawson, Han Seok Ko, and Valina L Dawson. Genetic animal models of parkinson's disease. *Neuron*, 66:646–661, 2010.

BD DeBusschere and GT Kovacs. Portable cell-based biosensor system using integrated cmos cell-cartridges. *Biosens Bioelectron*, 16:543–556, 2001.

TB Demarse, DA Wagenaar, AW Blau, and SM Potter. The neurally controlled animat: Biological brains acting with simulated bodies. *Auton Robots*, 11:305–310, 2001.

DC Duffy, JC McDonald, OJA Schueller, and GM Whitesides. Rapid prototyping of microfluidic systems in poly(dimethylsiloxane). *Anal Chem*, 70:4974–4984, 1998.

A Durukan and T Tatlisumak. Ischemic stroke in mice and rats. *Methods Mol Biol*, 573:95–114, 2009.

R Dutta, J McDonough, X Yin, J Peterson, A Chang, T Torres, T Gudz, WB Macklin, DA Lewis, RJ Fox, R Rudick, K Mirnics, and BD Trapp. Mitochondrial dysfunction as a cause of axonal degeneration in multiple sclerosis patients. *Ann Neurol*, 59:478–489, 2006.

BJ Dworak and BC Wheeler. Novel mea platform with pdms microtunnels enables the detection of action potential propagation from isolated axons in culture. *Lab Chip*, 9:404–410, 2009.

JP Eckmann, O Feinerman, L Gruendlinger, E Moses, J Soriano, and T Tlusty. The physics of living neural networks. *Physics Reports*, 449:54–76, 2007.

AK Engel, P Fries, and W Singer. Dynamic predictions: oscillations and synchrony in top-down processing. *Nat Rev Neurosci*, 2:704–716, 2001.

F Esposti and MG Signorini. Synchronization of neurons in micro-electrode array cultures. *Eur Phys J*, 97:547–554, 2008.

D Eytan and S Marom. Dynamics and effective topology underlying synchronization in networks of cortical neurons. *J Neurosci*, 26:8465–8476, 2006.

D Eytan, A Minerbi, N Ziv, and S Marom. Dopamine-induced dispersion of correlations between action potentials in networks of cortical neurons. *J Neurophysiol*, 92:1817–1824, 2004.

CL Faingold. Emergent properties of cns neuronal networks as targets for pharmacology: application to anticonvulsant drug action. *Prog Neurobiol*, 72:55–85, 2004.

E Fantini, P Athias, M Courtois, and A Grynberg. A simple gas-flow chamber for cultured cell electrophysiology in a controlled atmosphere. *Pflugers Arch*, 409: 632–634, 1987.

A Feigenspan and R Weiler. Electrophysiological properties of mouse horizontal cell gabaa receptors. *J Neurophysiol*, 92:2789–2801, 2004.

M Fejtl, A Stett, W Nisch, KH Boven, and A Moller. *On Micro-Electrode Array Revival: Its Development, Sophistication of Recording, and Stimulation*. Springer, 2006.

G Fisone, Kn Håkansson, A Borgkvist, and E Santini. Signaling in the basal ganglia: postsynaptic and presynaptic mechanisms. *Physiol Behav*, 92:8–14, 2007.

ID Forsythe and RT Coates. A chamber for electrophysiological recording from cultured neurones allowing perfusion and temperature control. *J Neurosci Methods*, 25:19–27, 1988.

U Frey, U Egert, F Heer, S Hafizovic, and A Hierlemann. Microelectronic system for high-resolution mapping of extracellular electric fields applied to brain slices. *Biosens Bioelectron*, 24:2191–2198, 2009.

S Fujii, H Sasaki, K Ito, K Kaneko, and H Kato. Temperature dependence of synaptic responses in guinea pig hippocampal ca1 neurons in vitro. *Cell Mol Neurobiol*, 22(4):379–391, Aug 2002.

M Gandolfo, A Maccione, M Tedesco, S Martinoia, and L Berdondini. Tracking burst patterns in hippocampal cultures with high-density cmos-meas. *J Neural Eng*, 7:056001, 2010.

Y Gao, D Majumdar, B Jovanovic, C Shaifer, PC Lin, A Zijlstra, DJ Webb, and D Li. A versatile valve-enabled microfluidic cell co-culture platform and demonstration of its applications to neurobiology and cancer biology. *Biomed Microdevices*, 13:539–548, 2011.

M Garofalo, T Nieus, P Massobrio, and S Martinoia. Evaluation of the performance of information theory-based methods and cross-correlation to estimate the functional connectivity in cortical networks. *PLoS One*, 4:e6482, 2009.

D Ghezzi, A Menegon, A Pedrocchi, F Valtorta, and G Ferrigno. A micro-electrode array device coupled to a laser-based system for the local stimulation of neurons by optical release of glutamate. *J Neurosci Methods*, 175:70–78, 2008.

H Golan, T Levav, A Mendelsohn, and M Huleihel. Involvement of tumor necrosis factor alpha in hippocampal development and function. *Cereb Cortex*, 14:97–105, 2004.

Z Gottesfeld, D Teitelbaum, C Webb, and R Arnon. Changes in the gaba system in experimental allergic encephalomyelitis-induced paralysis. *J Neurochem*, 27: 695–699, 1976.

B Gourévitch and JJ Eggermont. A nonparametric approach for detection of bursts in spike trains. *J Neurosci Methods*, 160:349–358, 2007.

A Gramowski, S Stuwe, K Jugelt, D Schiffmann, J Loock, O Schroder, GW Gross, and DG Weiss. Detecting neurotoxicity through electrical activity changes of neuronal networks on multielectrode neurochips. *ALTEX*, Special Issue 2,22:414–419, 2005.

SA Gray, JK Kusel, KM Shaffer, YS Shubin, DA Stenger, and JJ Pancrazio. Design and demonstration of an automated cell-based biosensor. *Biosens Bioelectron*, 16: 535–542, 2001.

A Grinvald, A Manker, and M Segal. Visualization of the spread of electrical activity in rat hippocampal slices by voltage-sensitive optical probes. *J Physiol*, 333:269–291, 1982.

G Gross and J Kowalski. *Experimental and Theoretical Analysis of Random Nerve Cell Network Dynamic.* Prentice-Hall, 1991.

G. W. Gross. Simultaneous single unit recording in vitro with a photoetched laser deinsulated gold multimicroelectrode surface. *IEEE Trans Biomed Eng*, 26:273–279, 1979.

GW Gross and FU Schwalm. A closed flow chamber for long-term multichannel recording and optical monitoring. *J Neurosci Methods*, 52:73–85, 1994.

GW Gross, AN Williams, and JH Lucas. Recording of spontaneous activity with photoetched microelectrode surfaces from mouse spinal neurons in culture. *J Neurosci Methods*, 5:13–22, 1982.

PG Gross, EP Kartalov, A Scherer, and LP Weiner. Applications of microfluidics for neuronal studies. *J Neurol Sci*, 252:135–143, 2007.

KS Guillory and RA Normann. A 100-channel system for real time detection and storage of extracellular spike waveforms. *J Neurosci Methods*, 91:21–29, 1999.

K Gupta, DH Kim, D Ellison, C Smith, A Kundu, J Tuan, KY Suh, and A Levchenko. Lab-on-a-chip devices as an emerging platform for stem cell biology. *Lab Chip*, 10:2019–2031, 2010.

ME Gurney, H Pu, AY Chiu, MC Dal Canto, CY Polchow, DD Alexander, J Caliendo, A Hentati, YW Kwon, and HX Deng. Motor neuron degeneration in mice that express a human cu,zn superoxide dismutase mutation. *Science*, 264: 1772–1775, 1994.

N Gustafson, E Gireesh-Dharmaraj, U Czubayko, KT Blackwell, and D Plenz. A comparative voltage and current-clamp analysis of feedback and feedforward

synaptic transmission in the striatal microcircuit in vitro. *J Neurophysiol*, 95: 737–752, 2006.

AC Guyton and JE Hall. *Textbook of Medical Physiology*. Elsevier, 2011.

AM Habets, AM Van Dongen, F Van Huizen, and MA Corner. Spontaneous neuronal firing patterns in fetal rat cortical networks during development in vitro: a quantitative analysis. *Exp Brain Res*, 69:43–52, 1987.

S Hafizovic, F Heer, T Ugniwenko, U Frey, A Blau, C Ziegler, and A Hierlemann. A cmos-based microelectrode array for interaction with neuronal cultures. *J Neurosci Methods*, 164:93–106, 2007.

D Hakkoum, L Stoppini, and D Muller. Interleukin-6 promotes sprouting and functional recovery in lesioned organotypic hippocampal slice cultures. *J Neurochem*, 100:747–757, 2007.

CM Hales, JD Rolston, and SM Potter. How to culture, record and stimulate neuronal networks on micro-electrode arrays (meas). *J Vis Exp*, 2010.

D Han, YN Rao, JC Principe, and K Gugel. Real-time pca (principal component analysis) implementation on dsp. *IEEE Int Joint Conf on Neural Networks*, 3: 2159–2162, 2004.

J Harris, H Lee, CT Tu, D Cribbs, C Cotman, and NL Jeon. Preparing e18 cortical rat neurons for compartmentalization in a microfluidic device. *J Vis Exp. 2007*, 8:305, 2007.

F Heer, S Hafizovic, T Ugniwenko, U Frey, W Franks, E Perriard, J-C Perriard, A Blau, C Ziegler, and A Hierlemann. Single-chip microelectronic system to interface with living cells. *Biosens Bioelectron*, 22:2546–2553, 2007.

SR Heidemann, P Lamoureux, K Ngo, M Reynolds, and RE Buxbaum. Open-dish incubator for live cell imaging with an inverted microscope. *Biotechniques*, 35: 708–714, 716, 2003.

RG Henry, M Shieh, DT Okuda, A Evangelista, ML Gorno-Tempini, and D Pelletier. Regional grey matter atrophy in clinically isolated syndromes at presentation. *J Neurol Neurosurg Psychiatry*, 79:1236–1244, 2008.

MO Heuschkel, M Fejtl, M Raggenbass, D Bertrand, and P Renaud. A three-dimensional multi-electrode array for multi-site stimulation and recording in acute brain slices. *J Neurosci Methods*, 114:135–148, 2002.

T Hirai and Y Yoneda. Functional alterations in immature cultured rat hippocampal neurons after sustained exposure to static magnetic fields. *J Neurosci Res*, 75: 230–240, 2004.

T Hirai, N Nakamichi, and Y Yoneda. Activator protein-1 complex expressed by magnetism in cultured rat hippocampal neurons. *Biochem Biophys Res Commun*, 292:200–207, 2002.

CL Ho, TY Mou, PS Chiang, CL Weng, and NH Chow. Mini chamber system for long-term maintenance and observation of cultured cells. *Biotechniques*, 38: 267–273, 2005.

F Hofmann and H Bading. Long term recordings with microelectrode arrays: studies of transcription-dependent neuronal plasticity and axonal regeneration. *J Physiol Paris*, 99:125–132, 2006.

S Hosmane, IH Yang, A Ruffin, N Thakor, and A Venkatesan. Circular compartmentalized microfluidic platform: Study of axon-glia interactions. *Lab Chip*, 10: 741–747, 2010.

KR Howell, A Kutiyanawalla, and A Pillai. Long-term continuous corticosterone treatment decreases vegf receptor-2 expression in frontal cortex. *PLoS One*, 6: e20198, 2011.

M Ichikawa, K Muramoto, K Kobayashi, M Kawahara, and Y Kuroda. Formation and maturation of synapses in primary cultures of rat cerebral cortical cells: an electron microscopic study. *Neurosci Res*, 16:95–103, 1993.

A Iglesias, J Bauer, T Litzenburger, A Schubart, and C Linington. T- and b-cell responses to myelin oligodendrocyte glycoprotein in experimental autoimmune encephalomyelitis and multiple sclerosis. *Glia*, 36:220–234, 2001.

ZH Inan and M Kuntalp. A study on fuzzy c-means clustering-based systems in automatic spike detection. *Comput Biol Med*, 37:1160–1166, 2007.

Y Jimbo, T Tateno, and HP Robinson. Simultaneous induction of pathway-specific potentiation and depression in networks of cortical neurons. *Biophys J*, 76:670–678, 1999.

Y Jimbo, A Kawana, P Parodi, and V Torre. The dynamics of a neuronal culture of dissociated cortical neurons of neonatal rats. *Biol Cybern*, 83:1–20, 2000.

Y Jimbo, N Kasai, K Torimitsu, and T Tateno. *MEA-Based Spike Recording in Cultured Neuronal Networks*. Springer, 2006.

AFM Johnstone, GW Gross, DG Weiss, OHU Schroeder, A Gramowski, and TJ Shafer. Microelectrode arrays: a physiologically based neurotoxicity testing platform for the 21st century. *Neurotoxicology*, 31:331–350, 2010.

IL Jones, P Livi, MK Lewandowska, M Fiscella, B Roscic, and A Hierlemann. The potential of microelectrode arrays and microelectronics for biomedical research and diagnostics. *Anal Bioanal Chem*, 399:2313–2329, 2011.

RW Joyner. Temperature effects on neuronal elements. *Fed Proc*, 40:2814–2818, 1981.

H Kaji, M Nishizawa, and T Matsue. Localized chemical stimulation to micropatterned cells using multiple laminar fluid flows. *Lab Chip*, 3:208–211, 2003.

TT Kanagasabapathi, K Wang, M Mellace, GJ Ramakers, and MM Decre. Dual compartment neurofluidic system for electrophysiological measurements in physically isolated neuronal cell cultures. *Conf Proc IEEE Eng Med Biol Soc*, 2009: 1655–1658, 2009.

TT Kanagasabapathi, D Ciliberti, S Martinoia, WJ Wadman, and MMJ Decré. Dual-compartment neurofluidic system for electrophysiological measurements in physically segregated and functionally connected neuronal cell culture. *Front Neuroeng*, 4:13, 2011.

Y Kawaguchi, CJ Wilson, SJ Augood, and PC Emson. Striatal interneurones: chemical, physiological and morphological characterization. *Trends Neurosci*, 18: 527–535, 1995.

A Keuer, R Schrott, J Taube, D Schmuck, H Beikirch, and W Baumann. Fpga based time detection of spikes within neural signals. In *Proc. Sensor Array and Multichannel Signal Processing Workshop*, pages 186–190, 2004.

D Khatami, Y Nam, G Brewer, and B Wheeler. Effect of bicuculline on the spontaneous and evoked activity of patterned embryonic hippocampal neurons cultured in vitro. *Conf Proc IEEE Eng Med Biol Soc*, 6:4059–4062, 2004.

N Kim, N Kehtarnavaz, MB Yeary, and S Thornton. Dsp-based hierarchical neural network modulation signal classification. *IEEE Trans Neural Netw*, 14:1065–1071, 2003.

CK Knox. Cross-correlation functions for a neuronal model. *Biophys J*, 14:567–582, 1974.

CK Knox. Detection of neuronal interactions using correlation analysis. *Trends Neurosci*, 4:222–225, 1981.

T Koos, JM Tepper, and CJ Wilson. Comparison of ipscs evoked by spiny and fast-spiking neurons in the neostriatum. *J Neurosci*, 24:7916–7922, 2004.

CR Kothapalli, E van Veen, S de Valence, S Chung, IK Zervantonakis, FB Gertler, and RD Kamm. A high-throughput microfluidic assay to study neurite response to growth factor gradients. *Lab Chip*, 11:497–507, 2011.

T Kraus, E Verpoorte, V Linder, W Franks, A Hierlemann, F Heer, S Hafizovic, T Fujii, NF de Rooij, and S Koster. Characterization of a microfluidic dispensing system for localised stimulation of cellular networks. *Lab Chip*, 6:218–229, 2006.

G Krause, S Lehmann, M Lehmann, I Freund, E Schreiber, and W Baumann. Measurement of electrical activity of long-term mammalian neuronal networks on semiconductor neurosensor chips and comparison with conventional microelectrode arrays. *Biosens Bioelectron*, 21:1272–1282, 2006.

Y Kubota and Y Kawaguchi. Dependence of gabaergic synaptic areas on the interneuron type and target size. *J Neurosci*, 20:375–386, 2000.

TN Kumar and CW Chong. An automated approach for locating multiple faulty luts in an fpga. *Microelectronics Reliability*, 48:1900–1906, 2008.

A Kunze, M Giugliano, A Valero, and P Renaud. Micropatterning neural cell cultures in 3d with a multi-layered scaffold. *Biomaterials*, 32:2088–2098, 2011a.

A Kunze, R Meissner, S Brando, and P Renaud. Co-pathological connected primary neurons in a microfluidic device for alzheimer studies. *Biotechnol Bioeng*, 108: 2241–2245, 2011b.

L Lanzaro, S Caserta, S Guido, L Sabetta, V Sibillo, and M Simeone. Controlled temperature water (or other fluid)-jacket co2 microscope stage incubator,patent number pct/it2005/000161, 2005.

R Lebar, C Lubetzki, C Vincent, P Lombrail, and JM Boutry. The m2 autoantigen of central nervous system myelin, a glycoprotein present in oligodendrocyte membrane. *Clin Exp Immunol*, 66:423–434, 1986.

MS Lewicki. A review of methods for spike sorting: the detection and classification of neural action potentials. *Network*, 9:R53–R78, 1998.

X Li, W Zhou, S Zeng, M Liu, and Q Luo. Long-term recording on multi-electrode array reveals degraded inhibitory connection in neuronal network development. *Biosens Bioelectron*, 22:1538–1543, 2007a.

Y Li, W Zhou, X Li, S Zeng, M Liu, and Q Luo. Characterization of synchronized bursts in cultured hippocampal neuronal networks with learning training on microelectrode arrays. *Biosens Bioelectron*, 22:2976–2982, 2007b.

JL Lin, MH Wu, CY Kuo, KD Lee, and YL Shen. Application of indium tin oxide (ito)-based microheater chip with uniform thermal distribution for perfusion cell culture outside a cell incubator. *Biomed Microdevices*, 12:389–398, 2010.

A Maccione, M Gandolfo, P Massobrio, A Novellino, S Martinoia, and M Chiappalone. A novel algorithm for precise identification of spikes in extracellularly recorded neuronal signals. *J Neurosci Methods*, 177:241–249, 2009.

L MacNabb. Application of cluster analysis towards the development of health region peer groups. *Proc of the Survey Methods Section*, 1:85–90, 2003.

E Maeda, HP Robinson, and A Kawana. The mechanisms of generation and propagation of synchronized bursting in developing networks of cortical neurons. *J Neurosci*, 15:6834–6845, 1995.

E Maeda, Y Kuroda, HP Robinson, and A Kawana. Modification of parallel activity elicited by propagating bursts in developing networks of rat cortical neurones. *Eur J Neurosci*, 10:488–496, 1998.

D Majumdar, Y Gao, D Li, and DJ Webb. Co-culture of neurons and glia in a novel microfluidic platform. *J Neurosci Methods*, 196:38–44, 2011.

S Marom and D Eytan. Learning in ex-vivo developing networks of cortical neurons. *Prog Brain Res*, 147:189–199, 2005.

S Martinoia, L Bonzano, M Chiappalone, M Tedesco, M Marcoli, and G Maura. In vitro cortical neuronal networks as a new high-sensitive system for biosensing applications. *Biosens Bioelectron*, 20:2071–2078, 2005.

JC McDonald, DC Duffy, JR Anderson, DT Chiu, H Wu, OJA Schueller, and GM Whitesides. Fabrication of microfluidic systems in poly(dimethylsiloxane). *Electrophoresis*, 21:27–40, 2000.

MJ McLean, RR Holcomb, AW Wamil, JD Pickett JD, and AV Cavopol. Blockade of sensory neuron action potentials by a static magnetic field in the 10 mt range. *Bioelectromagnetics*, 16:20–32, 1995.

MEA-Manual. *Multi Channel Systems*. MCS GmbH, http://www.multichannelsystems.com/fileadmin/userupload/Manuals/MEAManual.pdf., 2010.

MEA1060-Manual. *Multi Channel Systems*. MCS GmbH, http://www.multichannelsystems.com/uploads/media/MEA1060-Inv-BCManual01.pdf, 2011.

I Mendel, N Kerlero de Rosbo, and A Ben-Nun. A myelin oligodendrocyte glycoprotein peptide induces typical chronic experimental autoimmune encephalomyelitis in h-2b mice: fine specificity and t cell receptor v beta expression of encephalitogenic t cells. *Eur J Immunol*, 25:1951–1959, 1995.

DJ Mishelevich. On-line real-time digital computer separation of extracellular neuroelectric signals. *IEEE Trans Biomed Eng*, 17:147–150, 1970.

T Mizuno, G Zhang, H Takeuchi, J Kawanokuchi, J Wang, Y Sonobe, S Jin, N Takada, Y Komatsu, and A Suzumura. Interferon-gamma directly induces neurotoxicity through a neuron specific, calcium-permeable complex of ifn-gamma receptor and ampa glur1 receptor. *FASEB J*, 22:1797–1806, 2008.

JL Mohler, AW Partin, WB Isaacs, and DS Coffey. Time lapse videomicroscopic identification of dunning r-3327 adenocarcinoma and normal rat prostate cells. *J Urol*, 137:544–547, 1987.

P Mohseni and K Najafi. A fully integrated neural recording amplifier with dc input stabilization. 51:832–837, 2004.

SI Morefield, EW Keefer, and KD Chapman GW Gross. Drug evaluations using neuronal networks cultured on microelectrode arrays. *Biosens Bioelectron*, 15: 383–396, 2000.

FO Morin, Y Takamura, and E Tamiya. Investigating neuronal activity with planar microelectrode arrays: achievements and new perspectives. *J Biosci Bioeng*, 100: 131–143, 2005.

FO Morin, N Nishimura, L Griscom, B Lepioufle, H Fujita, Y Takamura, and E Tamiya. Constraining the connectivity of neuronal networks cultured on microelectrode arrays with microfluidic techniques: a step towards neuron-based functional chips. *Biosens Bioelectron*, 21:1093–1100, 2006.

N Morizet, F Amiel, ID Hamed, and T Ea. A comparative implementation of pca face recognition algorithm. *14th IEEE Int Conf on Electronics*, 1:865–868, 2007.

SJ Morrison, M Csete, AK Groves, W Melega, B Wold, and DJ Anderson. Culture in reduced levels of oxygen promotes clonogenic sympathoadrenal differentiation by isolated neural crest stem cells. *J Neurosci*, 20:7370–7376, 2000.

Y Mourzina, D Kaliaguine, P Schulte, and A Offenhäusser. Patterning chemical stimulation of reconstructed neuronal networks. *Anal Chim Acta*, 575:281–289, 2006.

J Mukai, T Shiina, and Y Jimbo. Continuous monitoring of developmental activity changes in cultured cortical networks. *Electrical Engineering in Japan*, 145:28–37, 2003.

L Muzio, F Cavasinni, C Marinaro, A Bergamaschi, A Bergami, C Porcheri, F Cerri, G Dina, A Quattrini, G Comi, R Furlan, and G Martino. Cxcl10 enhances blood cells migration in the sub-ventricular zone of mice affected by experimental autoimmune encephalomyelitis. *Mol Cell Neurosci*, 43:268–280, 2010.

Y Nam, JC Chang, BC Wheeler, and GJ Brewer. Gold-coated microelectrode array with thiol linked self-assembled monolayers for engineering neuronal cultures. 51: 158–165, 2004.

H Neumann, R Schweigreiter, T Yamashita, K Rosenkranz, H Wekerle, and YA Barde. Tumor necrosis factor inhibits neurite outgrowth and branching of hippocampal neurons by a rho-dependent mechanism. *J Neurosci*, 22:854–862, 2002.

MAL Nicolelis and S Ribeiro. Multielectrode recordings: the next steps. *Curr Opin Neurobiol*, 12:602–606, 2002.

A. Novellino, Bibiana Scelfo, T. Palosaari, A. Price, Tomasz Sobanski, T. J. Shafer, A. F M Johnstone, G. W. Gross, A. Gramowski, O. Schroeder, K. Jügelt, M. Chiappalone, F. Benfenati, S. Martinoia, M. T. Tedesco, E. Defranchi, P. D'Angelo, and M. Whelan. Development of micro-electrode array based tests for neurotoxicity: assessment of interlaboratory reproducibility with neuroactive chemicals. *Front Neuroeng*, 4:4, 2011.

I Obeid, MAL Nicolelis, and PD Wolf. A low power multichannel analog front end for portable neural signal recordings. *J Neurosci Methods*, 133:27–32, 2004.

MJ O'Donovan. The origin of spontaneous activity in developing networks of the vertebrate nervous system. *Curr Opin Neurobiol*, 9:94–104, 1999.

M Olsen, A Sarup, OM Larsson, and A Schousboe. Effect of hyperosmotic conditions on the expression of the betaine-gaba-transporter (bgt-1) in cultured mouse astrocytes. *Neurochem Res*, 30:855–865, 2005.

RH Olsson, DL Buhl, AM Sirota, G Buzsaki, and KD Wise. Band-tunable and multiplexed integrated circuits for simultaneous recording and stimulation with microelectrode arrays. *IEEE Trans Biomed Eng*, 52:1303–1311, 2005.

JJ Pancrazio, SA Gray, YS Shubin, N Kulagina, DS Cuttino, KM Shaffer, K Eisemann, A Curran, B Zim, GW Gross, and TJ O'Shaughnessy. A portable microelectrode array recording system incorporating cultured neuronal networks for neurotoxin detection. *Biosens Bioelectron*, 18:1339–1347, 2003.

J Park, H Koito, J Li, and A Han. Microfluidic compartmentalized co-culture platform for cns axon myelination research. *Biomed Microdevices*, 11:1145–1153, 2009a.

J Park, H Koito, J Li, and A Han. A multi-compartment cns neuron-glia co-culture microfluidic platform. *J Vis Exp*, 10:31, 2009b.

V Pasquale, P Massobrio, LL Bologna, M Chiappalone, and S Martinoia. Self-organization and neuronal avalanches in networks of dissociated cortical neurons. *Neuroscience*, 153:1354–1369, 2008.

V Pasquale, S Martinoia, and M Chiappalone. A self-adapting approach for the detection of bursts and network bursts in neuronal cultures. *J Comput Neurosci*, 29:213–229, 2010.

TM Pearce and JC Williams. Microtechnology: meet neurobiology. *Lab Chip*, 7: 30–40, 2007.

TM Pearce, JA Wilson, SG Oakes, SY Chiu, and JC Williams. Integrated microelectrode array and microfluidics for temperature clamp of sensory neurons in culture. *Lab Chip*, 5:97–101, 2005.

Y Perelman and R Ginosar. Analog frontend for multichannel neuronal recording system with spike and lfp separation. *J Neurosci Methods*, 153:21–26, 2006.

Y Perelman and R Ginosar. An integrated system for multichannel neuronal recording with spike/lfp separation, integrated a/d conversion and threshold detection. *IEEE Trans Biomed Eng*, 54:130–137, 2007.

DH Perkel, GL Gerstein, and GP Moore. Neuronal spike trains and stochastic point processes. i. the single spike train. *Biophys J*, 7:391–418, 1967.

S Petronis, M Stangegaard, CBV Christensen, and M Dufva. Transparent polymeric cell culture chip with integrated temperature control and uniform media perfusion. *Biotechniques*, 40:368–376, 2006.

C Picard, V Hearnden, M Massignani, S Achouri, G Battaglia, S MacNeil, and A Donald. A micro-incubator for cell and tissue imaging. *Biotechniques*, 48: 135–138, 2010.

J Pihl, J Sinclair, E Sahlin, M Karlsson, F Petterson, J Olofsson, and O Orwar. Microfluidic gradient-generating device for pharmacological profiling. *Anal Chem*, 77:3897–3903, 2005.

J Pine. Recording action potentials from cultured neurons with extracellular microcircuit electrodes. *J Neurosci Methods*, 2:19–31, 1980.

V Polikov, M Block, C Zhang, WM Reichert, and JS Hong. *In Vitro Models for Neuroelectrodes: A Paradigm for Studying Tissue Materials Interactions in the Brain.* CRC Press, 2008.

SM Potter. Distributed processing in cultured neuronal networks. *Prog Brain Res*, 130:49–62, 2001.

SM Potter and TB DeMarse. A new approach to neural cell culture for long-term studies. *J Neurosci Methods*, 110:17–24, 2001.

BR Preiss. *Data Structures and Algorithms with Object-Oriented Design Patterns in C++*. http://www.brpreiss.com/books/opus4/html/page493.html, 2009.

A Prina-Mello, E Farrell, PJ Prendergast, V Campbell, and JM Coey. Effects of static magnetic fields on primary cortical neurons. *Phys Scripta*, T118:205–207, 2005.

A Prina-Mello, E Farrell, PJ Prendergast, V Campbell, and JM Coey. Influence of strong static magnetic fields on primary cortical neurons. *Bioelectromagnetics*, 27:35–42, 2006.

D Qin, Y Xia, and GM Whitesides. Rapid prototyping of complex structures with feature sizes larger than 20 lm. *Adv Mater*, 8:917–919, 1996.

GA Qureshi and MS Baig. Quantitation of free amino acids in biological samples by high-performance liquid chromatography. application of the method in evaluating amino acid levels in cerebrospinal fluid and plasma of patients with multiple sclerosis. *J Chromatogr*, 459:237–244, 1988.

M Rafat, DR Raad, AC Rowat, and DT Auguste. Fabrication of reversibly adhesive fluidic devices using magnetism. *Lab Chip*, 9:3016–3019, 2009.

M Rasponi, F Piraino, N Sadr, M Laganà, A Redaelli, and M Moretti. Reliable magnetic reversible assembly of complex microfluidic devices: fabrication, characterization and biological validation. *Microfluid Nanofluid*, 10:1097–1107, 2011.

SK Ravula, MS Wang, MA McClain, SA Asress, B Frazier, and JD Glass. Spatiotemporal localization of injury potentials in drg neurons during vincristine-induced axonal degeneration. *Neurosci Lett*, 415:34–39, 2007.

SW Rhee, AM Taylor, CH Tu, DH Cribbs, CW Cotman, and NL Jeon. Patterned cell culture inside microfluidic devices. *Lab Chip*, 5:102–107, 2005.

R Rieger and JT Taylor. Design strategies for multi-channel low-noise recording systems. *Analog Integr Circ Sig Process*, 58:123–133, 2009.

R Rieger, Yen-Yow Pan, and J Taylor. Design strategies for multi-channel low-noise recording systems. In *Proc. IEEE Int. Symp. Circuits and Systems ISCAS 2007*, pages 561–564, 2007.

TM Rivers and FF Schwentker. Encephalomyelitis accompanied by myelin destruction experimentally produced in monkeys. *J Exp Med*, 61:689–702, 1935.

TM Rivers, DH Sprunt, and GP Berry. Observations on attempts to produce acute disseminated encephalomyelitis in monkeys. *J Exp Med*, 58:39–53, 1933.

JD Rolston, RE Gross, and SM Potter. A low-cost multielectrode system for data acquisition enabling real-time closed-loop processing with rapid recovery from stimulation artifacts. *Front Neuroeng*, 2:12, 2009.

EV Romanova, KA Fosser, SS Rubakhin, RG Nuzzo, and JV Sweedler. Engineering the morphology and electrophysiological parameters of cultured neurons by microfluidic surface patterning. *FASEB J*, 18:1267–1269, 2004.

GG Rose. The circumfusion system for multipurpose culture chambers. i. introduction to the mechanics, techniques, and basic results of a 12-chamber (in vitro) closed circulatory system. *J Cell Biol*, 32:89–112, 1967.

S Rossi, L Muzio, V De Chiara, G Grasselli, A Musella, G Musumeci, G Mandolesi, R De Ceglia, S Maida, E Biffi, A Pedrocchi, A Menegon, G Bernardi, R Furlan, G Martino, and D Centonze. Impaired striatal gaba transmission in experimental autoimmune encephalomyelitis. *Brain Behav Immun*, 25:947–956, 2011.

L Rowe, M Almasri, K Lee, N Fogleman, G J Brewer, Y Nam, BC Wheeler, J Vukasinovic, A Glezer, and AB Frazier. Active 3-d microscaffold system with fluid perfusion for culturing in vitro neuronal networks. *Lab Chip*, 7:475–482, 2007.

L Rubinsky, N Raichman, I Baruchi, M Shein, J Lavee, H Frenk, and E Ben-Jacob. Study of hypothermia on cultured neuronal networks using multi-electrode arrays. *J Neurosci Methods*, 160:288–293, 2007.

U Rutishauser, EM Schuman, and AN Mamelak. Online detection and sorting of extracellularly recorded action potentials in human medial temporal lobe recordings, in vivo. *J Neurosci Methods*, 154:204–224, 2006.

E Salinas and TJ Sejnowski. Correlated neuronal activity and the flow of neural information. *Nat Rev Neurosci*, 2:539–550, 2001.

R Schrott, A Keuer, J Taube, D Schmuck, H Beikirch, W Baumann, and E Schreiber. Real-time data analysis of action potentials. In *Proc. CIMSA Computational Intelligence for Measurement Systems and Applications 2004 IEEE Int. Conf*, pages 26–29, 2004.

R Segev, I Baruchi, E Hulata, and E Ben-Jacob. Hidden neuronal correlations in cultured networks. *Phys Rev Lett*, 92:118102, 2004.

JV Selinger, NV Kulagina, TJ O'Shaughnessy, W Ma, and JJ Pancrazio. Methods for characterizing interspike intervals and identifying bursts in neuronal activity. *J Neurosci Methods*, 162:64–71, 2007.

MN Shadlen and WT Newsome. The variable discharge of cortical neurons: implications for connectivity, computation, and information coding. *J Neurosci*, 18: 3870–3896, 1998.

G Shahaf and S Marom. Learning in networks of cortical neurons. *J Neurosci*, 21: 8782–8788, 2001.

P Shi, S Nedelec, H Wichterle, and LC Kam. Combined microfluidics/protein patterning platform for pharmacological interrogation of axon pathfinding. *Lab Chip*, 10:1005–1010, 2010.

HK Slocum, JC Parsons, EO Winslow, L Broderick, H Minderman, K Tóth, WR Greco, and YM Rustum. Time-lapse video reveals immediate heterogeneity and heritable damage among human ileocecal carcinoma hct-8 cells treated with raltitrexed (zd1694). *Cytometry*, 41:252–260, 2000.

DM Sokal, R Mason, and TL Parker. Multi-neuronal recordings reveal a differential effect of thapsigargin on bicuculline- or gabazine-induced epileptiform excitability in rat hippocampal neuronal networks. *Neuropharmacology*, 39:2408–2417, 2000.

H Sonnier, OV Kolomytkin, and AA Marino. Resting potential of excitable neuroblastoma cells in weak magnetic fields. *Cell Mol Life Sci*, 57:514–520, 2000.

D Stellwagen and RC Malenka. Synaptic scaling mediated by glial tnf-alpha. *Nature*, 440:1054–1059, 2006.

D Stellwagen, EC Beattie, JY Seo, and RC Malenka. Differential regulation of ampa receptor and gaba receptor trafficking by tumor necrosis factor-alpha. *J Neurosci*, 25:3219–3228, 2005.

A Stett, U Egert, E Guenther, F Hofmann, T Meyer, W Nisch, and H Haemmerle. Biological application of microelectrode arrays in drug discovery and basic research. *Anal Bioanal Chem*, 377:486–495, 2003.

CF Stevens and AM Zador. Input synchrony and the irregular firing of cortical neurons. *Nat Neurosci*, 1:210–217, 1998.

J Streit, A Tscherter, MO Heuschkel, and P Renaud. The generation of rhythmic activity in dissociated cultures of rat spinal cord. *Eur J Neurosci*, 14:191–202, 2001.

A Sun, DD Zeng, and H Chen. Burst detection from multiple data streams: A network-based approach. 40:258–267, 2010.

JH Sung, C Kam, and ML Shuler. A microfluidic device for a pharmacokinetic-pharmacodynamic (pk-pd) model on a chip. *Lab Chip*, 10:446–455, 2010.

JA Sykes and EB Moore. A new chamber for tissue culture. *Proc Soc Exp Biol Med*, 100:125–127, 1959.

DC Tam. An alternate burst analysis for detecting intra-burst firings based on inter-burst periods. *Neurocomputing*, 44-46:1155–1159, 2002.

G Tao, S Datta, R He, F Nelson, JS Wolinsky, and PA Narayana. Deep gray matter atrophy in multiple sclerosis: a tensor based morphometry. *J Neurol Sci*, 282: 39–46, 2009.

T Tateno and Y Jimbo. Activity-dependent enhancement in the reliability of correlated spike timings in cultured cortical neurons. *Biol Cybern*, 80:45–55, 1999.

AM Taylor and NL Jeon. Micro-scale and microfluidic devices for neurobiology. *Curr Opin Neurobiol*, 20:640–647, 2010.

AM Taylor, SW Rhee, CH Tu, DH Cribbs, CW Cotman, and NL Jeon. Microfluidic multicompartment device for neuroscience research. *Langmuir*, 19:1551–1556, 2003.

AM Taylor, DC Dieterich, HT Ito, SA Kim, and EM Schuman. Microfluidic local perfusion chambers for the visualization and manipulation of synapses. *Neuron*, 66:57–68, 2010.

JM Tepper, T Koós, and CJ Wilson. Gabaergic microcircuits in the neostriatum. *Trends Neurosci*, 27:662–669, 2004.

JM Tepper, ED Abercrombie, and JP Bolam. Basal ganglia macrocircuits. *Prog Brain Res*, 160:3–7, 2007.

PH Thakur, H Lu, SS Hsiao, and KO Johnson. Automated optimal detection and classification of neural action potentials in extra-cellular recordings. *J Neurosci Methods*, 162:364–376, 2007.

S Tokdar, P Xi, RC Kelly, and RE Kass. Detection of bursts in extracellular spike trains using hidden semi-markov point process models. *J Comput Neurosci*, 29: 203–212, 2010.

S Toyotomi and Y Momose. Temperature-controlled perfusion apparatus for microscope using transparent conducting film heater. *Am J Physiol*, 256:C214–217, 1989.

J van Pelt, MA Corner, PS Wolters, WLC Rutten, and GJA Ramakers. Longterm stability and developmental changes in spontaneous network burst firing patterns in dissociated rat cerebral cortex cell cultures on multielectrode arrays. *Neurosci Lett*, 361:86–89, 2004a.

J van Pelt, PS Wolters, MA Corner, WLC Rutten, and GJA Ramakers. Long-term characterization of firing dynamics of spontaneous bursts in cultured neural networks. *IEEE Trans Biomed Eng*, 51:2051–2062, 2004b.

J van Pelt, I Vajda, PS Wolters, MA Corner, and GJA Ramakers. Dynamics and plasticity in developing neuronal networks in vitro. *Prog Brain Res*, 147:173–188, 2005.

KS Vikman, B Owe-Larsson, J Brask, KS Kristensson, and RH Hill. Interferon-gamma-induced changes in synaptic activity and ampa receptor clustering in hippocampal cultures. *Brain Res*, 896:18–29, 2001.

HC von Büdingen, N Tanuma, P Villoslada, JC Ouallet, SL Hauser, and CP Genain. Immune responses against the myelin/oligodendrocyte glycoprotein in experimental autoimmune demyelination. *J Clin Immunol*, 21:155–170, 2001.

HC von Büdingen, T Menge, SL Hauser, and CP Genain. Restrictive and diversifying elements of the anti-myelin/oligodendrocyte glycoprotein antibody response in primate experimental allergic encephalomyelitis. *Immunogenetics*, 58:122–128, 2006.

J Vukasinovic, DK Cullen, MC LaPlaca, and A Glezer. A microperfused incubator for tissue mimetic 3d cultures. *Biomed Microdevices*, 11:1155–1165, 2009.

T Vyshkina, I Banisor, YY Shugart, TP Leist, and B Kalman. Genetic variants of complex i in multiple sclerosis. *J Neurol Sci*, 228:55–64, 2005.

DA Wagenaar and SM Potter. A versatile all-channel stimulator for electrode arrays, with real-time control. *J Neural Eng*, 1:39–45, 2004.

DA Wagenaar, TB DeMarse, and SM Potter. Meabench: A toolset for multi-electrode data acquisition and on-line analysis. *Proc 2nd Int IEEE EMBS Conf on Neural Engineering*, 1:518–521, 2005.

DA Wagenaar, Z Nadasdy, and SM Potter. Persistent dynamic attractors in activity patterns of cultured neuronal networks. *Phys Rev E Stat Nonlin Soft Matter Phys*, 73:051907, 2006a.

DA Wagenaar, J Pine, and SM Potter. An extremely rich repertoire of bursting patterns during the development of cortical cultures. *BMC Neurosci*, 7:11, 2006b.

J Wang, L Ren, L Li, W Liu, J Zhou, W Yu, D Tong, and S Chen. Microfluidics: a new cosset for neurobiology. *Lab Chip*, 9:644–652, 2009.

Y Wang, D Feng, G Liu, Q Luo, Y Xu, S Lin, J Fei, and L Xu. Gamma-aminobutyric acid transporter 1 negatively regulates t cell-mediated immune responses and ameliorates autoimmune inflammation in the cns. *J Immunol*, 181:8226–8236, 2008.

PT Watkins, G Santhanam, KV Shenoy, and RR Harrison. Validation of adaptive threshold spike detector for neural recording. *Conf Proc IEEE Eng Med Biol Soc*, 6:4079–4082, 2004.

BC Wheeler and WJ Heetderks. A comparison of techniques for classification of multiple neural signals. *IEEE Trans Biomed Eng*, 29:752–759, 1982.

N Willumsen. Increased throughput in ion channel drug development and exploration by automation of electrophysiology. *Am Biotechol Lab*, 24:20–23, 2006.

CJ Wilson and Y Kawaguchi. The origins of two-state spontaneous membrane potential fluctuations of neostriatal spiny neurons. *J Neurosci*, 16:2397–2410, 1996.

D Wlodkowic and JM Cooper. Microfabricated analytical systems for integrated cancer cytomics. *Anal Bioanal Chem*, 398:193–209, 2010.

BM Wright. A simple control system for co2 in incubators. *J Clin Pathol*, 17: 100–102, 1964.

G Wrobel, Y Zhang, HJ Krause, N Wolters, F Sommerhage, A Offenhäusser, and S Ingebrandt. Influence of the first amplifier stage in mea systems on extracellular signal shapes. *Biosens Bioelectron*, 22:1092–1096, 2007.

MH Wu, SB Huang, and GB Lee. Microfluidic cell culture systems for drug research. *Lab Chip*, 10:939–956, 2010.

Y Xia, J McClelland, R Gupta, D Qin, XM Zhao, LL Sohn, RJ Celotta, and GM Whitesides. Replica molding using polymeric materials: A practical step toward nanomanufacturing. *Adv Mat*, 9:147–149, 1997.

K Xiang, DE Earl, KM Davis, DR Giovannucci, LJ Greenfield, and EI Tietz. Chronic benzodiazepine administration potentiates high voltage-activated calcium currents in hippocampal ca1 neurons. *J Pharmacol Exp Ther*, 327:872–883, 2008.

XILINX-Inc. *Xilinx Spartan-3 Platform FPGAs*. XILINX Inc., http://www.xilinx.com/company/press/kits/spartan3/S3PressFAQ.pdf, 2003.

XILINX-Inc. *Spartan-3 FPGA family data sheet*. XILINX Inc., http://www.xilinx.com/support/documentation/datasheets, 2008.

XILINX-Inc. *Extended Spartan-3A, Spartan-3E and Spartan-3 FPGA families*. XILINX Inc., http://www.xilinx.com/support/documentation/userguides/ug331.pdf, 2009.

ZQ Xiong and JO McNamara. Fleeting activation of ionotropic glutamate receptors sensitizes cortical neurons to complement attack. *Neuron*, 36:363–374, 2002.

XW Yang and SA Shamma. A totally automated system for the detection and classification of neural spikes. *IEEE Trans Biomed Eng*, 35:806–816, 1988.

EW Young and DJ Beebe. Fundamentals of microfluidic cell culture in controlled microenvironments. *Chem Soc Rev*, 39:1036–1048, 2010.

EW Young and CA Simmons. Macro- and microscale fluid flow systems for endothelial cell biology. *Lab Chip*, 10:143–160, 2010.

R Zhang, J Yamada, Y Hayashi, Z Wu, S Koyama, and H Nakanishi. Inhibition of nmda-induced outward currents by interleukin-1beta in hippocampal neurons. *Biochem Biophys Res Commun*, 372:816–820, 2008.

B Zhu, L Luo, GR Moore, DW Paty, and MS Cynader. Dendritic and synaptic pathology in experimental autoimmune encephalomyelitis. *Am J Pathol*, 162: 1639–1650, 2003.

X Zhu, LY Chu, BH Chueh, M Shen, B Hazarika, N Phadke, and S Takayama. Arrays of horizontally-oriented mini-reservoirs generate steady microfluidic flows for continuous perfusion cell culture and gradient generation. *Analyst*, 129:1026–1031, 2004.

MO Ziehn, AAA Avedisian, S Tiwari-Woodruff, and RR Voskuhl. Hippocampal ca1 atrophy and synaptic loss during experimental autoimmune encephalomyelitis, eae. *Lab Invest*, 90:774–786, 2010.

A Zviagintsev, Y Perelman, and R Ginosar. Algorithms and architectures for low power spike detection and alignment. *J Neural Eng*, 3:35–42, 2006.